Sea Grant College Program

Massachusetts Institute
of Technology
Cambridge, Massachusetts
02139

TIME SERIES ANALYSIS OF OCEAN WAVES

Douglas G. Dommermuth
Nitindra R. Joglekar

MITSG 87-8TN

Revised June 1986

Sea Grant College Program
Massachusetts Institute of Technology
Cambridge, MA 02139

Grant No: NA84-AA-D-00046
Project No: R/O-18

TABLE OF CONTENTS

ABSTRACT

In this report, the simulation of ocean wave kinematics by digital convolution techniques is presented. In deep water, the vertical attenuation and horizontal propagation of ocean waves are solved analytically. In shallow water, the vertical-attenuation and horizontal-propagation problems are solved using the fast Fourier transform. It is shown that the convolution integrals required to simulate irregular waves are more efficient than summing sinusoids. Guidelines for the processing of real wave data are established. The technique is validated by comparing data acquired in a wave tank with the simulated result. Applications of this method are demonstrated with example problems.

For information concerning computer programs which implement these simulation techniques, contact:

Professor J. Kim Vandiver
MIT Room 5-222
Cambridge, MA 02139
(617) 253-4366

CHAPTER 1

ANALYSIS OF OCEAN WAVES IN THE TIME DOMAIN

1.1 THE FREQUENCY DOMAIN VERSUS THE TIME DOMAIN

Time-domain analysis can be very useful for the design of offshore structures. However, time-domain analysis is not performed very often because the software in use today is inefficient. Instead frequency-domain analysis is used. A frequency-domain analysis is made efficient by the many linearizations that are imposed. The motions, exciting and restraining forces, and wave kinematics are linearized to perform a frequency-domain analysis. But these linearizations make the frequency domain a worse model of reality than the time domain because the time domain does model nonlinearities. Also, physically, the time domain is a better choice than the frequency domain because natural phenomena change with time, not with frequency. Both the frequency domain and time domain have certain advantages and disadvantages which make the proper choice for analysis extremely important.

The response of an offshore structure to a storm is very nonlinear. Since the frequency domain cannot model nonlinearities, it cannot model response to storms. It models the response of an offshore structure under normal operating conditions. It is best used during preliminary design, in the early stages of the design spiral, when there are many possible solutions. It is an efficient and inexpensive way of eliminating poor design choices. Unlike the frequency domain, the time domain can model the response of an offshore structure to a storm. It is best used during final design, near the end of the design spiral, when only one or two designs are being considered. Poor design choices that are not found by a frequency-domain analysis can be found by a time-domain analysis.

Together with model tests, the time domain can be a valuable method of design. If it is used properly, it will certainly help to avoid accidents such as befell the Ocean Ranger and Glomar Explorer. This is especiallly important as the search for oil is extended into deeper and harsher environments.

Time-domain analysis will become more attractive as it becomes more efficient. Its inefficiency leads to very expensive and extremely long computer simulations. One of the leading contributors to this inefficiency is the algorithm which models irregular seas. This paper will

demonstrate an efficient method for modeling irregular seas.

1.2 APPLICATIONS OF TIME-DOMAIN ANALYSIS

Time-domain analysis of an offshore structure's response to ocean waves can identify poor design choices. Specifically, the ocean engineer is most interested in preventing structural failure. Other design objectives include flood prevention, station-keeping ability, and good seakeeping characteristics. Time-domain analysis can help meet all of these design objectives. Useful applications of time-domain analysis include dynamic response of jackets, hybrid towers, guyed towers, and risers. Other applications include seakeeping response of semisubmersibles and tension-leg platforms. As seen in Figure 1, all of these structures are made of slender cylinders. In general, Morison's equation can be used to model the dynamic response of a cylinder to an ocean wave when the cylinder's diameter is smaller than the wave's length. The application of Morison's equation is controversial. Yet, for the problems we want to solve, Morison's equation gives results which are in good agreement with experiments.

1.3 MORISON'S EQUATION

For forces normal to a cylinder's axis, Morison's equation can be expressed as (Figure 2)

$$\vec{F_n} = C_a \rho \nabla (\vec{\dot{u}_n} - \vec{\ddot{x}_n}) + \rho \nabla \vec{\dot{u}_n} + C_d \frac{1}{2} \rho A |\vec{u_n} - \vec{\dot{x}_n}| (\vec{u_n} - \vec{\dot{x}_n}) \qquad (1.1)$$

where the variables have the following definitions:

1) $\vec{F_n}$ is the vector of hydrodynamic forces normal to the cylinder's axis,

2) C_a is the added-mass coefficient and C_d is the viscous-drag coefficient for flow normal to the cylinder's axis,

3) ρ is the mass density of water,

4) ∇ is the volume of the cylinder,

5) A is the projected area in the direction of the normal, and

6) $\vec{u_n}$, $\vec{\dot{x}_n}$, $\vec{\dot{u}_n}$, and $\vec{\ddot{x}_n}$ are normal components of the water-particle velocity, the cylinder's velocity, the water-particle acceleration, and the cylinder's acceleration respectively.

The first term in the equation is called the added-mass force. This term models forces proportional to acceleration. The second term models forces proportional to the gradient of pressure. The last term models viscous forces. Morison's equation does not model diffraction. However, Morison's equation can be a good model of the hydrodynamic forces acting on cylinders with diameters less than one-quarter of the wave length. Furthermore, unlike

most potential flow models, Morison's equation does model viscous forces. These forces can be the greatest proportion of the total force acting on offshore structures.

Similiarly, the hydrodynamic forces acting in-line with a cylinder's axis can be expressed as (Figure 3)

$$\vec{F_t} = C_a \rho \forall (\dot{\vec{u}}_t - \ddot{\vec{x}}_t) + P_D A \vec{t} + C_d \frac{1}{2} \rho A |\vec{u}_t - \dot{\vec{x}}_t| (\vec{u}_t - \dot{\vec{x}}_t) \qquad (1.2)$$

where the variables have the following definitions:

1) $\vec{F_t}$ is the vector of hydrodynamic forces in-line with the cylinder's axis,

2) C_a is the added-mass coefficient of an equivalent sphere having a cross-sectional area equal to the area of the end of the cylinder and C_d is the viscous drag coefficient of an equivalent disc that has the same area as the end of the cylinder,

3) $\vec{t}$ is the unit vector in-line with the cylinder's axis,

4) P_D is the dynamic component of pressure,

5) $\forall$ is the volume of the equivalent sphere,

6) A is the area of the end of the cylinder, and

7) $\vec{u}_t$, $\dot{\vec{x}}_t$, $\dot{\vec{u}}_t$, and $\ddot{\vec{x}}_t$ are in-line components of the water-particle velocity, the cylinder's velocity, the water-particle acceleration, and the cylinder's acceleration respectively.

The water-particle velocities, accelerations, and pressures are required in Morison's equation. Furthermore, the free-suface elevation must be known so that the

hydrodynamic forces acting on all submerged cylinders can be calculated. Presently, the algorithm used to compute these quantities is very inefficient. In this paper, a more efficient method for computing these quantities will be developed.

1.4 SUMMARY OF CHAPTER ONE

The response of offshore structures to ocean waves can be analyzed in either the frequency domain or time domain. Frequency-domain analysis is best used during preliminary design, whereas time-domain analysis is best used during final design. Time-domain analysis is not used as often as it should be because it is inefficient, but it can become more efficient. For certain offshore structures, Morison's equation can be used to model the hydrodynamic forces. Presently, the algorithm used to compute the wave properties required by Morison's equation is very inefficient. A more efficient method will be developed in this paper. First, Airy wave theory will be reviewed. Then a theory of irregular waves will be developed which is based on Airy wave theory. This theory is more efficient than what is used today.

CHAPTER 2

REGULAR AND IRREGULAR WAVES

2.1 AIRY WAVE THEORY

Subject to certain limitations, Airy wave theory can be a very useful model of ocean waves. To understand those limitations, we must review the theory's derivation. Our final objective will be a model for irregular waves. Since irregular waves are a superposition of regular waves, we will use many Airy waves to simulate irregular waves. Therefore, the theory of irregular waves which we will develop will have limitations similiar to those of Airy waves.

We will define our coordinate system such that the Z-axis is positive up and the X-axis positive to the right. Furthermore, we will fix the origin at the mean waterline (Figure 4).

The first assumption we will make is that the fluid is inviscid or ideal.

$$\gamma = 0. \tag{2.1}$$

where γ is the kinematic viscosity. Since we have assumed an ideal fluid, there will be no energy dissipation due to viscous damping. This is valid because we are only interested in waves that travel short distances in the neighborhood of the offshore structure. For these short distances, we do not expect that the viscous damping will have a significant effect.

The second assumption we will make is that the fluid is incompressible.

$$\frac{\partial \rho}{\partial t} = \frac{\partial \rho}{\partial x} = \frac{\partial \rho}{\partial z} = 0. \tag{2.2}$$

where ρ is the density of the fluid. Intuitively, this seems to be a reasonable assumption. However, it is possible to model the compressibility of the fluid. In fact, even for water, compressibility can significantly affect added-mass and wave-damping calculations.

The third assumption we will make is that the fluid is irrotational.

$$\nabla \times \vec{V} \tag{2.3}$$

where ∇ is the del operator and $\vec{V}$ is the fluid particle

velocity vector. This important assumption enables us to express the velocity field in terms of the gradient of a scalar function Φ .

$$\vec{V} = \nabla\Phi \tag{2.4}$$

where Φ is defined as the velocity potential. Le Mehaute in his book An Introduction to Hydrodynamics and Water Waves, gives a good discussion of irrotational motion:

> A deep water swell, i.e., wave generated by wind traveling out of the generating area, is probably the motion which most closely approaches the condition of irrotationality. But under wind action the free surface shearing stress induces rotationality (and turbulence) in the direction of wave travel... Also, in shallow water, the bottom friction induces rotationality.... Rotationality at the crest in the direction of wave travel will reduce the limit wave steepness... Rotationality in the oposite direction will theoretically increase the limit wave steepness.

Using these arguments, we expect our theory to become less valid as the wave becomes steeper and the water shallower. These are limitations to the theory we propose. However, as we will soon discover, they are not very strong limitations.

By the continuity principle, equal amounts of fluid must enter and exit a control volume. Therefore,

$$\nabla^2\Phi = 0. \qquad \text{in the fluid.} \tag{2.5}$$

This equation is called Laplace's equation. It is the governing differential equation.

We must solve Laplace's equation and also satisfy the free-surface and bottom-boundary conditions. The bottom-boundary condition is that no fluid can move across the bottom - the normal component of fluid velocity must be zero.

$$\frac{\partial \bar{\Phi}}{\partial z} = 0. \qquad \text{on } z=-h, \quad (2.6)$$

where h is the water depth. This boundary condition does not allow for sloped bottoms. However, in the neighborhood of the offshore structure the bottom will be horizontal. For rigid, hard, horizontal bottoms, this boundary condition is exact.

The kinematic boundary condition on the free surface is that the fluid particles near the free surface can only move tangentially to the free surface. The nonlinear boundary condition is

$$\frac{D(z-\eta)}{Dt} = -\frac{\partial \eta}{\partial t} - \frac{\partial \eta}{\partial x}\frac{\partial \bar{\Phi}}{\partial x} + \frac{\partial \bar{\Phi}}{\partial z} = 0. \qquad \text{on } z=\eta, \quad (2.7)$$

where $\frac{D}{Dt}$ is the substantial derivative, and η is the free-surface elevation. This equation can be linearized if we assume that that the product of $\frac{\partial \eta}{\partial x}$ and $\frac{\partial \bar{\Phi}}{\partial x}$ is very small compared to the other terms in the equation. (This is the fourth assumption we have made.) This is a limitation on the steepness of the waves we can model because $\frac{\partial \eta}{\partial x}$ and $\frac{\partial \bar{\Phi}}{\partial x}$ are measures of the slope of the wave. It is a much stronger

limitation on steepness than that due to irrotationality. The linearized kinematic boundary condition on the free surface becomes

$$\frac{\partial \Phi}{\partial z} = \frac{\partial \eta}{\partial t} \qquad \text{on } z=0. \qquad (2.8)$$

Unlike the fully nonlinear boundary condition, the linear boundary condition is satisfied on the mean waterline. Since the steepness of the wave is small, the potential, the free-surface elevation, and their derivatives evaluated on the free surface can be expanded in a Taylor series expansion about the mean waterline.

The dynamic boundary condition on the free surface is that the pressure must be continuous across the free surface - the water pressure immediately below the free surface must be equal to the air pressure immediately above. We can use Bernoulli's equation to show

$$\frac{\partial \Phi}{\partial t} + \frac{1}{2} \nabla\Phi \cdot \nabla\Phi + g\eta = 0. \qquad \text{on } z=\eta \ , \qquad (2.9)$$

where g is the acceleration of gravity. Since it is consistent with our earlier assumption that the slope of the wave is small, we can neglect the nonlinear terms. Then the linearized dynamic boundary condition on the free surface becomes

$$\eta = -\frac{1}{g}\frac{\partial \Phi}{\partial t} \qquad \text{on } z=0. \qquad (2.10)$$

This boundary condition is also satisfied on the mean waterline.

The kinematic and dynamic boundary conditions on the free surface can be combined into

$$\frac{\partial^2 \bar{\Phi}}{\partial t^2} + g\frac{\partial \bar{\Phi}}{\partial z} = 0. \qquad \text{on } z=0. \qquad (2.11)$$

This is called the free-surface boundary condition or the wave equation.

A solution of Laplace's equation which satisfies the bottom and free-surface boundary conditions is

$$\bar{\Phi} = Re\ -\frac{i\omega A}{k}\frac{\cosh(k(z+h))}{\sinh(kh)}\, e^{i(kx-\omega t)} \qquad (2.12)$$

where ω is the wave frequency, k is the wave number, A is the wave amplitude, and t is time. (In equation (2.12) we have used complex notation. Throughout this report we will use the symbol Re to indicate that the real part must be taken.) Furthermore, the wave frequency and wave number must satisfy the dispersion relation.

$$\omega^2 = kg\tanh(kh) \qquad (2.13)$$

We can use the dispersion relation to find the speed of a wave crest.

$$c = \frac{\omega}{k} = \sqrt{\frac{g}{k}\tanh(kh)} \qquad (2.14)$$

where c is called the phase velocity. The phase

velocity is a nonlinear function of frequency and wavelength because

$$k = 2\pi/\lambda \tag{2.15}$$

where λ is the wavelength. In general, for the same water depth, longer waves will travel faster than shorter waves. This phenomenon is called dispersion, and it explains why equation 2.13 is called the dispersion relation.

The derivation of Airy wave theory requires us to assume:

1) the wave's amplitude is much smaller than the wavelength,

2) the fluid is irrotational,

3) the fluid is ideal, and

4) the fluid is incompressible.

These assumptions limit the type of wave motion we can model well. Basically, Airy wave theory is not a good model of steep waves or waves traveling in shallow water. In general, Airy wave theory is a good model of long ocean waves in a region slightly below the free surface and slightly above the bottom. Le Mehaute has suggested a range for which Airy wave theory would be suitable (Figure 5).

The results of Airy wave theory for finite and infinite water depths respectively are summarized in Tables G.1 and G.2. Airy wave theory is the basis for the theory of irregular waves which will be developed in this paper.

2.2 THEORY OF IRREGULAR WAVES

Presently, a finite number of regular waves are superposed to model irregular seas. Each regular wave has a distinct frequency and random phase. For example, the free surface elevation in two dimensions is given by

$$\eta = Re \sum_{n=1}^{N} A_n e^{i(k_n x - \omega_n t)} \tag{2.16}$$

where N is the number of regular wave components, A_n is a complex wave amplitude with random phase, k_n is a wave number, x is the distance propagated, ω_n is a wave frequency, and t is time. Other wave properties can also be represented in this manner. This technique is called sum of sinusoids. It is based on the principle of superposition. It is inefficient because it requires many multiplications and additions. Another, less obvious, and undesireable characteristic is the discrete representation of the seastate. Consequently, the distribution of wave energy is not continuous. Furthermore, this method does not allow for wave breaking. When a wave becomes too steep, it will break. Sum of sinusoids can

create waves that are so steep they are physically impossible. This paper will demonstrate an alternative method to sum of sinusoids whcih is more efficient and gives a continuous distribution of energy. However, it also does not allow for wave breaking. Furthermore, since it is based on Airy wave theory, it is subject to the same limitations as that theory.

2.3 SUMMARY OF CHAPTER TWO

Subject to certain limitations, Airy wave theory can be a very useful model of ocean waves. In general, Airy wave theory is not a good model of very steep waves or waves in very shallow water. Airy wave theory is a good model of long waves in deep water. Since Airy wave theory is linear, many regular waves can be superposed to model irregular seas. As the number of regular waves approaches infinity, the distribution of wave energy becomes continuous, and the Fourier series becomes a Fourier transform. In the next chapter it will be shown how Fourier transforms and convolution integrals can be used to model waves more efficiently than sum of sinusoids. .

CHAPTER 3

THE CONTINUOUS SPECTRUM OF OCEAN WAVES

3.1 FOURIER TRANSFORMS AND INVERSE FOURIER TRANSFORMS

To begin this problem, the Fourier transform and its inverse will be defined. This will not be a rigorous analysis, but it will be a good introduction to the applications of the Fourier transform. For example, suppose we know a function in the time domain. The fourier transform of this function can be used to find its expression in the frequency domain as follows:

$$F(\omega) = \int_{-\infty}^{\infty} f(t)\, e^{i\omega t}\, dt \tag{3.1}$$

where $f(t)$ is in the time domain and $F(\omega)$ is in the frequency domain. $f(t)$ might represent the free-surface elevation, the water-particle velocity or acceleration, or the water pressure. The inverse Fourier transform is defined as

$$f(t) = \frac{1}{2\pi} \int_{-\infty}^{\infty} F(\omega)\, e^{-i\omega t}\, dt \tag{3.2}$$

Therefore, equation (3.1) can now be expressed as

$$f(t) = \frac{1}{2\pi} \int_{-\infty}^{\infty} \int_{-\infty}^{\infty} f(\tau) e^{i\omega\tau} d\tau e^{-i\omega t} d\omega \tag{3.3}$$

In certain cases the order of integration can be changed.

$$f(t) = \int_{-\infty}^{\infty} d\tau f(\tau) \frac{1}{2\pi} \int_{-\infty}^{\infty} d\omega e^{-i\omega(t-\tau)} \tag{3.4}$$

Since the second integral is a delta function,

$$f(t) = \int_{-\infty}^{\infty} d\tau f(\tau) \delta(t-\tau) = f(t) \tag{3.5}$$

Therefore, it has been shown that the inverse fourier transform of the transform of $f(t)$ is $f(t)$. This is very convenient because the wave properties we know in the frequency domain, as a result Airy wave theory, can also be expressed in the time domain. However, there are limitations to this theory. In general, the Fourier transform of a function will exist if the absolute value of the function integrated over the range from $-\infty$ to ∞ exists. This rather modest beginning leads to a very important result - the convolution theorem.

3.2 THE CONVOLUTION THEOREM IN THE TIME DOMAIN

Having defined the fourier transform and its inverse, the convolution theorem can now be derived. For example, suppose we know a transfer function in the frequency domain which will convert the horizontal component of water-particle velocity into the vertical component of water-particle velocity. This relationship can be expressed as

$$W(\omega) = H(\omega)\,U(\omega) \qquad \text{frequency Space} \qquad (3.6)$$

where $W(\omega)$ is the vertical component, $U(\omega)$ is the horizontal component, and $H(\omega)$ is the transfer function. All of these functions are in the frequency domain, and in general, they are complex.

But $H(\omega)$ and $U(\omega)$ can be expressed in terms of their Fourier transforms. Therefore, equation 3.6 becomes

$$W(\omega) = \int_{-\infty}^{\infty} h(\tau)\,d\tau \int_{-\infty}^{\infty} u(\sigma)\, e^{i\omega\sigma}\, d\sigma \qquad (3.7)$$

where $h(t)$ and $u(t)$ are real functions in the time domain.

This equation can be rearranged.

$$W(\omega) = \int_{-\infty}^{\infty} h(\tau) \int_{-\infty}^{\infty} u(\sigma)\, e^{i\omega(\sigma+\tau)}\, d\sigma\, d\tau \qquad (3.8)$$

Now let $\sigma + \tau = t$. Then equation 3.8 becomes

$$W(\omega) = \int_{-\infty}^{\infty} h(\tau) \int_{-\infty}^{\infty} u(t-\tau) e^{i\omega t} dt\, d\tau \qquad (3.9)$$

Under certain conditions the order of integration can be changed. Then equation 3.9 becomes

$$W(\omega) = \int_{-\infty}^{\infty} \int_{-\infty}^{\infty} h(\tau) u(t-\tau) d\tau\, e^{i\omega t} dt \qquad (3.10)$$

But this is by definition the Fourier transform of $w(t)$. Therefore,

$$w(t) = \int_{-\infty}^{\infty} h(\tau) u(t-\tau) d\tau \equiv C\mathcal{O}\left(h(t), u(t)\right) \qquad (3.11)$$

The final integral is called the convolution of $h(t)$ with $u(t)$. The convolution integral enables us to generate a time series of the vertical component of water-particle velocity directly from the time series of the horizontal component of water-particle velocity.

3.3 THE FOURIER TRANSFORM AND CONVOLUTION INTEGRAL

The Fourier transform and the convolution integral will be used in this paper to develop efficient algorithms for modeling ocean waves. For instance, the vertical attenuation and horizontal propagation of ocean waves can be modeled by Fourier transforms.

A time series represents a history of events at a single point in space. A time series can be transformed so that it represents another time series at the same point in space or at a different point in space. Some operations which do not "move" a time series of ocean waves in space include differentiation, integration, and Hilbert transforms. (A Hilbert transform is a phase shift of ninety-degrees in the frequency domain.) The operations which do "move" a time series through space include vertical attenuation and horizontal propagation.

A time series of the free-surface elevation will be convolved with transfer functions to generate time series of the dynamic water pressure, and the horizontal and vertical components of water-particle velocity and acceleration. Transfer functions will also be developed to model the vertical attenuation and horizontal propagation of ocean waves. The six time series that are required for a wave-force analysis will be known everywhere in space and they will be generated from one time series.

3.4 THE TIME AND WAVE-FREQUENCY DOMAIN

As the number of discrete waves N goes to infinity while the difference between neighboring wave frequencies and wave numbers goes to zero, the summation in equation 2.16 approaches its integral representation,

$$\eta = Re \frac{1}{2\pi} \int_{-\infty}^{\infty} A(\omega) e^{i(kx - \omega t)} d\omega \qquad (3.12)$$

where $A(\omega)$ is a complex amplitude which varies continuously with wave frequency and has a random phase. Equation 2.16 is a Fourier transform in the time and wave-frequency domain. As long as $A(\omega)$ has certain properties, we are now free to use the very powerful tools of Fourier transform analysis. Specifically, we will be most interested in the convolution of equation 3.12 with the inverse fourier transforms of transfer functions which we will develop in the frequency domain. Those transfer functions will be based on Airy wave theory.

3.5 THE SPACE AND WAVE-NUMBER DOMAIN

Equation 3.12 can alternatively be expressed as

$$\eta = Re \frac{1}{2\pi} \int_{-\infty}^{\infty} A(k) e^{i(kx - \omega t)} dk \qquad (3.13)$$

where $A(k)$ is a complex amplitude which varies continuously with wave number and has a random phase. Therefore, we can also express equation (2.16) as a Fourier transform in the space and wave-number domain. Both equations (3.12) and (3.13) have certain advantages and disadvantages.

The disadvantage of equation (3.13) is that its inverse Fourier transform requires an integration along the X-axis. Physically, this is a very difficult thing to do because it

would require many samples of the ocean wave along a straight line. However, this method is used to solve the Cauchy-Poisson problem. The advantage of equation (3.12) is that it represents the free-surface elevation at a single point in space. In the real world, wave-rider buoys have been doing this measurement for a long time. But this method does require long time records to model the horizontal propagation of irregular waves over long distances. However, time-domain analysis of offshore structures will not require us to simulate the propagation of irregular waves over long distances.

3.6 SUMMARY OF CHAPTER THREE

Given a time series of the free-surface elevation at one point in space, time series of water particle velocities and accelerations, and pressure can be generated at other points in space. The given time series can be either measured or simulated data. The generated time series can represent wave kinematics at points in a grid. During a time-domain simulation, the wave kinematics required by Morison's equation can be interpolated from the grid. The convolution integrals necessary to perform this analysis are usually more efficient than sum of sinusoids.

CHAPTER 4

TRANSFER FUNCTIONS FOR ANALYSIS OF OCEAN WAVES

4.1 EFFICIENT MODELING OF OCEAN WAVES

For very complicated offshore structures, calculating the wave kinematics at grid points is more efficient than calculating wave kinematics for every finite element. This would be especially true for offshore platforms. (However, for risers, it is probably more efficient to calculate the wave kinematics for every finite element instead of a mesh of points.) In particular, the methods of digital-signal processing are well-suited for a grid.

The coordinate system we will adopt for the grid is given in figure 6. The X-axis is positive to the right, and the Z-axis is positive upwards. The number of grid points along the horizontal is ℓ, and the number along the vertical is d. The free-surface elevation at the upper-left corner of the grid is given. It is required to know the wave kinematics at every grid point at each time step.

To move from one grid point to another grid point parallel to the mean waterline will be called horizontal propagation. To move downward will be called vertical attenuation.

There are numerous ways to calculate time series of the wave kinematics at all grid points when the the free-surface elevation at one grid point is the only known time series. However, there are very few good methods. For instance, using one convolution integral to generate the time series of the horizontal-water particle acceleration at the bottom-right corner from the time series of the free-surface elevation at the origin is not very efficient. It is not very efficient because evaluating the convolution integral would require many multiplications and additions.

A far more efficient method is to do the convolution integral in steps. For instance, use an impulse response function that models horizontal propagation to move the free-surface elevation at the left side of the grid to the right side. This is a very good first step because the impulse response function that models horizontal propagation requires many sample points. It is best to do the the convolution integrals that require the most effort first. Even though the ultimate goal is to find the horizontal water-particle acceleration at the bottom-right corner, there are many time series that can be calculated at

intermediate steps. This is what makes this particular method so efficient. Now that the free-surface elevation is known at the right side of the grid, the horizontal water-particle velocity at the mean waterline can be found. The impulse response function that performs this operation requires fewer sample points than the impulse response function for horizontal propagation. Then use an impulse response function that models vertical attenuation to move the horizontal water-particle velocity at the mean waterline down to the bottom of the grid. This impulse response function requires very few sample points. To find the water-particle acceleration, differentiate the water-particle velocity with respect to time. This operation requires only two sample points. Therefore, in addition to calculating the horizontal water-particle at the bottom corner, three other time series were calculated at intermediate steps. Those three other time series were also required, and they can also be used to generate other time series within the same column of grid points. This is what makes this method much more efficient than using one impulse response function to do horizontal propagation, vertical attenuation, etc. Figures 7 and 8 give the algorithms used for generating time series in this paper.

4.2 THE TRANSFER FUNCTIONS IN DEEP WATER

The dispersion relation in deep water is

$$\omega^2 = kg \tag{4.1}$$

where ω is the wave frequency, k is the wave number, and g is the acceleration of gravity.

The transfer function for modeling horizontal propagation is

$$H(\omega) = e^{ik\Delta x} \tag{4.2}$$

where Δx is the distance propagated to the right. This transfer function is used to move the free-surface elevation at the origin horizontally.

The transfer function for modeling vertical attenuation is

$$H(\omega) = e^{|k|\Delta z} \tag{4.3}$$

where Δz is the negative distance below the mean waterline. This transfer function is used to find water-particle velocities and pressure below the mean waterline.

The transfer function for differentiation is

$$H(\omega) = i\omega \tag{4.4}$$

This transfer function is used to find the vertical

water-particle velocity on the mean waterline from the free-surface elevation. It is also used to convert water-particle velocities into accelerations.

The transfer function for converting the free-surface elevation into the horizontal water-particle velocity on the mean waterline is

$$H(\omega) = |\omega| \qquad \eta \longrightarrow \bar{u} \tag{4.5}$$

This transfer function is similiar to a differentiator, but it does not induce a phase shift.

4.3 THE TRANSFER FUNCTIONS IN WATER OF FINITE DEPTH

The transfer functions in water of finite depth are similiar to those in water of infinite depth. However, one major difference is the dispersion relation. The dispersion relation in water of finite depth is

$$\omega^2 = kg\tanh(kh) \tag{4.6}$$

where ω is the wave frequency, k is the wave number, g is the acceleration of gravity, and h is the water depth.

The transfer function for modeling horizontal propagation is

$$H(\omega) = e^{ik\Delta x} \qquad \text{Horizontal Propagation} \tag{4.7}$$

where ΔX is the distance propagated to the right. It is a positive number. This transfer function is used move the free-surface elevation at the origin horizontally.

The transfer function for modeling vertical attenuation of the horizontal water-particle velocity and the dynamic pressure is

$$H(\omega) = \frac{\cosh(k(\Delta z + h))}{\cosh(kh)} \qquad (4.8)$$

where Δz is the negative distance below the mean waterline.

The transfer function for modeling vertical attenuation of the vertical water-particle velocity is

$$H(\omega) = \frac{\sinh(k(\Delta z + h))}{\sinh(kh)} \qquad (4.9)$$

The transfer function for differentiation is

$$H(\omega) = i\omega \qquad (4.10)$$

This transfer function is used to find the vertical water-particle velocity on the mean waterline from the free-surface elevation. It is also used to convert water-particle velocities into accelerations.

The transfer function for converting the free-surface elevation into the horizontal water-particle velocity on the mean waterline is

$$H(\omega) = \frac{|\omega|}{\tanh(|k|h)} \qquad \eta \rightarrow \nabla \phi(x,\omega,t) \qquad (4.11)$$

4.4 SUMMARY OF CHAPTER FOUR

An efficient algorithm for calculating wave kinematics in a grid has been discussed. The transfer functions in water of infinite and finite depth have been presented. The resulting impulse response functions will now be discussed in detail.

CHAPTER 5

DIFFERENTIATING TIME SERIES OF OCEAN WAVES

A time series of the free-surface elevation can be differentiated with respect to time to generate a time series of the vertical water particle velocity. This is true for both infinite and finite water depths. Physically, there is no justification for performing this operation. However, according to Airy wave theory differentiating the free-surface elevation with respect to time gives the vertical water-particle velocity. Similiarly, time series of the water particle accelerations can be generated from time series of the water particle velocities by differentiation with respect to time.

5.1 THEORY OF DIFFERENTIATION OF SINUSOIDAL WAVES

The equation for a sinusoidal wave in complex notation is

$$f(t) = e^{i\omega t} \qquad \text{Wave} \tag{5.1}$$

where ω is the frequency and t represents time.

Differentiating this function with respect to time gives

$$f'(t) = i\omega e^{i\omega t} \tag{5.2}$$

where $f'(t)$ is the first derivative of $f(t)$.

In this manner, time series of the vertical water-particle velocity on the mean waterline can be generated from time series of the free-surface elevation. Similiarly, the horizontal and vertical water-particle accelerations can be generated from the horizontal and vertical water-particle velocities respectively.

5.2 NUMERICAL DIFFERENTIATION OF SINUSOIDAL WAVES

The approximate derivative of $f(t)$ as given by the central difference method is

$$f'(t) \sim \frac{f(t+\Delta t) - f(t-\Delta t)}{2\Delta t} \tag{5.3}$$

where Δt is the time step and n is an index.

As discussed in appendix A, there are two types of errors associated with this approximation. The first type of error is due to truncation. The truncation error is reduced by taking smaller time steps or by using a higher order differentiator. The second type of error is due to

roundoff or noise. This type of error is best eliminated by a filter. Furthermore, this method becomes less accurate as the number of sample ponts per wave is reduced.

5.3 SUMMARY OF CHAPTER FIVE

Numerical differentiation is a very efficient method for generating time series. However, it must be used carefully because it does amplify noise.

CHAPTER 6

THE HORIZONTAL WATER-PARTICLE VELOCITY

A time series of the free-surface elevation can be differentated with respect to time to generate a time series of the vertical water-particle velocity on the mean waterline. This is true in water of either infinite or finite depth. A time series of the horizontal water-particle velocity can be generated in a similiar manner.

6.1 HORIZONTAL WATER-PARTICLE VELOCITY - DEEP WATER

The dispersion relation in deep water is

$$\omega^2 = kg \tag{6.1}$$

where ω is the wave frequency, k is the wave number, and g is the acceleration of gravity.

The transfer function for converting the free-surface elevation into the horizontal water-particle velocity on the mean waterline is

$$H(\omega) = |\omega| \qquad (6.2)$$

This transfer function does not have a Fourier transform, but it does have a fourier series. The coefficients of the impulse response function have been derived in appendix B, equation B.6.

$$h(n\Delta t) = \begin{cases} \frac{\pi}{2\Delta t^2} & n = 0 \\ 0. & n \text{ even} \\ \frac{-2}{\pi (n\Delta t)^2} & n \text{ odd} \end{cases} \qquad (6.3)$$

where Δt is the time step.

A plot of this function is given in figure 9. It is a symmetric function which rapidly approaches zero as the time becomes large. In fact, the coefficients of the impulse response function are inversely proportional to the square of time.

When the convolution integral is evaluated numerically, the range of integration should not extend beyond the time when the amplitude of the impulse response function becomes less than a certain tolerance. The time at which this function is less than a certain tolerance is

$$T \geq \frac{2\Delta t}{\pi} \frac{1}{\sqrt{\theta}} \tag{6.4}$$

where θ is a fraction of $h(n\Delta t)$ at $n=0$.

The corresponding number of sample points is

$$n \geq \frac{2}{\pi} \frac{1}{\sqrt{\theta}} \tag{6.5}$$

where $T = n\Delta t$.

6.2 HORIZONTAL WATER-PARTICLE VELOCITY - FINITE DEPTH

The dispersion relation in water of finite depth is

$$\omega^2 = kg \tanh(kh) \tag{6.6}$$

where ω is the wave frequency, k is the wave number, g is the acceleration of gravity, and h is the water depth.

The transfer function for converting the free-surface elevation into the horizontal water-particle velocity on the mean waterline is $\eta \longrightarrow u(m.w.l)$

$$H(\omega) = \frac{|\omega|}{\tanh(|k|h)} \tag{6.7}$$

This function does not have a Fourier transform, but it does have a Fourier series. But even the Fourier series solution cannot be expressed in terms of elementary

functions. However, the fast Fourier transform can be used to evaluate the Fourier coefficients. Figure 10 compares the impulse response functions for infinite and finite water depths. Even though the water depth is very shallow, the two functions are very similiar. Therefore, the behaviour of the function for infinite water depth case can be used to size the function for the finite water depth case.

6.3 SUMMARY OF CHAPTER SIX

The impulse response function for transforming a time series of the free-surface elevation into a time series of the horizontal water-particle velocity on the mean waterline in deep water has been derived. The impulse response function for water of finite depth must be evaluated numerically. However, the theoretical solution for deep water can be used to size the numerical solution for water of finite depth.

CHAPTER 7

THE VERTICAL-ATTENUATION PROBLEM

A point far below the free surface does not feel a wave's disturbance as much as a point near the free surface. This phenomenon is called vertical attenuation. According to Airy wave theory, the vertical attenuation of waves varies exponentially as a function of the distance from the free surface.

7.1 VERTICAL ATTENUATION IN DEEP WATER

The dispersion relation in deep water is

$$\omega^2 = kg \tag{7.1}$$

where ω is the wave frequency, k is the wave number, and g is the acceleration of gravity.

The transfer function for vertical attenuation in deep water is

$$H(\omega) = e^{k/\Delta z} \tag{7.2}$$

where Δz is the negative distance below the mean waterline.

The inverse Fourier transform of this transfer function has been derived in appendix C, equation C.15.

$$h(t) = \frac{1}{2}\sqrt{\frac{-g}{\pi \Delta z}}\ \exp\left(\frac{g t^2}{4 \Delta z}\right) \tag{7.3}$$

A plot of this function is given in figure 11. It is a symmetric function which rapidly approaches zero as the time becomes large. In fact, the function converges exponentially.

When the convolution integral is evaluated numerically, the range of integration should not extend beyond the time when the amplitude of the function in equation 7.3 becomes less than a certain tolerance. The time at which this function is less than a certain tolerance is

$$|T| \geq 2\sqrt{\frac{\Delta z \ln \theta}{g}} \tag{7.4}$$

where θ is a fraction of the value of $h(t)$ at $t = 0$.

The corresponding number of sample points is

$$|n| \geq \frac{2}{\Delta t}\sqrt{\frac{\Delta z \ln \theta}{g}} \tag{7.5}$$

where $T = n \Delta t$.

7.2 VERTICAL ATTENUATION IN WATER OF FINITE DEPTH

The dispersion relation in water of finite depth is

$$\omega^2 = kg\tanh(kh) \tag{7.6}$$

where ω is the wave frequency, k is the wave number, g is the acceleration of gravity, and h is the water depth.

The transfer functions for vertical attenuation in water of finite depth are

$$H_1(\omega) = \frac{\cosh(k(z+h))}{\cosh(kh)} \qquad \text{Pressure}$$

$$H_2(\omega) = \frac{\sinh(k(z+h))}{\sinh(kh)} \qquad \text{h. Velocity } u \text{ + acceleration } a \tag{7.7}$$

where the first transfer function models the vertical attenuation of the "dynamic pressure" and the horizontal water-paticle velocity and acceleration. The second transfer function models the vertical attenuation of the vertical water-particle velocity and acceleration. These transfer functions cannot be expressed in terms of elementary functions. However, the fast Fourier transform can be used to evaluate their inverse Fourier transforms. Figure 12 compares the impulse response functions for infinite and finite water depths. Even though the water depth is very shallow in these examples, the two functions are very similiar. Therefore, the behaviour of the function

for attenuation in deep water case can be used to size the impulse response functions for the finite water depth case.

7.3 SUMMARY OF CHAPTER SEVEN

The inverse Fourier transform for vertical attenuation in deep water has been derived. The impulse response functions for water of finite depth must be evaluated numerically. However, the theoretical solution for deep water can be used to size the numerical solutions for water of finite depth.

CHAPTER 8

THE HORIZONTAL-PROPAGATION PROBLEM

A single wave moves horizontally at a rate equal to its phase velocity. A wave's phase velocity is a function of the wave's frequency and the water depth. This phenomenon is called dispersion. The front of a wave group moves at a rate equal to its group velocity. For waves traveling over short distances, the phase velocity is a good measure of a wave's speed. (The model proposed in this paper does not simulate group effects.) Given a time history of the free-surface elevation at a point in space, the free-surface elevation at neighboring points can be found by convolving the original time series with the impulse response function of the appropiate transfer function.

8.1 HORIZONTAL PROPAGATION IN DEEP WATER

The dispersion relation in deep water is

$$\omega^2 = kg \tag{8.1}$$

where ω is the wave frequency, k is the wave number, and g is the acceleration of gravity.

The transfer function for horizontal propagation in deep water is (phase speeds) NO GROUPS ! !

$$H(\omega) = e^{ikx} \tag{8.2}$$

where x is the positive distance propagated.

The inverse Fourier transform of this transfer function has been derived in appendix D, equation D.10.

$$h(t) = \sqrt{\frac{g}{2\pi x}}\left[\left(\frac{1}{2} + C\left(\sqrt{\frac{g}{2\pi x}}\,t\right)\right)\cos\left(\frac{gt^2}{4x}\right) + \left(\frac{1}{2} + S\left(\sqrt{\frac{g}{2\pi x}}\,t\right)\right)\sin\left(\frac{gt^2}{4x}\right)\right] \tag{8.3}$$

where $C(y)$ and $S(y)$ are the cosine and sine Fresnel integrals.

F.-14

Figure 8.13 shows that for this function the period of oscillation becomes smaller while the amplitude of oscillation remains constant as the time goes to positive infinity. As time goes to negative infinity, the function approaches zero very rapidly. The method of asymptotics will now be used to explain these phenomena.

The cosine and sine Fresnel integrals approach 0.5 as their arguments go to infinity. Therefore,

$$h(t) \rightarrow \sqrt{\frac{g}{\pi \Delta x}} \cos\left(\frac{g t^2}{4 \Delta x} - \frac{\pi}{4}\right) \text{ as } \sqrt{\frac{g}{2\pi \Delta x}}\, t \rightarrow +\infty \qquad (8.4)$$

The amplitude of oscillation is constant and the period of oscillation becomes smaller because of the the argument of the cosine function is an nonlinear function of time. This is in agreement with figure 13.

In fact, if one is given the apparent period of oscillation, the time at which it occurs is given by

$$\frac{g(T_t + T_A)}{4\Delta x} - \frac{g T_t^2}{4 \Delta x} = 2\pi \qquad (8.5)$$

where T_A is the apparent period.

Now solve for the time in terms of the apparent period.

$$T_t \equiv \frac{4\pi \Delta x}{g T_A} - \frac{T_A}{2} \qquad (8.6)$$

In particular, if the apparent period is chosen as $2\Delta t$ which is the period of ocillation of a wave sampled at the nyquist rate, equation 8.5 becomes

$$T_t = \frac{2\pi \Delta x}{g \Delta t} - \Delta t \qquad (8.7)$$

Therefore, the time at which the apparent period equals $2\Delta t$ is directly proportional to the distance propagated and inversely proportional to the time step. As

the distance of propagation increases, the amount of effort required to evaluate the convolution integral increases linearly. For very large distances, the effort required to evaluate the convolution integral could become enormous. But this particular model is not meant for simulating the propagation of waves over large distances. For very large distances wave group effects would become important.

When the convolution integral for horizontal propagation is evaluated numerically, the range of integration for positive time should not extend beyond the time when the apparent period equals two times the time step. Therefore, the number of sample points of the impulse response function for positive time is

$$n_+ \geq \frac{2\pi\Delta x}{g\Delta t^2} - 1 \tag{8.8}$$

where $T_+ = n_+ \Delta t$.

Since the first term is much greater than one,

$$n_+ \approx \frac{2\pi\Delta x}{g\Delta t^2} \tag{8.9}$$

For negative arguments, the cosine and sine Fresnel integrals behave like

$$\begin{aligned} C(z) &= -\frac{1}{2} - f(z)\sin\left(\frac{\pi}{2}z^2\right) + g(z)\cos\left(\frac{\pi}{2}z^2\right) \\ S(z) &= -\frac{1}{2} + f(z)\cos\left(\frac{\pi}{2}z^2\right) + g(z)\sin\left(\frac{\pi}{2}z^2\right) \end{aligned} \tag{8.10}$$

where the functions $f(z)$ and $g(z)$ are defined in chapter seven of Abramowitz and Stegun.

As time goes to negative infinity the cosine and sine Fresnel integrals approach -0.5. The leading order behaviour of equation 8.3 is

$$h(t) \rightarrow -\frac{2\Delta x}{\pi g t^3} \quad as \quad \sqrt{\frac{g}{2\pi\Delta x}}\, t \longrightarrow -\infty \tag{8.11}$$

Therefore, the amplitude of the function is directly proportional to the distance propagated and inversely proportional to the time cubed.

When the convolution integral is evaluated numerically, the range of integration for negative time should not extend beyond the time when the amplitude of the impulse response function becomes less than a certain tolerance. The time at which this function is less than a certain tolerance is

$$T_- \leq -\left(\frac{32}{\theta^2\pi}\right)^{1/6}\left(\frac{\Delta x}{g}\right)^{1/2} \tag{8.12}$$

where θ is a fraction of the value of $h(t)$ at $t=0$.

The corresponding number of sample points is

$$n_- \geq \left(\frac{32}{\theta^2\pi}\right)^{1/6}\left(\frac{\Delta x}{g}\right)^{1/2}\frac{1}{\Delta t} \tag{8.13}$$

where $T_- = -n_- \Delta t$.

Equations 8.9 and 8.12 are very useful for evaluating the convolution integral when the inverse Fourier transform is given by equation 8.3. However, equation 8.3 is only applicable when the cut-off frequency is infinite. But the impulse response function for finite depth will be evaluated numerically. Its cut-off frequency will be finite. For deep water, the inverse Fourier transform of equation 8.2 for a finite cut-off frequency is (equation D.11)

$$h(t)=\sqrt{\frac{g}{2\pi\Delta x}}\left[\left(C\left(\sqrt{\frac{2\Delta x}{\pi g}}\,\omega_c-\sqrt{\frac{g}{2\pi\Delta x}}\,t\right)+C\left(\sqrt{\frac{g}{2\pi\Delta x}}\,t\right)\right)\cos\left(\frac{gt^2}{4\Delta x}\right)\right. \tag{8.14}$$
$$\left.+\left(S\left(\sqrt{\frac{2\Delta x}{\pi g}}\,\omega_c-\sqrt{\frac{g}{2\pi\Delta x}}\,t\right)+S\left(\sqrt{\frac{g}{2\pi\Delta x}}\,t\right)\right)\sin\left(\frac{gt^2}{4\Delta x}\right)\right]$$

where ω_c is the cut-off frequency.

Figure 14 shows that the behaviour of this function is quite different from the function plotted in figure 13. As the time goes to positive infinity the function approaches zero. If the time at which the function goes to zero is less than the time at which the apparent period equals $2\Delta t$, the convolution integral will give incorrect results. The function goes to zero when the argument of the cosine and sine Fresnel integrals changes sign.

$$T_0 = \frac{2\Delta x\,\omega_c}{g} \tag{8.15}$$

where T_0 represents the time at which the function approaches zero.

When the Fast Fourier trnasform is used to evaluate the impulse response function,

$$\omega_c = \frac{\pi}{\Delta t} \tag{8.16}$$

Therefore,

$$T_o = \frac{2\pi\Delta X}{g\Delta t} \tag{8.17}$$

Consequently, T_o and T_f are equal, and the error caused by the finite cut-off frequency affects the convolution integral very little.

8.2 HORIZONTAL PROPAGATION IN WATER OF FINITE DEPTH

The dispersion relation in water of finite depth is

$$\omega^2 = Kg\tanh(Kh) \tag{8.18}$$

where ω is the wave frequency, K is the wave number, g is the acceleration of gravity, and h is the water depth.

The transfer function for horizontal propagation in water of finite depth is

$$H(\omega) = e^{iK\Delta X} \tag{8.19}$$

where ΔX is the positive distance propagated.

This inverse Fourier transform does not have a solution in closed form. However, the fast Fourier transform can be used to evaluate it. Figure F-16 15 compares the impulse response functions for infinite and finite water depths. Even though the water depth is very shallow, the two functions are very similiar. At shallower water depths, Airy wave theory would not be valid. Therefore, the asymptotic analysis performed for the deep water case can be used to size the impulse response function for the finite water depth case.

8.3 SUMMARY OF CHAPTER EIGHT

An aysmptotic analysis has been made of the inverse Fourier transforms of the transfer functions for performing horizontal propagation. The function for deep water has a closed form solution. The impulse response function for water of finite depth must be evaluated numerically. However, the theoretical solution for deep water can be used to size the numerical solution for water of finite depth.

CHAPTER 9

GUIDELINES

The guidelines for efficient and accurate convolution computations are discussed here. These guidelines are used to choose parameters that are necessary inputs for setting up the computation.

9.1 Constraints

Four types of constraints were developed in the formulation of the technique:

i. Differentiation: Minimum of 8 samples per period

ii. Horizontal particle velocity: Size of impulse response function,

$$n_v = \frac{2}{\pi}\sqrt{\frac{1}{\theta}}$$

iii. Vertical Attenuation: Size of impulse response function,

$$n_a = \frac{2}{Dt}\sqrt{\frac{Dz\ \ln\theta}{g}}$$

iv. Horizontal propagation, size of impulse response function:

For positive real time,

$$n_+ = \frac{2\pi\ Dx}{S(dt)^2}$$

For negative real time,

$$n_- = \left(\frac{32}{\theta^2\pi}\right)^{1/6}\left(\frac{Dx}{g}\right)^{1/2}\frac{1}{Dt}$$

where Dt = time increment

Dz = vertical distance of propagation

Dx = horizontal distance of propagation

g = acceleration due to gravity

θ = tolerance

In the analysis θ, the level of tolerance is set at 0.001; θ is the fraction of the value of the impulse response function at t=0.

The first two constraints do not need any further comment. The vertical attenuation problem does not give rise to difficulty in the numerical computation because the transfer function is essentially an exponential decay. The horizontal propagation problem can be difficult to compute and usually dictates the size of computations.

9.2 Phase Error During Propagation

As the waves are propagated by the convolution process, errors in phase increase with the distance travelled. For a given propagation distance Dx, the shortest wave length waves in the time series travel the greatest number of wave lengths and therefore have the largest likelihood of building up a phase error. In the programs the user must choose the largest phase error which can be tolerated for the shortest wave length waves. We usually use $\pi/4$ radians. Let:

F_c = cut off frequency

F_s = sampling frequency

N = number of sample points

The magnitude and the phase of the transfer function for horizontal propagation are shown here.

Let $R = F_s/2\,F_c$, R must be greater than 1, we recommend 4

Let $\alpha = Dx/L_c$

where L_c is the length of the wave with frequency F_c. The maximum

phase error is

$$\Delta Q_{max} = \Delta K \cdot Dx$$

$$= \frac{2K\ \Delta f}{C_g}\ Dx$$

$$= \frac{2\pi R}{N}\ F_c\ (\frac{Dx}{L_c})(\frac{L_c}{C_g})\ ,$$

$$= \frac{4\pi R\alpha}{N}$$

Here ΔK = error in the wave number k

C_g = group velocity

N = number of sample points

when ΔQ_{max} = $\pi/4$, (The maximum phase error is set by the user.)

then N = $16\ \alpha\ R$

9.3 Choice of Parameters

Typically, the analyst is faced with any one of the following problems:

i. Given a distance (Dx) and the cut off frequency of the wave, Fc, the objective is to select Dt and N. It is recommended that

$$Dt = Tc/8$$

so that $R = 4$

where $1/T_c$ is the cut off frequency, Fc

Then $N = 64\ \alpha$

The maximum phase error associated with this choice is $\pi/4$ radians.

ii. Given the cut off frequency and the size of impulse response function. The objective is to find out the number of wave lengths over which the time series can be propagated. Once again

$$Dt = Tc/8$$

$$\frac{Dx}{L_c} = \frac{N}{64}$$

The maximum phase error associated with this choice is $\frac{\pi}{4}$ radians.

iii. Given the distance and the number of points in the convolution, the objective is to establish the theoretical cut-off (shortest) wave simulated.

$$L_c = \frac{16\ R\ Dx}{N}$$

9.4 Interpolation

The convolution method is set up to compute the kinematics at a number of grid points. Between the grid points a quadratic interpolation scheme

is employed. The grid spacing ought to be $\frac{L_c}{8}$ or less, where L_c is the shortest wave length.

When the grid spacing is less than $L_c/8$, then the quadratic interpolator will accurately calculate the kinematics at any location between the grid points. When the grid spacing is greater than an eighth of a wave length, a quadratic polynomial does not provide a good approximation to a sinusoidal curve.

1. If the grid spacing s is not as per the recommendation, the intermediate points will show an error in phase.

2. The smaller grid spacing requires a large number of grid points and thus a larger memory is needed for the computations.

9.5 Summary of Chapter 9

1. The time step $Dt \leq \frac{T_c}{8}$ or $R = \frac{f_s}{2fc} \geq 4$

2. The grid size should be as small as possible to reduce memory/computation requirements.

3. The grid spacing should be less than $\frac{L_c}{8}$ for accurate interpolations.

4. For phase error $\Delta Q_{max} \leq \pi/4$

   Convolution size $N = 16 \alpha R$

5. Phase error

If a lower phase error is sought, a suitably high N has to be used.

CHAPTER 10

NUMERICAL STUDY

10.1 Introduction

This section presents the results of a study carried out to establish the accuracy and stability of the numerical solution. The simulation of ocean waves by convolution has several potential sources of numerical error. The computed impulse response functions for a finite cut off frequency are accurate only for a limited range. It has been shown that the distance (Dx), time step (Dt), and size of the convolution must be chosen so as to have an acceptable level of accuracy in the computed results. Furthermore, error gets compounded due to the fact that for a time stepping operation, computed values at a given instant are used as inputs for the next time step. This can lead to an unstable solution.

To check stability and accuracy in this section, the results of the convolution method are compared to the results of an alternative formulation, the sum of sinusoids, which does not utilize convolution.

In all of the simulations, the sizes of the convolutions have been chosen so as to satisfy the requirements laid down in the formulation of the impulse response functions. The acceptable level of error used here is $L_c/8$ (or $\pi/4$ in phase).

The numerical study is presented as three examples. The first is a single sinusoidal wave. The second and third are examples of random wave simulation.

10.2 Example 1: Regular Wave

A model scale wave of 0.5 second period and a wave amplitude of 0.1 feet is propagated 5, 10, and 15 wave lengths, which corresponds to 6.4, 12.8, and 19.5 feet. The wave length is 1.28 feet. The results are shown in Figures 16, 17, and 18. The convolution and exact solution are plotted together. The two time history plots are indistinguishable.

10.3 Example 2: Horizontal Propagation of Random Waves

A sum of N=32 sine waves is used to simulate a model scale random sea state. The lowest and highest frequency components are 0.5 Hz and 1.75 Hz, corresponding to wave lengths of 20 feet and 1.67 feet respectively. These waves are propagated exactly by sum of sines techniques and numerically by convolution distances of 2.5, 5.0, and 7.5 feet. This corresponds to 1.5, 3.0, and 4.5 wave lengths of the shortest wave.

The results are shown in Figures 19, 20, and 21. The results are well within the desired accuracy.

10.4 Example 3: Horizontal and Vertical Propagation of Random Waves

A sea state with a significant wave height of 20 feet and a mean period of ten seconds was approximated by a sum of sinusoids. These waves were propagated exactly and by convolution to a point 300 feet horizontally and 25 feet down the water column. At this point kinematics were computed. The water depth is 250 feet.

Figure 22 shows the water particle vertical displacement or amplitude at that point assuming linear theory. Figures 23 and 24 show the horizontal and vertical velocity components for both the exact and

numerical convolution results. Figures 25 and 26 present the accelerations in the horizontal and vertical directions. In each case the agreement is very good. It is concluded the kinematics convolution techniques are accurate when the guidelines are followed.

Figures 27 and 28 show the consequences of two common pitfalls. One is the effect of grid spacing on interpolation results and the other is undersampling.

For the generation of kinematics between grid points, a quadratic interpolation scheme was employed. This scheme can accommodate a curve with at most two points of inflection between grid points. It is recommended that the grid spacing be less than 1/8 of the shortest wave length to circumvent this kind of error. Figure 27 shows the simulated waves for a grid spacing of $L_c/8$, $L_c/4$, and $L_c/2$ compared to an exact sinusoidal wave. The phase error caused by the interpolation can clearly be seen here. The error increases for larger grid spacing. In the example the wave length is 1.28 feet and the propagated distance is 0.48 feet or 3/8 of a wave length. The grid spacing of the $L_c/8$ gives excellent results because no interpolation is required, but the coarser grid spacings result in substantial errors.

In Figure 28, the error is caused by undersampling. A regular wave of period 0.5 seconds is sampled at 0.15 seconds (clearly violating the suggested criterion), $Dt = T_c/8$. Figure 28 shows the results of the convolution method along with the theoretical sine wave sampled at the same interval. Since the nature of the wave form is not correctly defined due to undersampling, the convolution gives incorrect results.

10.5 Summary of Chapter 10

Using numerically simulated waves the convolution method has been shown to be both stable and accurate when carried out in accordance with the guidelines presented. In the next chapter the propagation of waves using convolution techniques is compared to the propagation of experimentally measured waves in a towing tank.

CHAPTER 11

EXPERIMENTAL STUDY

The objective of the experimental study was to ascertain the accuracy of the estimations of horizontal propagation and vertical attenuation for real waves, which include measurement noise and wave non-linearities.

Wave data was collected at the M.I.T. towing tank. A typical test set up is shown in Figure 29. Measurements were made at probes 1 and 2 simultaneously, along with the pressure variation directly under probe 2. These histories were taped on an anolog tape recorder (Tandberg 100) and subsequently digitized. The time history of wave elevation at probe 1 is the input to the convolution computation, which then predicts propagated time history at probe 2. These predictions are then compared with the measured history at probe 2. The pressure gauge output is scaled to yield attenuated wave amplitude at that depth. Thus the results of vertical attenuation can be checked.

11.1 Sinusoidal waves

Initially a sine wave of 0.7 Hz frequency was generated. The wave height was 0.1 feet. The computed and measured values of the propagated wave at probe 2 (1.625, 0.0) feet and at the pressure transducer (1.625, -0.6146) feet are plotted in Figures 30 and 31. The agreement of the horizontally propagated results (Figure 30) is very good. There is some error in the vertically attenuated results. This is attributed to the error in the positioning of the pressure gauge and the tendency of the pressure transducer to drift and not due to the convolution.

11.2 Random waves

Pseudo-random waves were generated in the tank based on a Pierson Moskowitz Spectrum. The peak frequency was 1.0 Hz and the significant wave height was 1.25 inches. The water depth was approximately 4 feet. Figures 32 and 33 show typical spectra of the wave data taken at probe 1 and 2 respectively. (These were computed by a maximum entropy spectral estimator using 1024 data points). The spectra show that the highest wave frequency of interest is 3.0 Hz. There is some difference between the two spectra (especially at high frequency), hence a slight discrepancy in the convolution results may be expected at high frequencies (above 2.00 Hz).

Figures 34 and 35 present the propagated and measured random waves at a distance of (1.625, 0.0) feet and (1.625, -0.6146) feet. This corresponds to 3 wave lengths of the shortest wave assumed to be present. The results are in good agreement, except for pressure transducer errors and except for high frequency fluctuations, which can be explained by the discrepancy in the spectral contents as discussed above. High frequency capillary waves are generated by interaction with the tank walls and non-linear wave effects.

On the whole, the errors are well within the acceptable limits, and it is concluded that real random waves can be propagated using this technique.

11.3 Summary of Chapter 11

The convolution method gives accurate results for real wave propagation problems.

CHAPTER 12

COMPUTATIONAL EFFICIENCY

Most users consider the time domain analysis as computationally inefficient and CPU-time consuming. An attempt has been made to gauge the time/memory required for the time series analysis of waves by the convolution procedure. In all the cases presented here, comparison has been made with the other time domain alternative, the sum of sinusoids.

In these results both approaches have been used to compute the kinematics at a number of grid points. These grid points are identical for both the methods, and the computation for intermediate points is carried out using an interpolation scheme identical in both the methods. Hence the results presented here are for equivalent operations.

The exact requirements are system dependent. The results presented here are valid for data processed on a VAX 11/750 machine and were gathered with a system routine called "getcpu".

12.1 Results

Figure 38 shows the CPU time required for the computation of wave kinematics (1 displacement, 2 velocities, and 2 accelerations) against the number of frequency components used to model the spectrum. The grid size is 6x6 and the duration of the time series was 100 time steps. It is seen that the sum of sinusoids approach needs a linearly increasing time while the convolution method is independent of the number of frequency components. The two methods break even at n=16 (which is used as a reference for further studies). The convolution method is 7 times faster

than a 150 component sum of sines.

Figure 39 shows the CPU time needed for processing a time series of increasingly longer duration. For this example, the number of components was 16 and the grid size was 6x6. It is seen that for short duration the convolution approach takes more time than the sum of sines approach, but if longer histories (involving more than a hundred time steps) are to be processed, the convolution method is more efficient.

Figure 38 shows the CPU time (in seconds) needed for different grid sizes. For this example, the number of frequency components was 16, the break even point. The number of time steps was 100. Generally for a low number of grid points the sinusoidal method is more efficient. But for larger grid sizes the convolution method is more efficient. However, it is also clear that the larger grid size requires larger memory on the system (regardless of the method). Typically on a VAX 11/750, a (3x3) grid needed 1250 blocks, a (6x6) grid needed 4813 blocks, and a (10x10) grid needed 13,063 blocks.

12.2 Summary of Chapter 12

The convolution approach offers substantial advantage when simulating a large number of sinusoidal components or very long record lengths. The grid size alone does not strongly favor either method.

CHAPTER 13

STRETCHED LINEAR CORRECTION

13.1 Introduction

The computation of wave kinematics up to the instantaneous free surface is carried out using the stretched linear correction. The formulation of wave kinematics computations subject to this correction is presented here along with a simple example to demonstrate the results.

13.2 Background

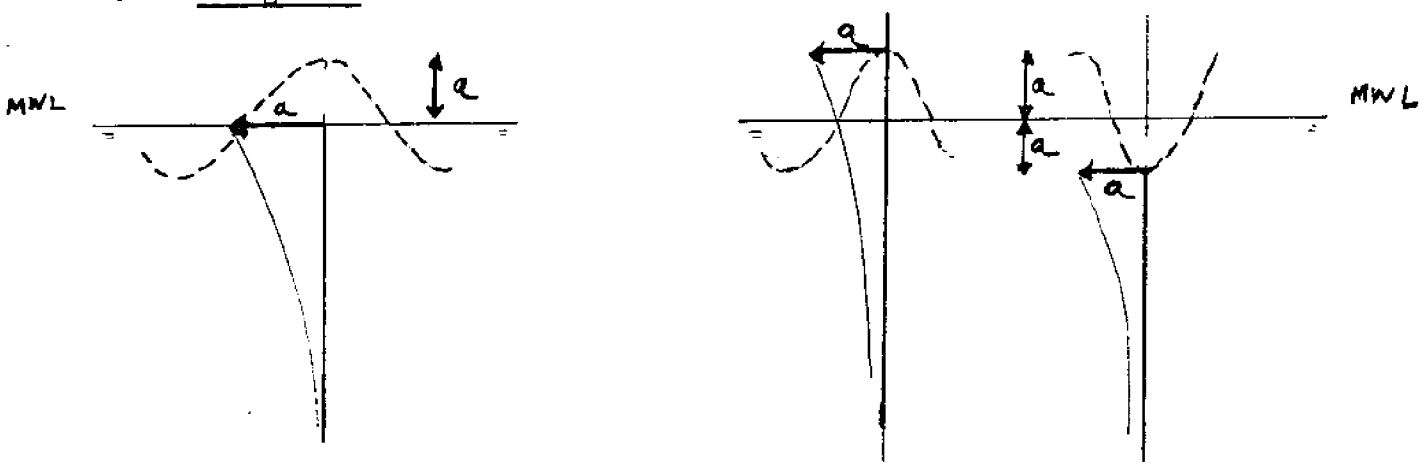

Linear Theory

Stretched Linear Theory

In the linear water wave theory, the wave kinematics are computed up to the mean water level (MWL) at any time instant. The typical variation of the water particle displacement is shown in the figure. (The dotted line shows the instantaneous water particle displacement, and "a" is the wave amplitude.) The adjacent figure shows the stretched linear correction, where the variation of the displacement starts with the instantaneous free surface location. Similar corrections are made to the

dynamic pressure, velocity and acceleration computations.

This approximation is important in the computation of shear forces and bending moments on vertical piles. The results with stretched linear correction will show a higher force and moment at the wave crest and lower values under the trough, when compared to the ordinary computation without the correction.

13.3 Formulation

For the stretched linear correction, the wave kinematics at any time instant have to be assigned to the free surface at that instant. The kinematics below the free surface have to be corrected accordingly.

The transfer function for vertical attenuation is a function of the distance between the grid point and the free surface so that equation (7.2) will be interpreted as

$$H(\omega) = e^{|K|Z_M}$$

where $H(\omega)$ = transfer function

K = wave number

Z_M = distance of a grid point from the free surface

At any grid point, this distance (Z_M) will change with every time increment. The impulse response function corresponding to this transfer function ought to be recalculated at every time step. This would null the advantage gained by the convolution method over the sum of sinusoids.

A solution to this problem lies in computing the impulse response functions just once, and then letting the grid points move with the free surface in accordance with the stretched linear correction.

The convolutions now provide wave kinematics at fixed distances

beneath the instantaneous free surface on a moving grid of points. To obtain the correct kinematics at a fixed point requires interpolation at each time step between adjacent moving grid points. For example, a fixed point a depth Z_o beneath the MWL has an instantaneous depth $Z_M = Z_o + \eta(t)$ with respect to the moving grid. The kinematics at Z_m are readily available by interpolation.

This formulation lends itself to an easy implementation because the original structure of the wave kinematics computation creates the impulse response function just once and is amenable to interpolations over the grid structure.

13.4 Example

The stretched linear correction is demonstrated for a sinusoidal wave. The particulars for the problem are:

1. wave amplitude 10 feet
2. wave period 14.59 seconds
3. point of propagation (250, -25) feet
4. water depth 250 feet
5. Dt is chosen as 0.5 seconds.

In this case T_c = 14.59 seconds. According to the guidelines,

$$DT \leq \frac{T_c}{8}$$

Therefore, Dt complies with the requirements.

Figure 39 shows the water particle displacement history at the point of interest. The history predicted by sinusoidal theory (but without stretched linear correction) is plotted on the same curve. This figure illustrates the effect of the correction. The corrected wave kinematics

have a higher value at the wave crest (and a lower value at the wave trough) than the values computed by the computations without the correction.

13.5 Summary of Chapter 13

The implementation of stretched linear correction during computation of wave kinematics using the convolution techniques can be done efficiently by interpolating within a grid, instead of computing the impulse response functions at each instant. An example shows the results for the case of a simple sinusoidal wave.

CHAPTER 14

CONCLUSIONS

An alternative to sum of sinusoids has been presented. Instead of a discrete sum of sinusoids, the Fourier transform and convolution integrals are used to represent a continuous distribution of sinusoids. The method proposed in this report is much faster than the sum of sinusoids. A number of examples for demonstrating the use of this method have been included.

14.1 Limitations of the Proposed Method

The proposed model of ocean waves is linear. It will not model wave breaking and other non-linear phenomena. Wave grouping is also not modelled. The proposed method could be used to simulate wave spreading, but it would require assembling many two-dimensional problems. The proposed method is not good for propagating waves over large distances. This method of simulating ocean waves will be efficient only when the wave kinematics need be evaluated at many points. Sum of sinusoids would probably be more efficient when the wave kinematics are to be evaluated at fewer points.

14.2 Advantages of the Proposed Method

Unlike sum of sinusoids, the proposed model of ocean waves gives a continuous distribution of wave energy. In fact, data taken from a wave-rider buoy can be used directly. Alternatively, data generated by an ARMA model can be used. For very complex offshore structures that would require the wave kinematics at many points in a grid, the proposed method is much more efficient than sum of sinusoids.

APPENDIX A

DIFFERENTIATION

Differentiation with respect to time is used to generate time series of the vertical water-particle velocity and acceleration, and the horizontal water-particle acceleration. The differentiation is done by using the central difference method. Whenever differentiation is performed numerically, the accuracy and noise amplification should be carefully investigated. The central difference method is

$$f'(t) \sim \frac{f(t+\Delta t) - f(t-\Delta t)}{2\Delta t} \tag{A.1}$$

where $f'(t)$ is the derivative of the function $f(t)$ at time t. Δt is the time step.

If $f(t+\Delta t)$ and $f(t-\Delta t)$ are expanded in a Taylor series, the truncation error can be found. Then

$$f'(t) = \frac{f(t+\Delta t) - f(t-\Delta t)}{2\Delta t} - \frac{\Delta t^2 f^{(3)}(\xi)}{6} \tag{A.2}$$

where $f^{(3)}(\xi)$ is the third derivative of $f(t)$ evaluated

anywhere in the interval from $t-\Delta t$ to $t+\Delta t$.

Therefore, the truncation error is inversely proportional to the square of the time step. Furthermore, functions which do not have smooth second derivatives will have first derivatives that are not well predicted by the central difference method.

In particular, let us investigate the accuracy of the central difference method when it is applied to sinusoidal functions. Suppose the sinusoidal function is given by

$$f(t) = e^{i\omega t} \tag{A.3}$$

where ω is the frequency. Then the derivative of this function is simply

$$f'(t) = i\omega e^{i\omega t} \tag{A.4}$$

where the above equation is exact.

The approximate derivative as given by the central difference method is

$$f'(t) \sim \frac{e^{i\omega(t+\Delta t)} - e^{i\omega(t-\Delta t)}}{2\Delta t} \tag{A.5}$$

This can be expressed as

$$f'(t) \sim \frac{i\sin(\omega\Delta t)\, e^{i\omega t}}{\Delta t} \tag{A.6}$$

Now calculate the ratio of the approximate derivative to the exact derivative

$$R(\omega) = \frac{\sin(\omega \Delta t)}{\omega \Delta t} \qquad (A.7)$$

where $R(\omega)$ is the relative error. When $R(\omega)$ equals one, the approximate solution is exact. As ω approaches zero, the central difference method becomes a very poor approximation.

The relative error is plotted in Figure 40. There is no error as the frequency goes to zero. But as the frequency approaches two samples per wave period, the relative error goes to zero. This is called the nyquist rate. In theory, the highest wave frequency that can be modeled by the methods of digital-signal processing is the nyquist frequency. In practice, the sampling rate should never become lower than eight samples per wave period.

The derivative of a function contaminated with noise can have very large errors. In fact, the error can go up as the time step decreases. For instance, suppose $f(t+\Delta t)$ and $f(t-\Delta t)$ are contaminated with noise. Then

$$f(t+\Delta t) = \tilde{f}(t+\Delta t) + n(t+\Delta t)$$
$$f(t-\Delta t) = \tilde{f}(t-\Delta t) + n(t-\Delta t) \qquad (A.8)$$

where $n(t+\Delta t)$ and $n(t-\Delta t)$ represent noise. The formula for the first derivative then becomes

$$f'(t) = \frac{\bar{f}(t+\Delta t) - \hat{f}(t-\Delta t)}{2\Delta t} + \frac{n(t+\Delta t) - n(t-\Delta t)}{2\Delta t} \qquad (A.9)$$
$$- \frac{\Delta t^2}{6} f^{(3)}(\xi)$$

Therefore, noise leads to an error in the derivative that is inversely proportional to the time step. (Figures 41, 42, 43 show a time series contaminated with noise and the derivative that time series for two different time steps.) For the second derivative, the additional error term would be inversely proportional to the square of the time step. This is a very undesireable phenomenon. However, there are two relatively easy ways of avoiding this problem. The first way is to filter the noise out of the original time series and then differentiate. The second way is to create a differentiator that removes the noise as it differentiates. Of the two methods, the first method is more desireable for our purposes because it only requires that the preventive measures be taken only once.

APPENDIX B

THE HORIZONTAL WATER-PARTICLE VELOCITY

The free-surface elevation convolved with an impulse response function gives the horizontal water-particle velocity on the mean waterline. The convolution integral has the following form:

$$\overline{u(t)} = \int_{-\infty}^{\infty} h(\tau)\,\eta(t-\tau)\,d\tau \qquad \text{(B.1)}$$

where $u(t)$ represents the time series of the horizontal water-particle velocity, $\eta(t)$ represents the time series of the free-surface elevation, and $h(t)$ is the inverse Fourier transform of the transfer function. In fact, the inverse Fourier transform is not defined. However, the Fourier series solution does exist.

This integral can be evaluated numerically as

$$u(m\Delta t) = \sum_{n=-\infty}^{\infty} h(n\Delta t)\,\eta(m\Delta t - n\Delta t)\,\Delta t \qquad \text{(B.2)}$$

where Δt is the time step, and m and n are indices. $u(t)$ and $\eta(t)$ are both sinusoidal functions of time. In

fact, in deep water $u(t)$ and $\eta(t)$ can be expressed as

$$u(t) = |\omega| e^{i\omega t}$$
$$\eta(t) = e^{i\omega t} \qquad \text{(B.3)}$$

where ω represents the frequency of the sinusoid.

Now equation B.2 can be expressed as

$$|\omega| e^{in\Delta t\omega} = \sum_{n=-\infty}^{\infty} h(n\Delta t) e^{i(m\Delta t\omega - n\Delta t\omega)} \Delta t \qquad \text{(B.4)}$$

But the above equation is a complex fourier series. Therefore,

$$h(n\Delta t) = \frac{1}{2\pi} \int_{-\pi/\Delta t}^{\pi/\Delta t} |\omega| e^{in\Delta t\omega} d\omega \qquad \text{(B.5)}$$

The evaluation of this integral gives

$$h(n\Delta t) = \begin{cases} \frac{\pi}{2\Delta t^2} & \text{zero} \\ 0. \quad \text{for } n & \text{even} \\ \frac{-2}{\pi (n\Delta t)^2} & \text{odd} \end{cases} \qquad \text{(B.6)}$$

It is now clear that the impulse response function is inversely proportional to the square of time. This is a more rapid convergence rate than some other alternatives that could have been used to generate time series of the horizontal water-particle velocity on the mean waterline. For instance, a Hilbert transform could have been used to transform the vertical water-particle velocity into the

horizontal. But the Hilbert transform is only inversely proportional to time.

APPENDIX C

VERTICAL ATTENUATION

For very deep water, the transfer function in the frequency domain is

$$H(\omega) = \exp(|K|\Delta Z) \tag{C.1}$$

where ω is the wave frequency, K is the wave number, and ΔZ is the change in water depth (measured positive upwards). Since the transfer function is a real and symmetric function of frequency, the impulse response function will be a real and symmetric function of time. The inverse Fourier transform of the transfer function is given by

$$h(t) = \frac{1}{2\pi}\int_{-\infty}^{\infty} \exp\left(\frac{\omega^2 \Delta Z}{g}\right) e^{i\omega t}\, d\omega \tag{C.2}$$

where t represents time. The dispersion relation for infinite water depth has been substituted for K .

As expected, the imaginary part of the integrand is an odd function of frequency, and it will not make a contribution to the inverse Fourier transform. The Fourier transform can now be expressed as

$$h(t) = \frac{1}{\pi}\int_{-\infty}^{\infty} \exp\left(\frac{\omega^2 \Delta z}{g}\right)\cos(\omega t)\, d\omega \qquad \text{(C.3)}$$

Now integrate by parts.

$$h(t) = \frac{1}{\pi}\exp\left(\frac{\omega^2 \Delta z}{g}\right)\frac{\sin(\omega t)}{t}\Bigg|_0^{\infty}$$

$$-\frac{2}{\pi}\frac{\Delta z}{gt}\int_0^{\infty} \omega \exp\left(\frac{\omega^2 \Delta z}{g}\right)\sin(\omega t)\, d\omega \qquad \text{(C.4)}$$

Since the first term is zero,

$$h(t) = -\frac{2}{\pi}\frac{\Delta z}{gt}\int_0^{\infty} \omega \exp\left(\frac{\omega^2 \Delta z}{g}\right)\sin(\omega t)\, d\omega \qquad \text{(C.5)}$$

The derivative with respect to time of equation C.3 gives

$$h'(t) = -\frac{1}{\pi}\int_0^{\infty} \omega \exp\left(\frac{\omega^2 \Delta z}{g}\right)\sin(\omega t)\, d\omega \qquad \text{(C.6)}$$

Therefore, the impulse response function and its derivative are related to each other as follows:

$$h'(t) = \frac{gt}{2\Delta z}\, h(t) \qquad \text{(C.7)}$$

Integrate this expression with respect to time.

$$h(t) = C \exp\left(\frac{g t^2}{4 \Delta z}\right) \tag{C.8}$$

where C is a constant of integration.

To find the constant of integration, evaluate $h(t)$ at $t=0$. Therefore,

$$C = h(0) = \frac{1}{\pi} \int_0^\infty \exp\left(\frac{\omega^2 \Delta z}{g}\right) d\omega \tag{C.9}$$

A change of variables gives

$$C = \frac{1}{\pi} \sqrt{\frac{-g}{\Delta z}} \int_0^\infty \exp(-u^2)\, du \tag{C.10}$$

The square of this integral is

$$C^2 = \frac{-g}{\pi^2 \Delta z} \int_0^\infty \exp(-u^2)\, du \int_0^\infty \exp(-w^2)\, dw \tag{C.11}$$

This quantity can be expressed as

$$C^2 = \frac{-g}{\pi^2 \Delta z} \int_0^\infty \int_0^\infty \exp(-(u^2 + w^2))\, du\, dw \tag{C.12}$$

Now introduce polar coordinates.

$$C^2 = \frac{-g}{\pi^2 \Delta z} \int_0^\infty \int_0^{\pi/2} r \exp(-r^2)\, d\theta\, dr \tag{C.13}$$

Therefore, the constant of integration is

$$C = \frac{1}{2}\sqrt{\frac{-9}{\pi \Delta z}} \tag{C.14}$$

Furthermore, the final expression for the impulse response function is

$$h(t) = \frac{1}{2}\sqrt{\frac{-9}{\pi \Delta z}}\, \exp\left(\frac{9t^2}{4\Delta z}\right) \tag{C.15}$$

APPENDIX D

HORIZONTAL PROPAGATION

For very deep water, the transfer function in the frequency domain is

$$H(\omega) = \exp(iK\Delta X) \tag{D.1}$$

where ω is the wave frequency, K is the wave number, and ΔX is a positive distance over which a wave is going to be propagated. Since the real part of the transfer function is even and the imaginary part is odd, the impulse response function will be a real function of time. The inverse Fourier transform of the transfer function is give by

$$h(t) = \frac{1}{2\pi}\int_{-\infty}^{\infty}\left[\cos\left(\frac{\omega^2 sgn(\omega)\Delta X}{g}\right) - i\sin\left(\frac{\omega^2 sgn(\omega)\Delta X}{g}\right)\right]e^{i\omega t}\,d\omega \tag{D.2}$$

where t represents time. The dispersion relation for infinite water depth has been substituted for K .

The integrand can be expanded as

$$h(t) = \frac{1}{2\pi}\int_{-\infty}^{\infty}\left[\cos\left(\frac{\omega^2 sgn(\omega)\Delta X}{g}\right)\cos\omega t + i\cos\left(\frac{\omega^2 sgn(\omega)\Delta X}{g}\right)\sin\omega t\right.$$

$$\left. -i\sin\left(\frac{\omega^2 sgn(\omega)\Delta X}{g}\right)\cos\omega t + \sin\left(\frac{\omega^2 sgn(\omega)\Delta X}{g}\right)\sin\omega t\right]d\omega \tag{D.3}$$

As expected, the imaginary part of the integrand is an odd function of frequency, and it will not make a contribution to the inverse Fourier transform. The Fourier transform can now be expressed as

$$h(t)=\frac{1}{\pi}\int_{-\infty}^{\infty}\cos\left(\frac{\omega^2\Delta X}{g}-\omega t\right)d\omega \tag{D.4}$$

This integral is similiar to the indefinite integral given below.

$$I(x)=\int\cos\left(ax^2+2bx+c\right)dx \tag{D.5}$$

This integral can be arranged as

$$I(x)=\int\cos\left(\frac{(ax+b)^2}{a}-\frac{(b^2-ac)}{a}\right)dx \tag{D.6}$$

The expansion of the integral is

$$I(x)=\int\left[\cos\left(\frac{(ax+b)^2}{a}\right)\cos\left(\frac{(b^2-ac)}{a}\right)+\sin\left(\frac{(ax+b)^2}{a}\right)\sin\left(\frac{(b^2-ac)}{a}\right)\right]dx \tag{D.7}$$

This integral can be expressed as

$$I(x)=\sqrt{\frac{\pi}{2a}}\int\left[\sqrt{\frac{2a}{\pi}}\cos\left(\frac{\pi}{2}\left(\sqrt{\frac{2}{a\pi}}(ax+b)\right)^2\right)\cos\left(\frac{(b^2-ac)}{a}\right)+\sqrt{\frac{2a}{\pi}}\sin\left(\frac{\pi}{2}\left(\sqrt{\frac{2}{a\pi}}(ax+b)\right)^2\right)\sin\left(\frac{(b^2-ac)}{a}\right)\right]dx \tag{D.8}$$

Now express this integral in terms of Fresnel integrals.

$$I(x)=\sqrt{\frac{\pi}{2a}}\left[C\left(\sqrt{\frac{2}{a\pi}}(ax+b)\right)\cos\left(\frac{b^2-ac}{a}\right)+S\left(\sqrt{\frac{2}{a\pi}}(ax+b)\right)\sin\left(\frac{b^2-ac}{a}\right)\right] \tag{D.9}$$

where $C(y)$ and $S(y)$ are defined as $\int_0^y \cos\left(\frac{\pi}{2}t^2\right)dt$ and $\int_0^y \sin\left(\frac{\pi}{2}t^2\right)dt$ respectively.

Therefore, the integral for $h(t)$ can be expressed as

$$h(t)=\sqrt{\frac{g}{2\pi\Delta x}}\left[\left(\frac{1}{2}+C\left(\sqrt{\frac{g}{2\pi\Delta x}}t\right)\right)\cos\left(\frac{gt^2}{4\Delta x}\right)+\left(\frac{1}{2}+S\left(\sqrt{\frac{g}{2\pi\Delta x}}t\right)\right)\sin\left(\frac{gt^2}{4\Delta x}\right)\right] \tag{D.10}$$

For finite cut-off frequencies, $h(t)$ can be expressed as

$$h(t)=\sqrt{\frac{g}{2\pi\Delta x}}\left[\left(C\left(\sqrt{\frac{2\Delta x}{\pi g}}\omega_c-\sqrt{\frac{g}{2\pi\Delta x}}t\right)+C\left(\sqrt{\frac{g}{2\pi\Delta x}}t\right)\right)\cos\left(\frac{gt^2}{4\Delta x}\right)+\left(S\left(\sqrt{\frac{2\Delta x}{\pi g}}\omega_c-\sqrt{\frac{g}{2\pi\Delta x}}t\right)+S\left(\sqrt{\frac{g}{2\pi\Delta x}}t\right)\right)\sin\left(\frac{gt^2}{4\Delta x}\right)\right] \tag{D.11}$$

where ω_c is the cut-off frequency. This expression is useful for comparing theory to numerical results generated by the fast Fourier transform.

APPENDIX E

BIBLIOGRAPHY

Abramowitz, M. and Stegun, I.A. 1965. Handbook of Mathematical Functions. Dover, New York. Burke, Ben G. and Tighe, James T. 1972. "A Time Series Model for Dynamic Behavior of Offshore Structures," Society of Petroleum Engineers Journal, 156-170. Fuchs, R.A. 1954. "On the Theory of Irregular Waves," Proceedings of the First Conference on Ships and Waves, SNAME, 1-10. Le Mehaute, B. 1969. "An Introduction to Hydrodynamics and Water Waves - Volume II: Water Wave Theories," ESSA Technical Report ERL 118-pol 3-2, U.S. Government Printing Office. Zienkiewicz, O.C., Lewis, R.W., and Stagg, K.G. 1978. Numerical Methods in Offshore Engineering, John Wiley and Sons, New York.

APPENDIX F

FIGURES

FIGURE 1 TYPICAL OFFSHORE STRUCTURES

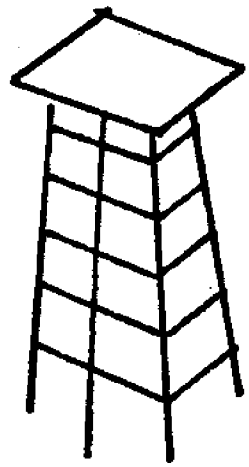

GRAVITY PLATFORM

RISER

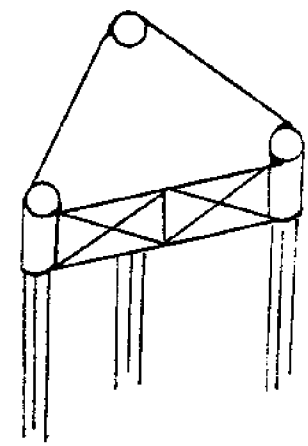

TENSION-LEG PLATFORM

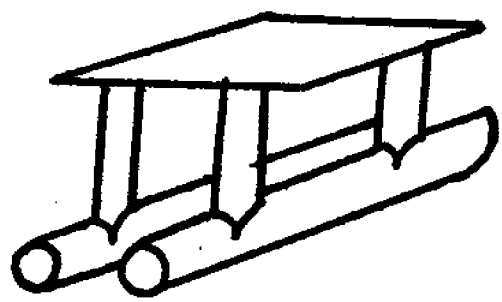

SEMISUBMERSIBLE

FIGURE 2 FLOW NORMAL TO A CYLINDER'S AXIS

This figure shows how Morison's equation is applied for flow normal to a cylinder's axis.

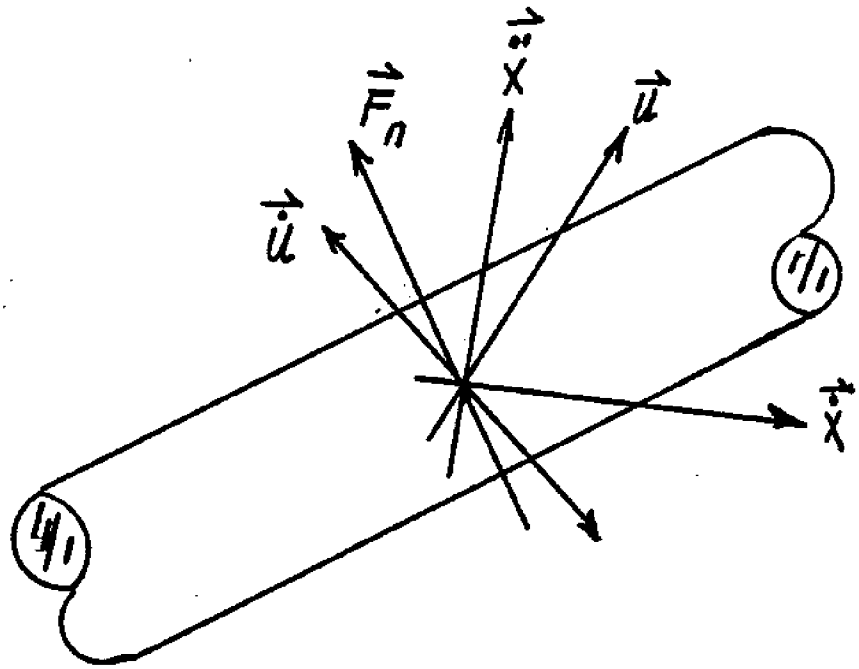

FIGURE 3 FLOW IN-LINE WITH A CYLINDER'S AXIS

This figure shows how Morison's equation is applied for flow in-line with a cylinder's axis.

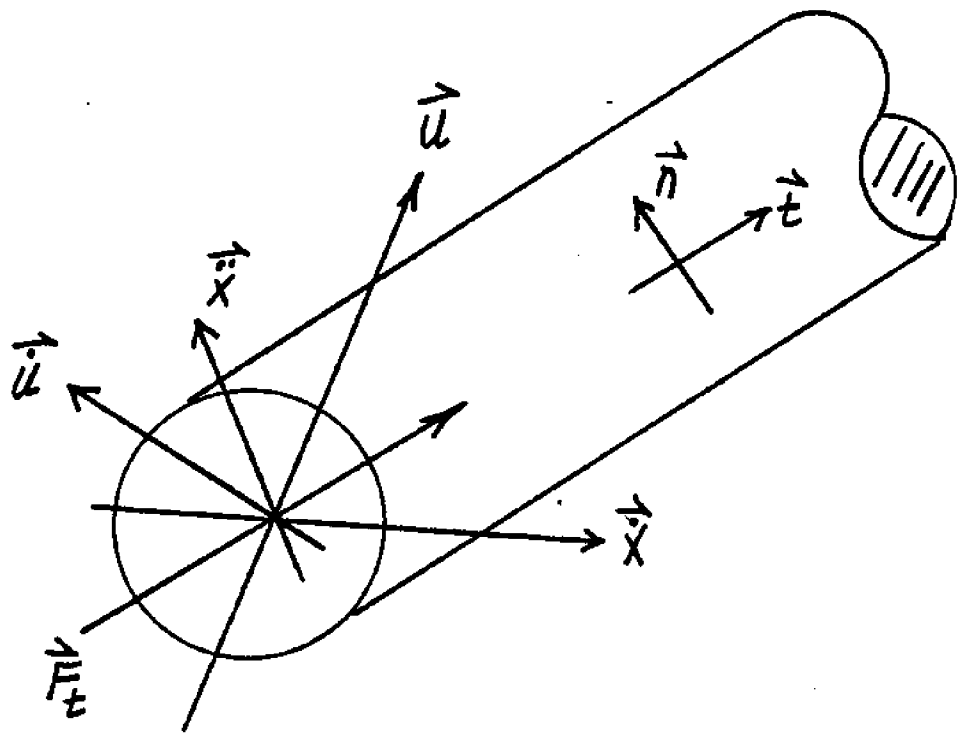

FIGURE 4 COORDINATE SYSTEM FOR AIRY WAVE THEORY

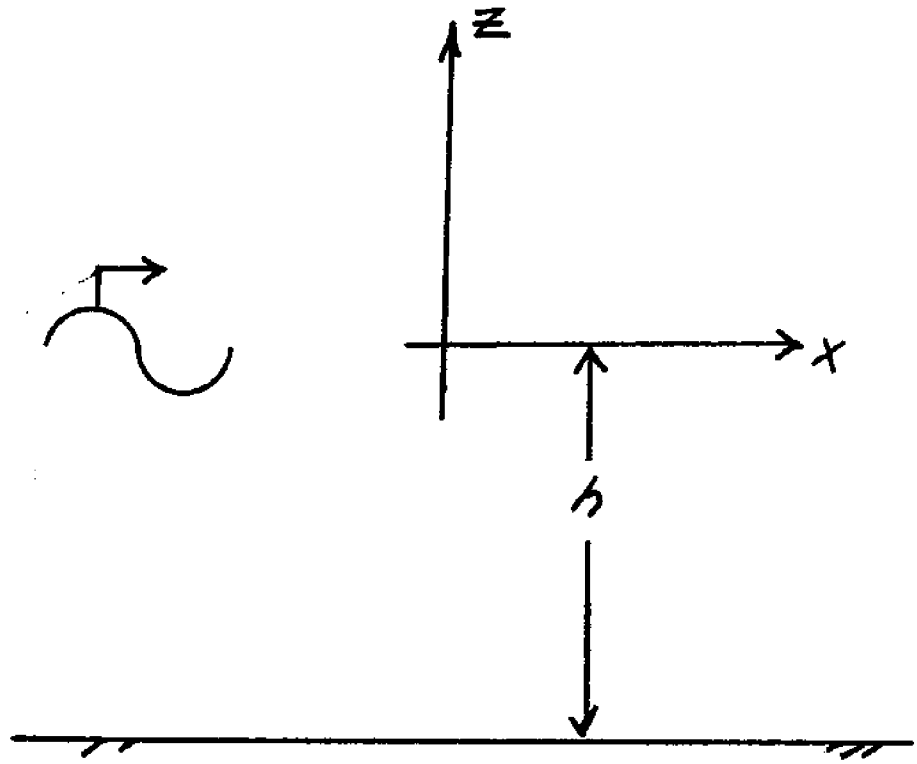

FIGURE 5 RANGE OF VALIDITY OF AIRY WAVE THEORY

(Adapted from Le Mehaute, 1969)

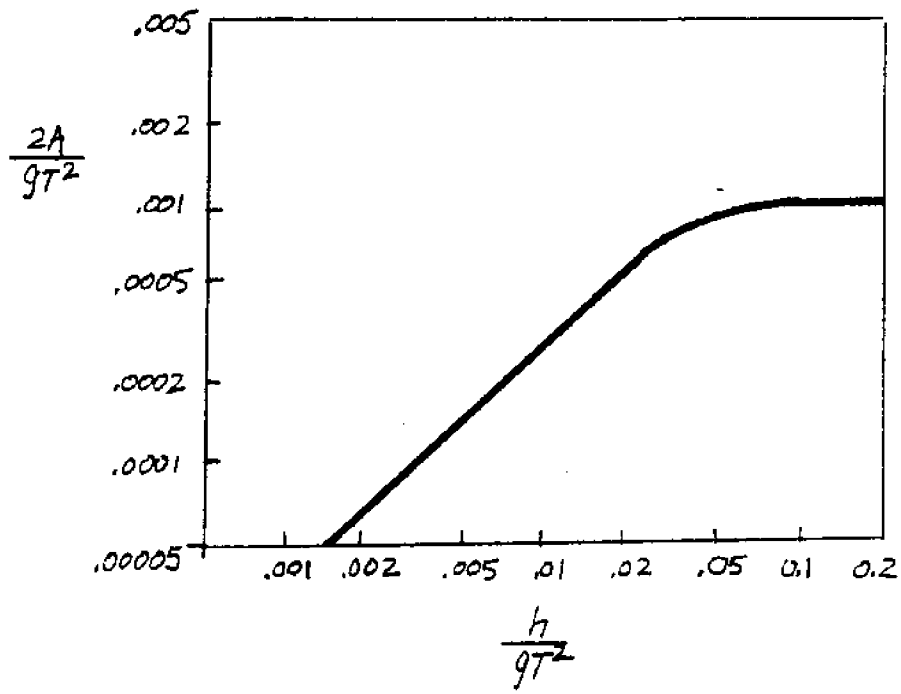

FIGURE 6 COORDINATE SYSTEM FOR THE GRID

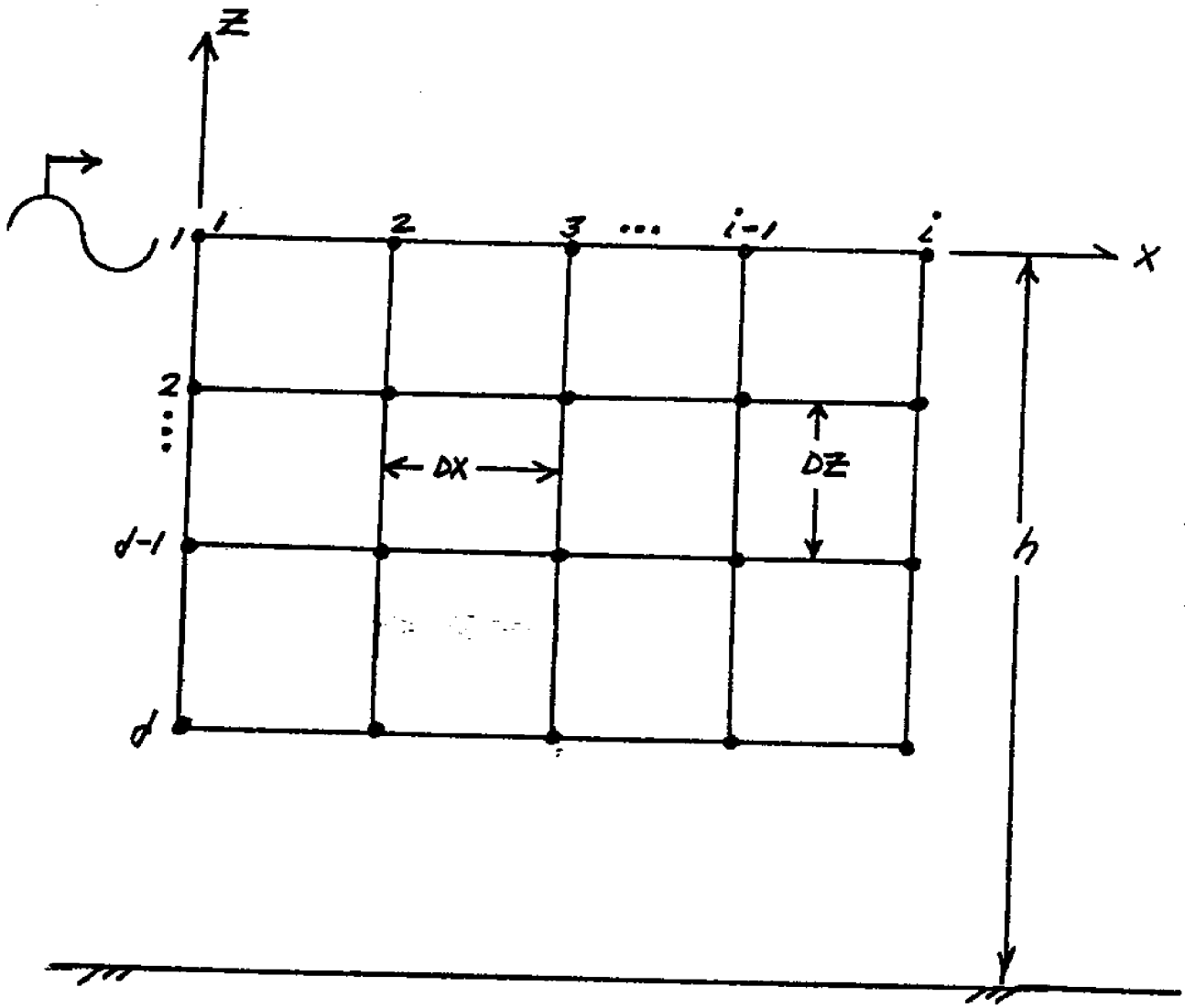

FIGURE 7 ALGORITHM FOR GENERATING WAVE KINEMATICS I

This figure describes an algorithm for finding the wave kinematics on the mean waterline.

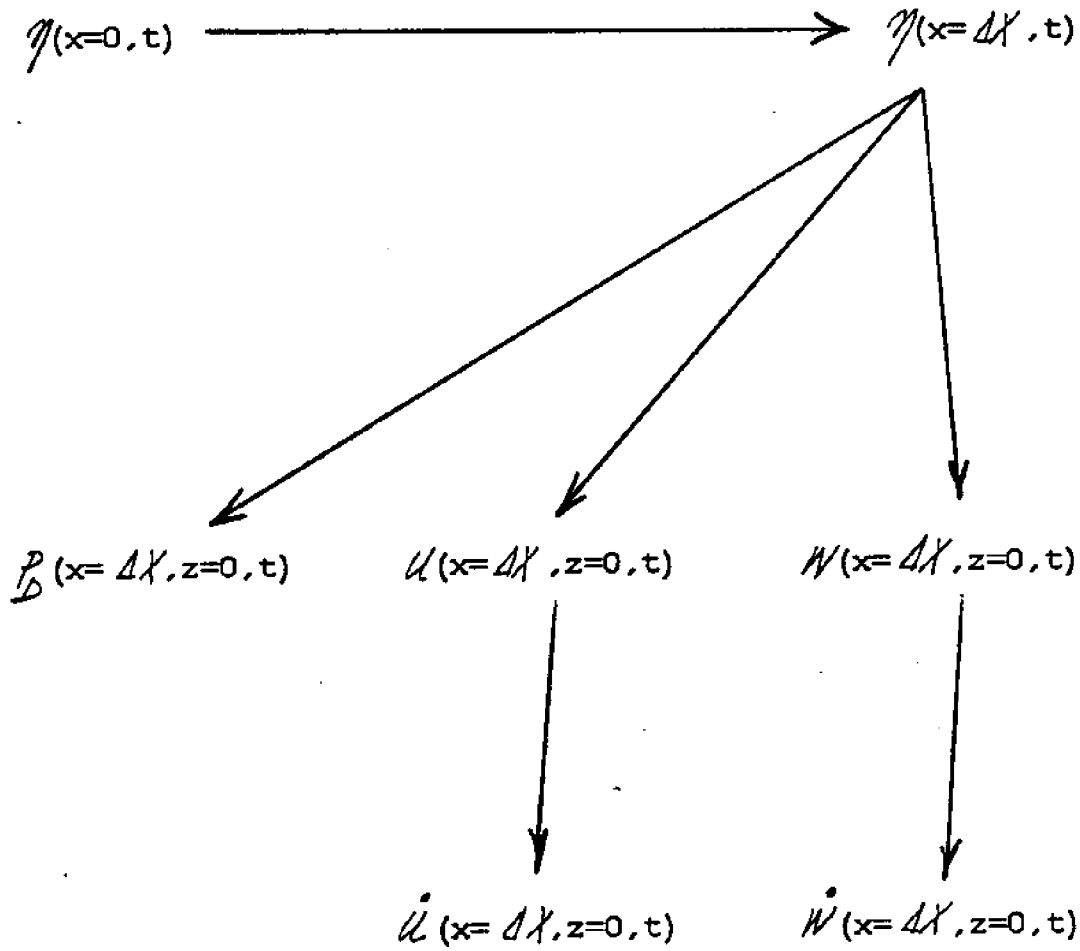

FIGURE 8 ALGORITHM FOR GENERATING WAVE KINEMATICS II

This figure describes an algorithm for finding the wave kinematics below the mean waterline.

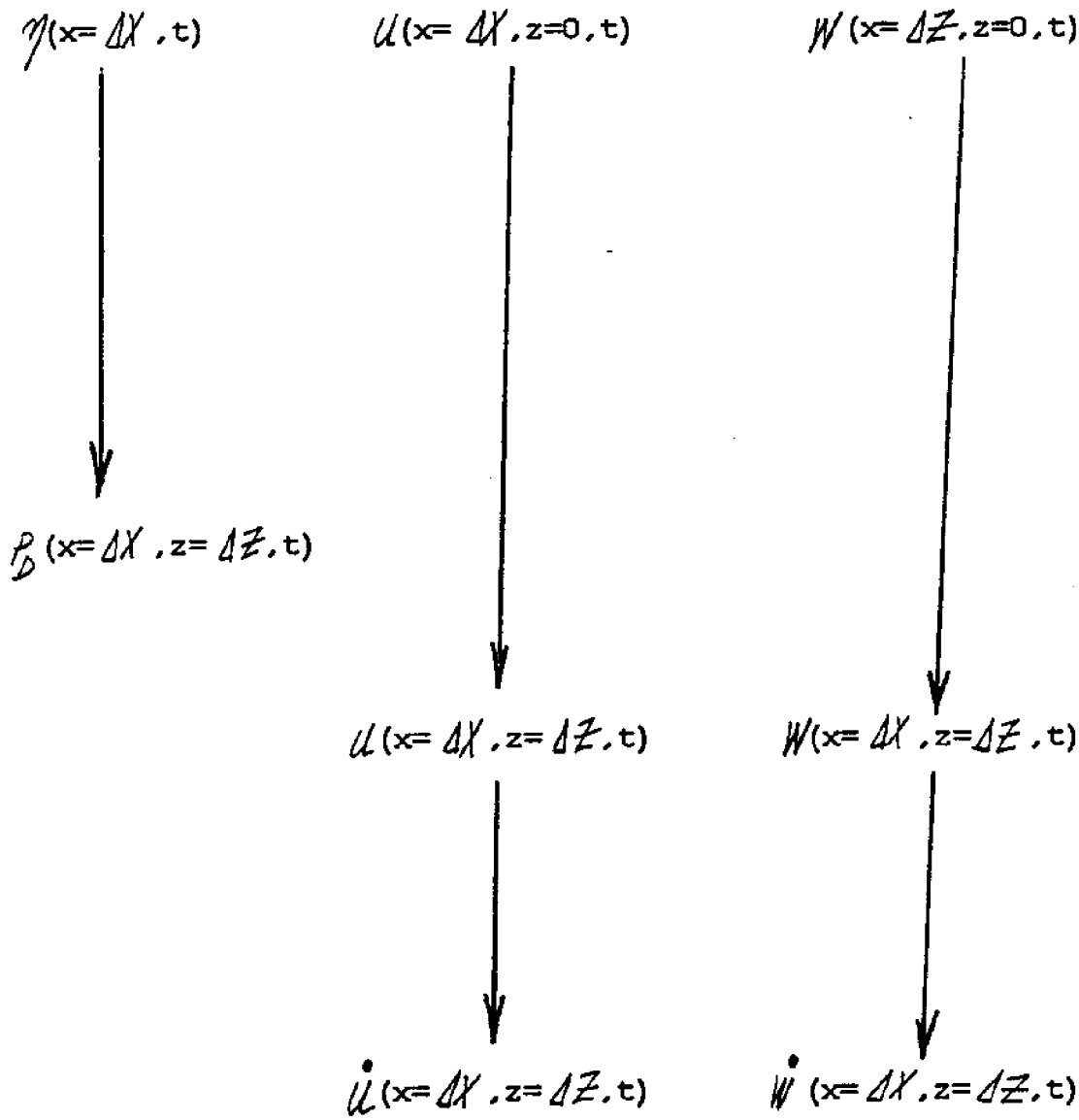

FIGURE 9 HORIZONTAL WATER-PARTICLE VELOCITY I

This figure shows an impulse response function for transforming the free-surface elevation into the horizontal water-particle velocity on the mean waterline in deep water. The time step is .25 seconds. Notice how rapidly the function approaches ~~zero~~ as the time becomes greater than or less than zero.

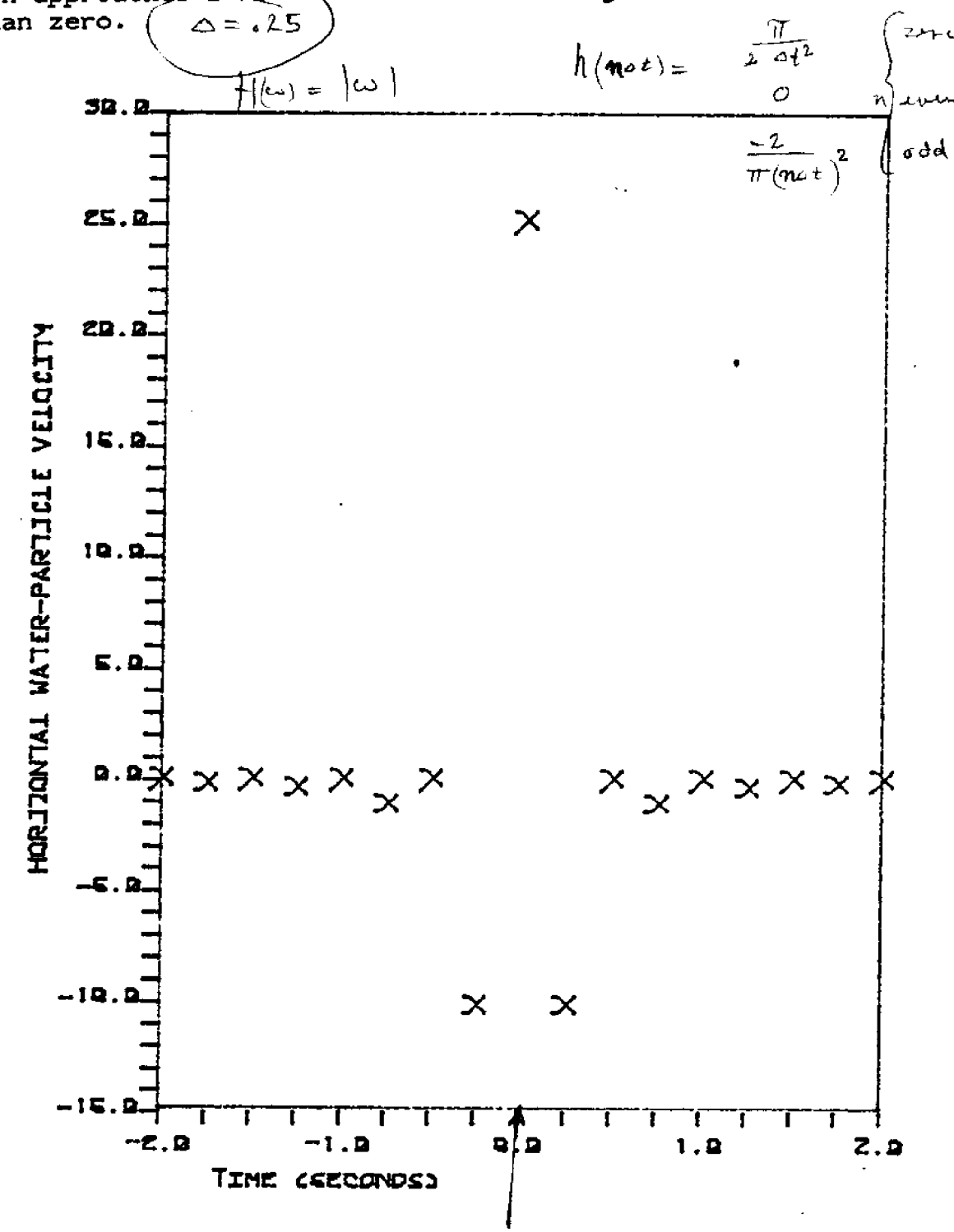

FIGURE 10 HORIZONTAL WATER-PARTICLE VELOCITY II

This figure shows an impulse response function for transforming the free-surface elevation into the horizontal water-particle velocity on the mean waterline in finite water depth. The time step is .25 seconds. The water depth is 25. feet. Even for this very shallow water depth the behaviour of the function differs very little from its behaviour in deep water.

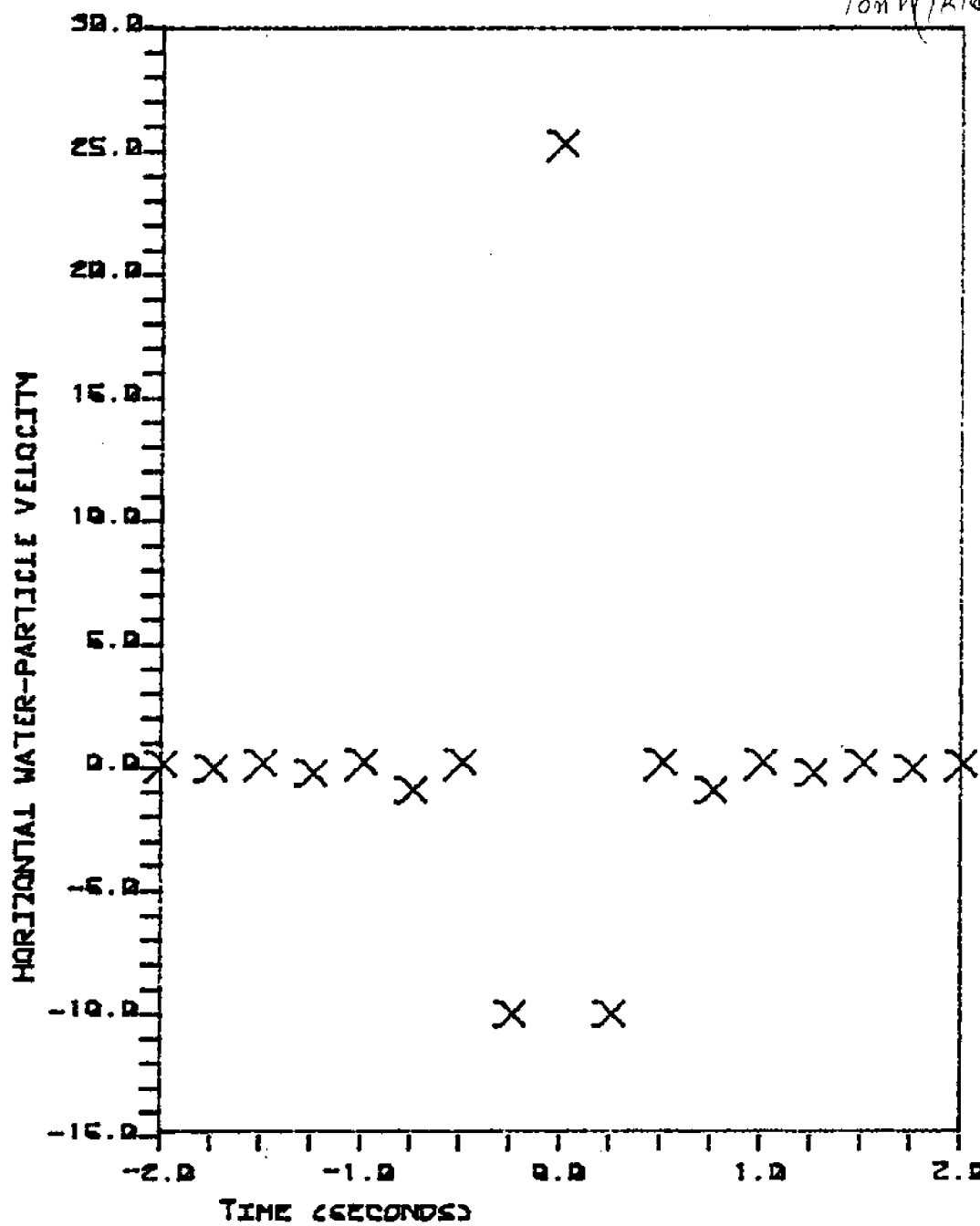

FIGURE 11 VERTICAL ATTENUATION IN DEEP WATER

This figure shows the inverse Fourier transform of the transfer function for modeling vertical attenuation in deep water. This function models the vertical attenuation over a change in depth of 25. feet.

$$h(t) = \frac{1}{2}\sqrt{\frac{-g}{\pi\sigma^2}}\, e^{\frac{gt^2}{4\sigma^2}}$$

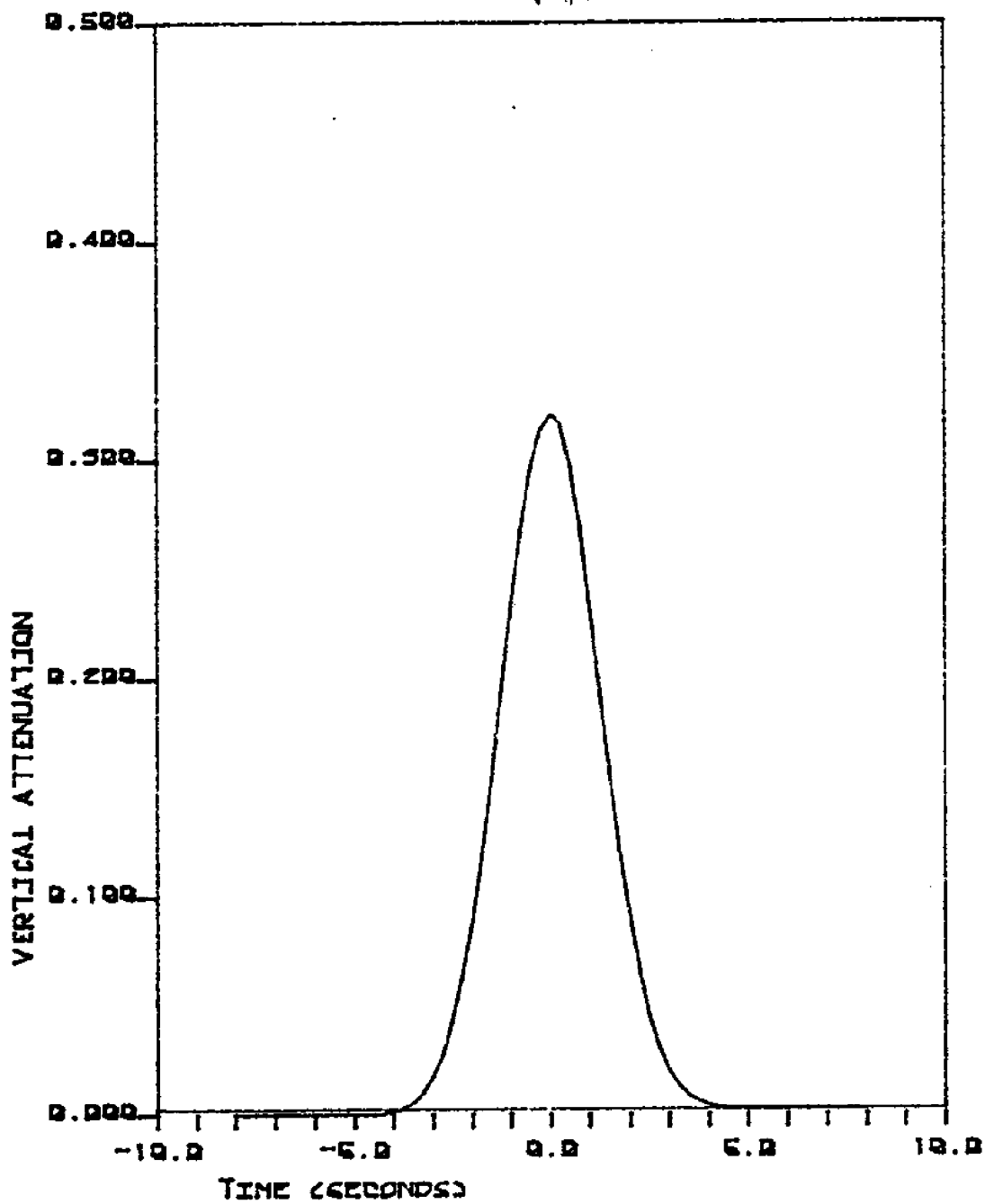

FIGURE 12 VERTICAL ATTENUATION IN WATER IN FINITE DEPTH

This figure shows impulse response functions for performing vertical attenuation in water of finite depth in comparison to the same function in deep water. The water depth is 50. feet. The distance over which the time series are attenuated is 25. feet. The time step is .25 seconds. The graph on the left is the impulse response function for the transfer function that contains the hyperbolic cosines. The graph on the right is the impulse response function for the transfer function that contains the hyperbolic sines. The symbols represent the finite depth results calculated by using the fast Fourier transform. The solid lines are deep water theory.

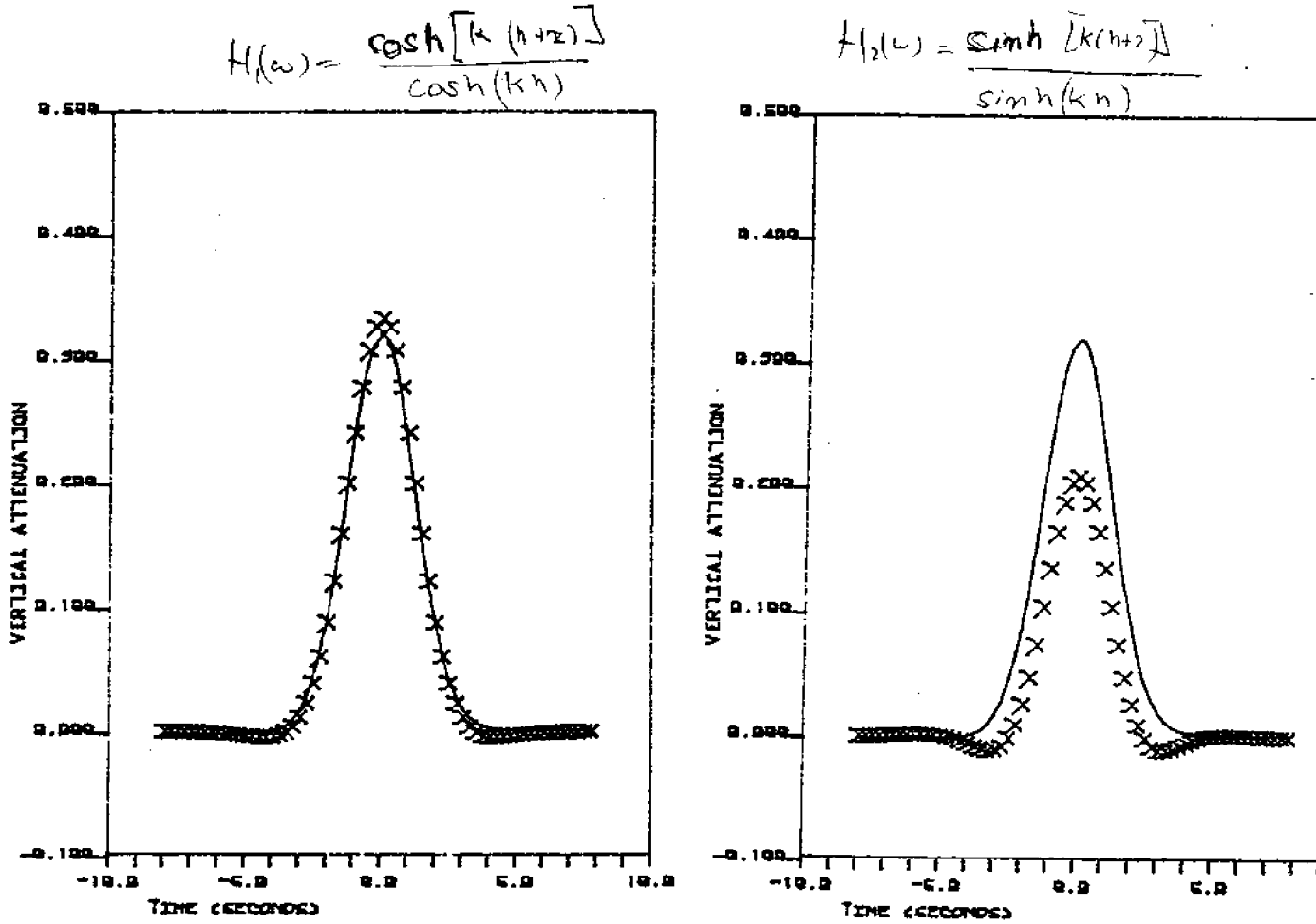

FIGURE 13 HORIZONTAL PROPAGATION IN DEEP WATER I

This figure shows the inverse fourier transform of the transfer function for horizontal propagation when there is no cut-off frequency. This function models the horizontal propagation over a distance of 25. feet.

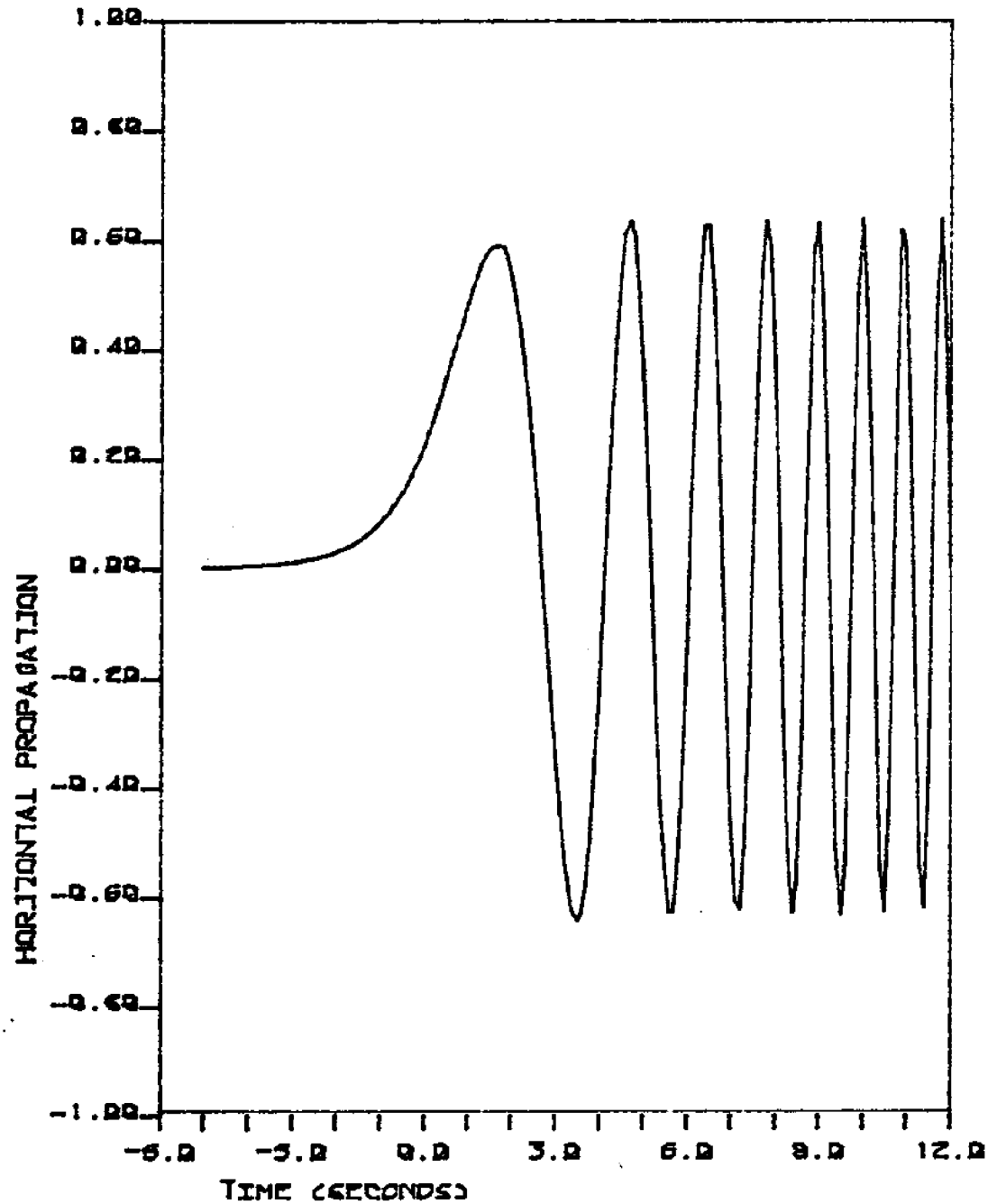

FIGURE 14 HORIZONTAL PROPAGATION IN DEEP WATER II

This figure shows the inverse fourier transform of the transfer function for horizontal propagation when there is a finite cut-off frequency. The cut-off frequency equals 1. Hz. The distance of propagation is 25. feet.

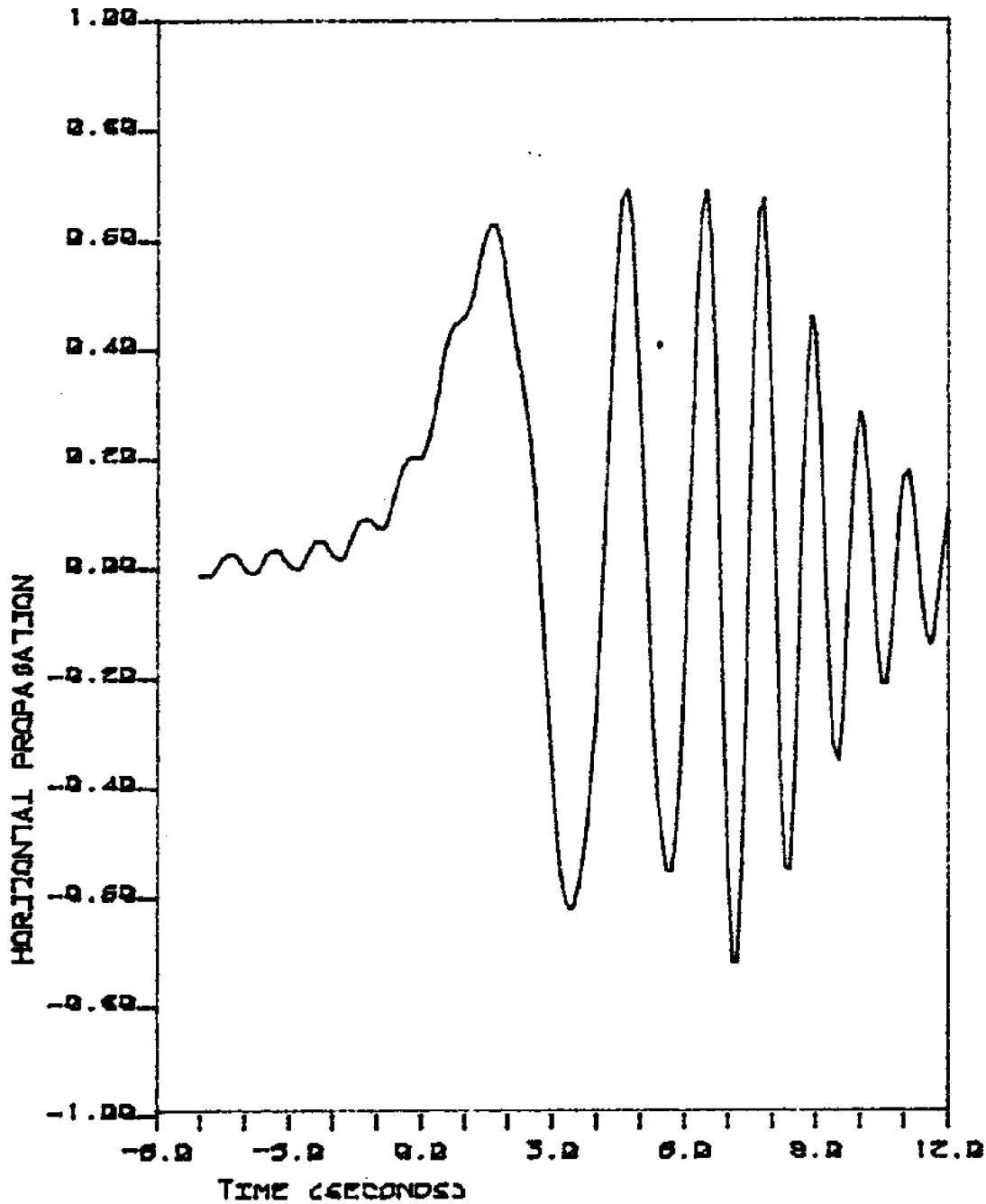

FIGURE 15 HORIZONTAL PROPAGATION IN FINITE WATER DEPTHS

This figure shows an impulse response function for performing horizontal propagation in water of finite depth in comparison to the same function in deep water. The water depth is 50. feet. The time step is 0.5 seconds. The distance of propagation is 25. feet. The symbols represent the finite depth results calculated by using the fast Fourier transform. The solid line is theory in deep water.

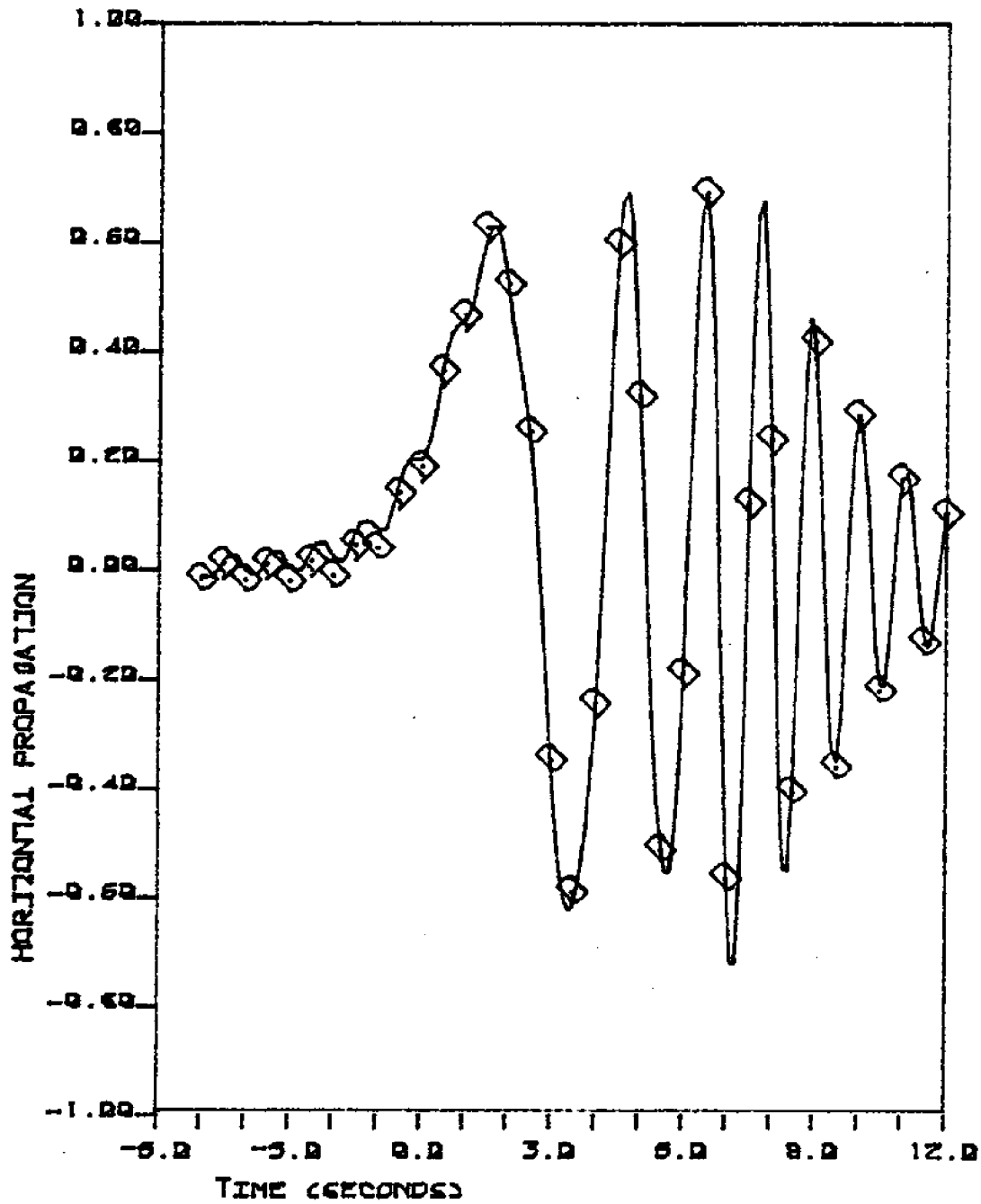

REGULAR WAVE : AMPLITUDE = 00.100 FEET PERIOD = 00.50 SEC

DT = 0.0625 SEC DEPTH = 004.0 FEET DATA SIZE = 2048

GRID IN X DIRECTION HAS 7 POINTS SPACED AT 03.2000 FEET

GRID IN Y DIRECTION HAS 3 POINTS SPACED AT 05.0000 FEET

RESULTS COMPUTED AT (006.400,-00.00) FEET

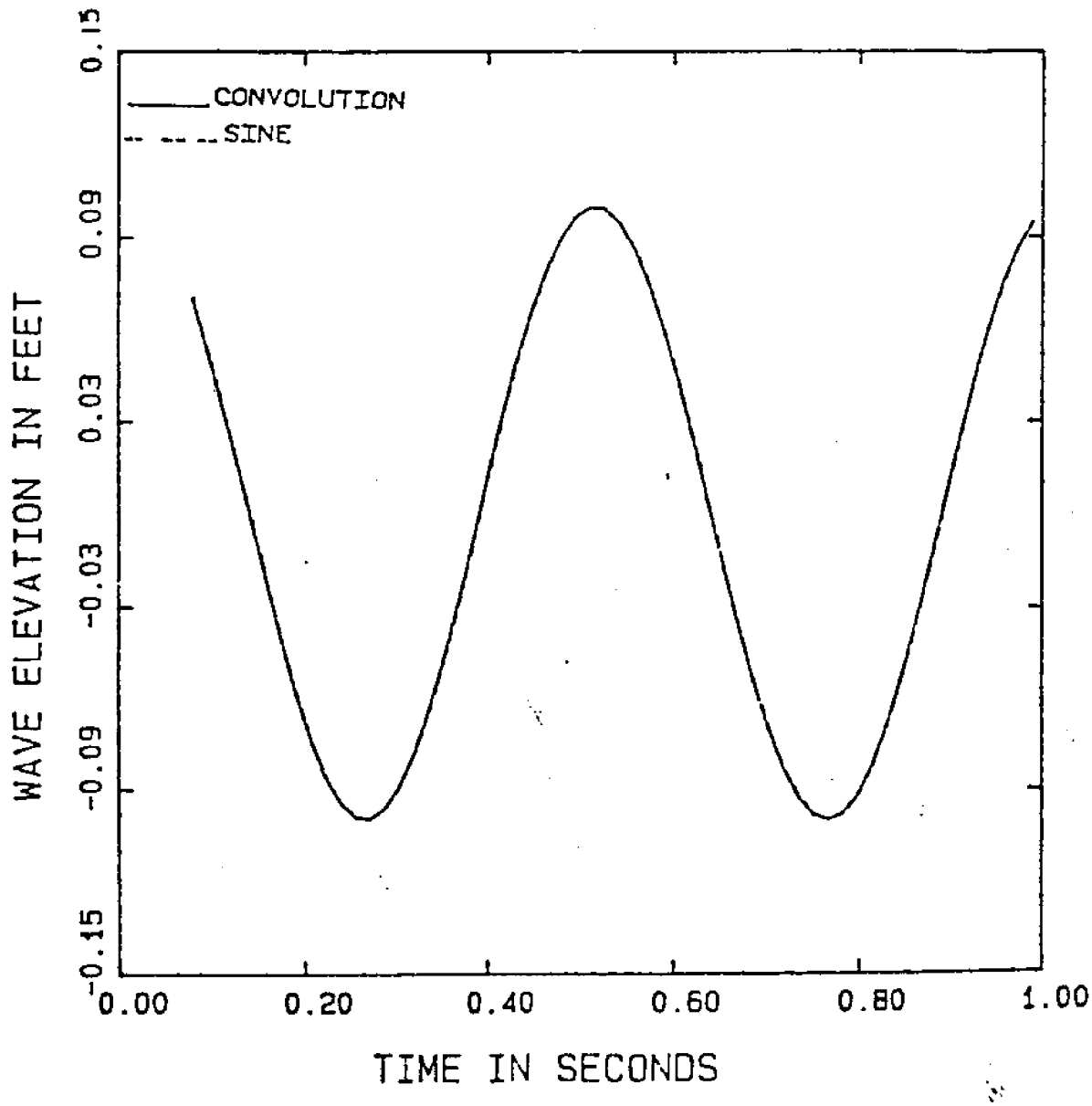

FIGURE 16 : SIMULATED WAVE AT 5 WAVELENGTHS

REGULAR WAVE : AMPLITUDE = 00.100 FEET PERIOD = 00.50 SEC

DT = 0.0625 SEC DEPTH = 004.0 FEET DATA SIZE = 2048

GRID IN X DIRECTION HAS 7 POINTS SPACED AT 03.2000 FEET

GRID IN Y DIRECTION HAS 3 POINTS SPACED AT 05.0000 FEET

RESULTS COMPUTED AT (012.800,-00.00) FEET

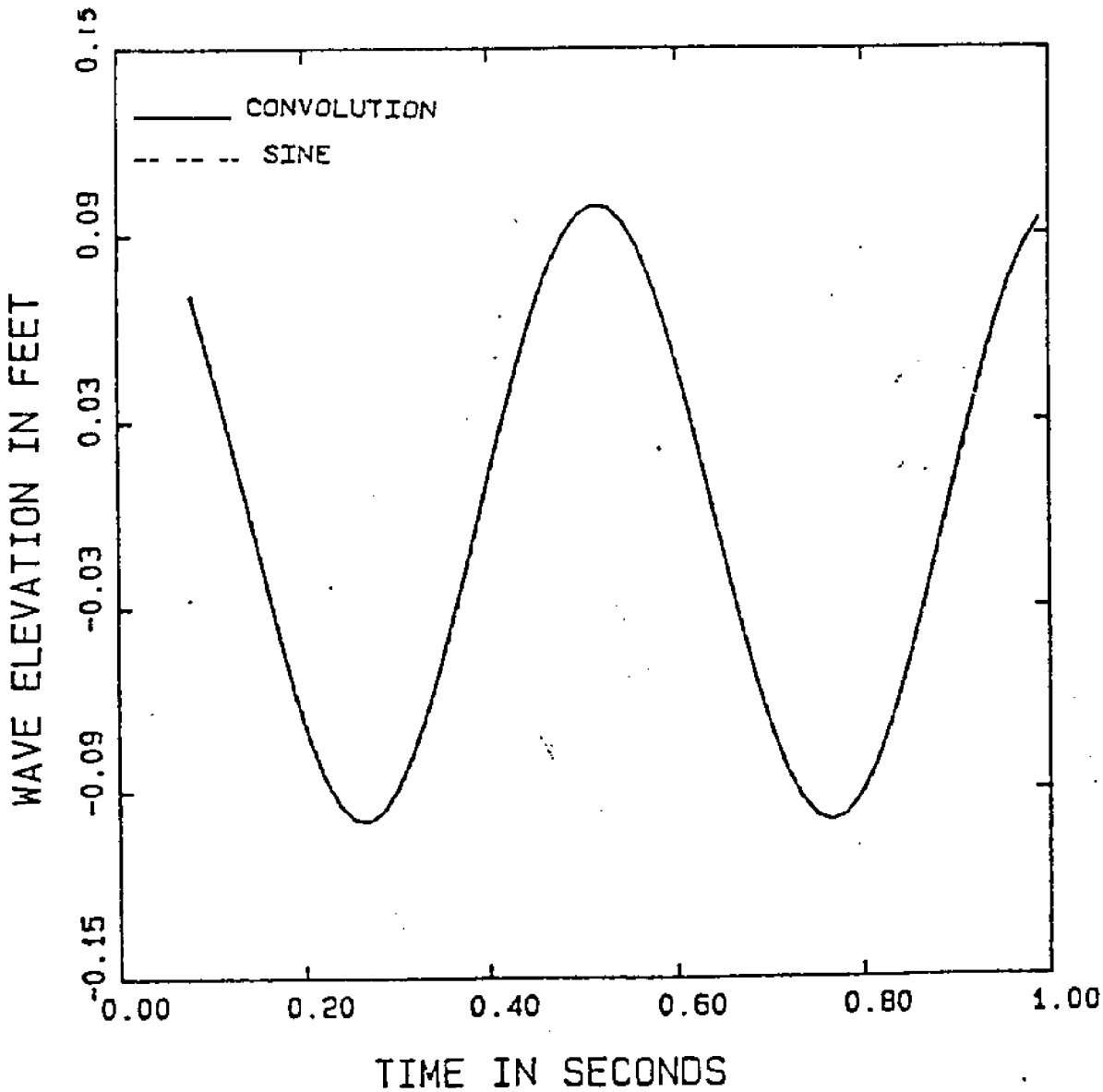

FIGURE 17 : SIMULATED WAVE AT 10 WAVELENGTHS

REGULAR WAVE : AMPLITUDE = 00.100 FEET PERIOD = 00.50 SEC

DT = 0.0625 SEC DEPTH = 004.0 FEET DATA SIZE = 2048

GRID IN X DIRECTION HAS 7 POINTS SPACED AT 03.2000 FEET

GRID IN Y DIRECTION HAS 3 POINTS SPACED AT 05.0000 FEET

RESULTS COMPUTED AT (019.200,-00.00) FEET

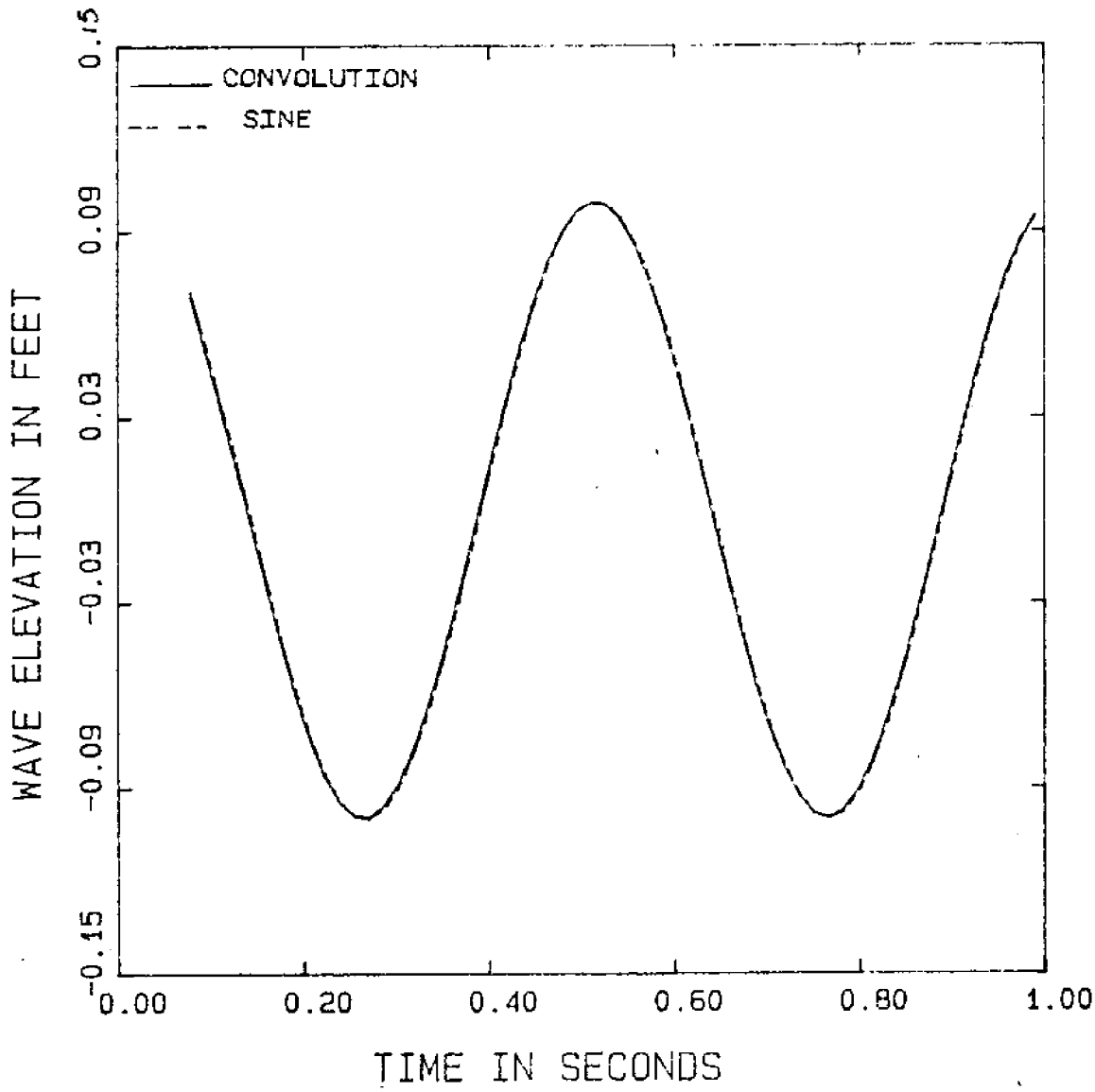

FIGURE 18 : SIMULATED WAVE AT 15 WAVELENGTHS

RANDOM WAVE : HEIGHT sig = 00.200 FEET PERIOD sig = 01.00 SEC

32 FREQUENCY COMPONENTS WITH MINIMUM = 0.50 HZ MAXIMUM = 1.78 HZ

DT = 0.0625 SEC DEPTH = 004.0 FEET DATA SIZE = 2048

GRID IN X DIRECTION HAS 3 POINTS SPACED AT 01.250 FEET

GRID IN Y DIRECTION HAS 3 POINTS SPACED AT 00.500 FEET

RESULTS COMPUTED AT (002.500,-00.00) FEET

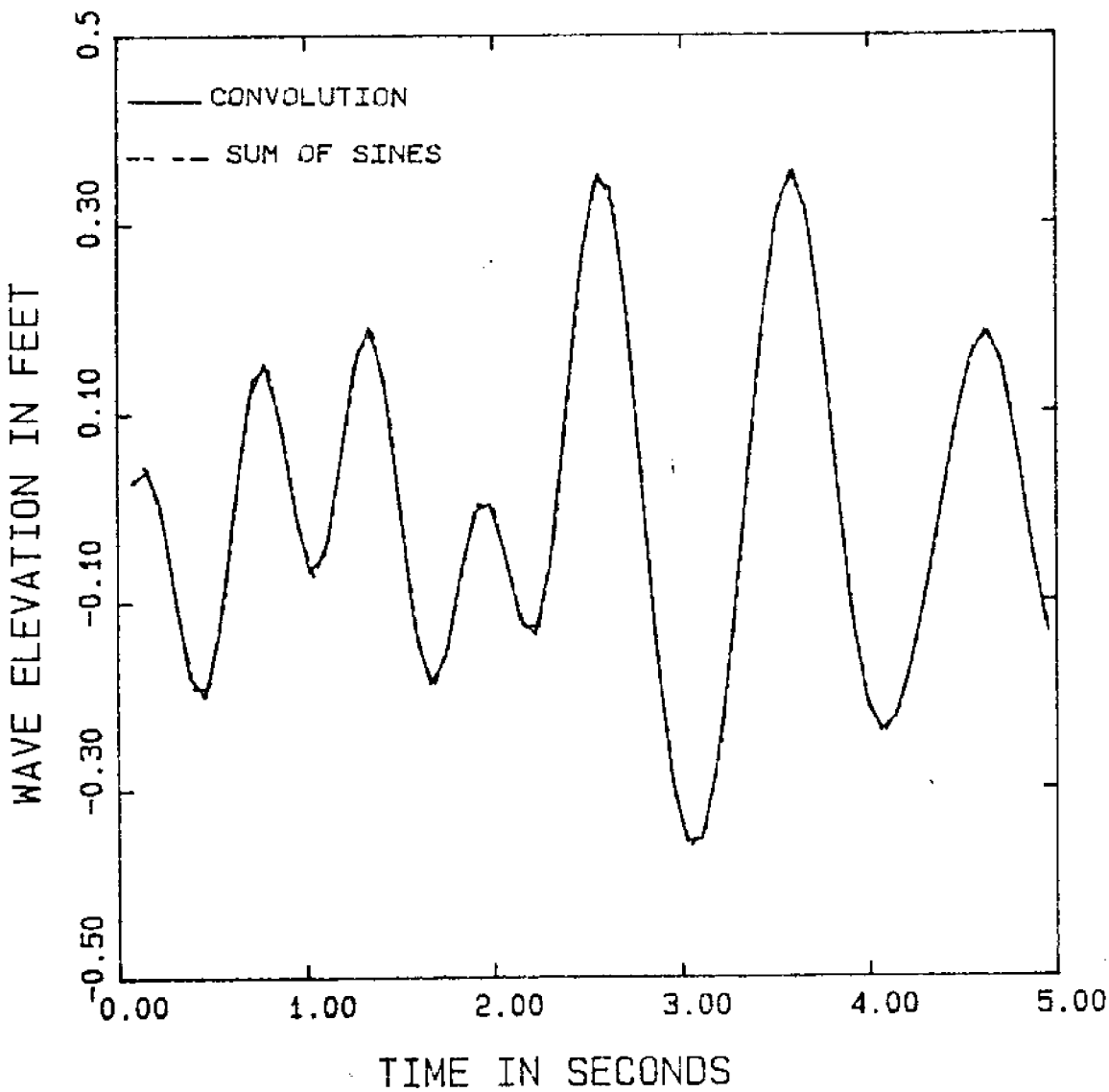

FIGURE 19: SIMULATED OVER 2.5 FEET (1.5 SHORTEST WAVE LENGTH)

RANDOM WAVE : HEIGHT sig = 00.200 FEET PERIOD sig = 01.00 SEC

32 FREQUENCY COMPONENTS WITH MINIMUM = 0.50 HZ MAXIMUM = 1.78 HZ

DT = 0.0625 SEC DEPTH = 004.0 FEET DATA SIZE = 2048

GRID IN X DIRECTION HAS 3 POINTS SPACED AT 01.250 FEET

GRID IN Y DIRECTION HAS 3 POINTS SPACED AT 00.500 FEET

RESULTS COMPUTED AT (005.000,-00.00) FEET

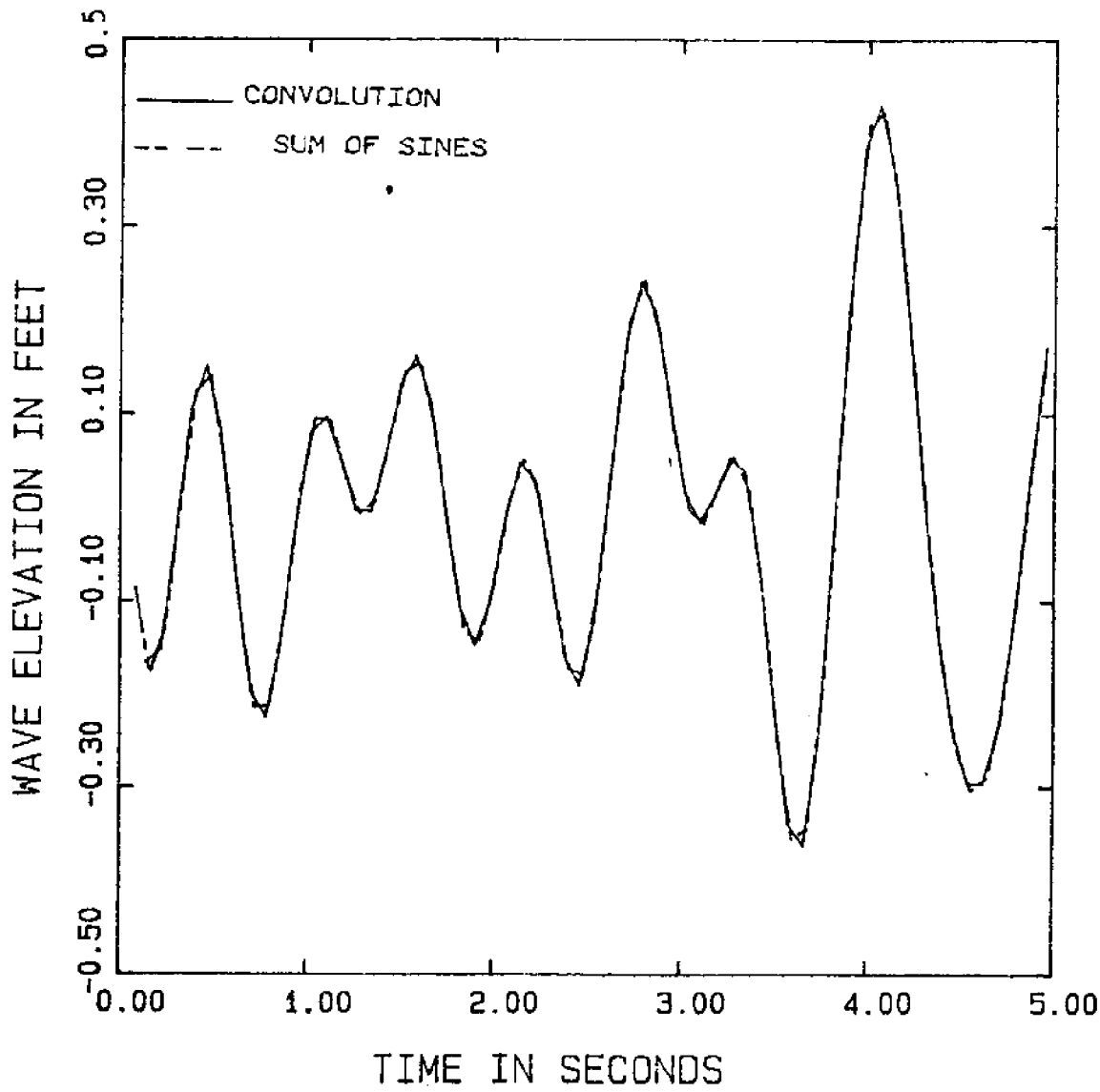

FIGURE 20: SIMULATED OVER 2.5 FEET (3.0 SHORTEST WAVE LENGTH)

RANDOM WAVE : HEIGHT sig = 00.200 FEET PERIOD sig = 01.00 SEC

32 FREQUENCY COMPONENTS WITH MINIMUM = 0.50 HZ MAXIMUM = 1.78 HZ

DT = 0.0625 SEC DEPTH = 004.0 FEET DATA SIZE = 2048

GRID IN X DIRECTION HAS 3 POINTS SPACED AT 01.250 FEET

GRID IN Y DIRECTION HAS 3 POINTS SPACED AT 00.500 FEET

RESULTS COMPUTED AT (007.500,-00.00) FEET

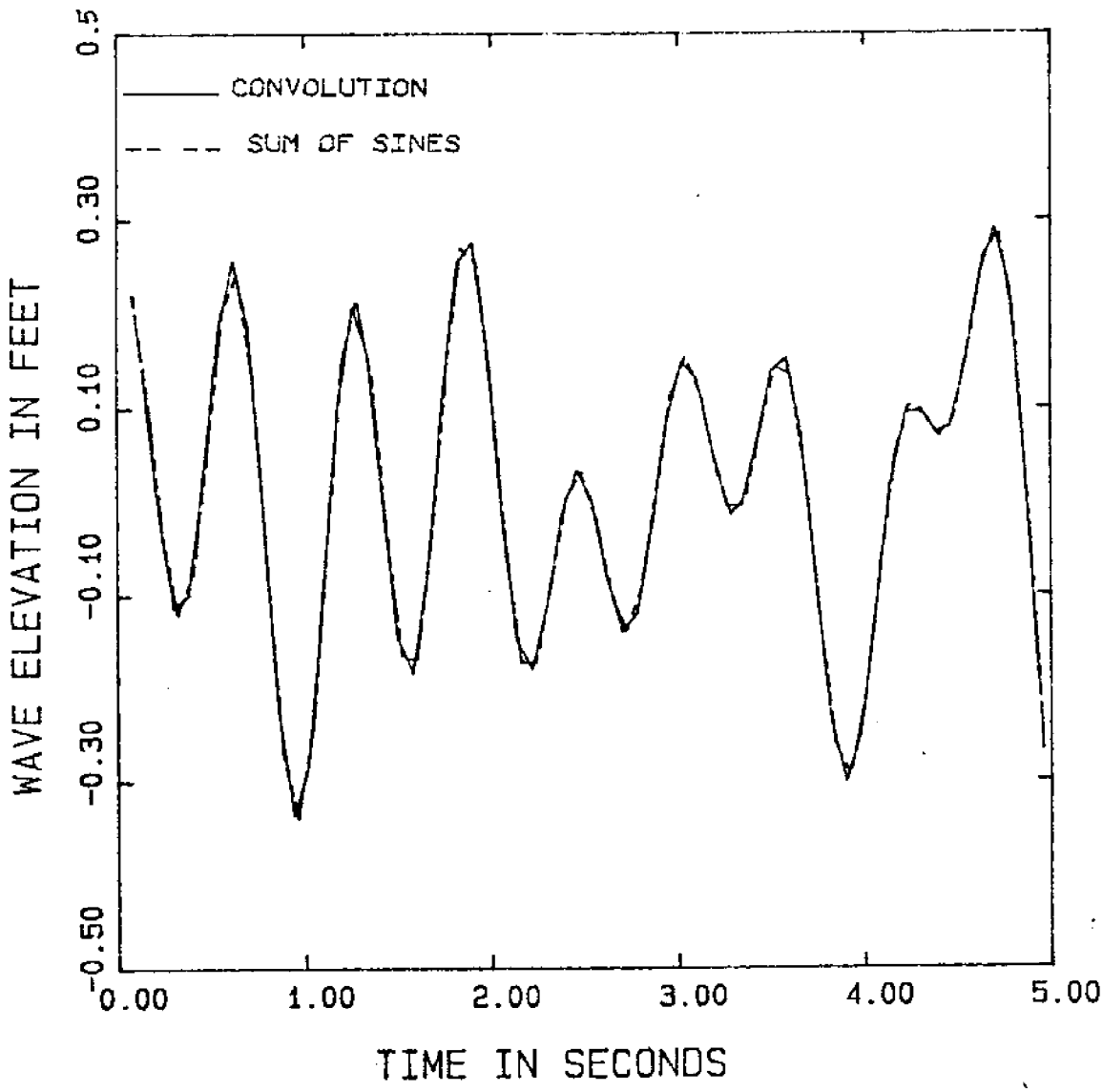

FIGURE 21: SIMULATED OVER 7.5 FEET (4.5 SHORTEST WAVE LENGTH)

RANDOM WAVE : HEIGHT sig = 20.00 FEET PERIOD sig = 10.00 SEC

32 FREQUENCY COMPONENTS WITH MINIMUM = 0.05 HZ MAXIMUM = 0.25 HZ

DT = 0.0625 SEC DEPTH = 250.0 FEET DATA SIZE = 2048

GRID IN X DIRECTION HAS 7 POINTS SPACED AT 50.000 FEET

GRID IN Y DIRECTION HAS 3 POINTS SPACED AT 25.000 FEET

RESULTS COMPUTED AT (300.000,-25.00) FEET

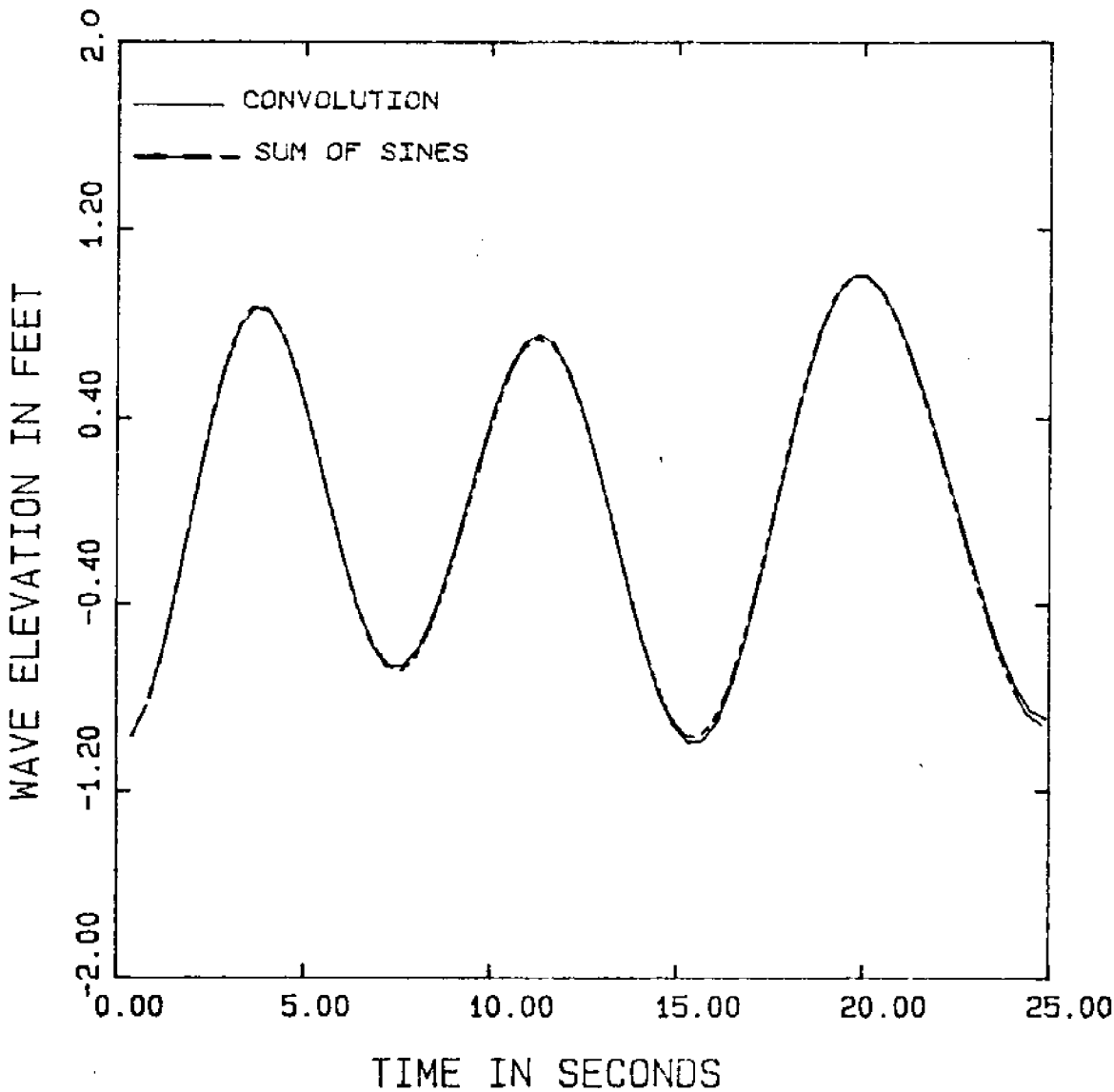

FIGURE 22: SIMULATED KINEMATICS (PARTICLE DISPLACEMENT)

RANDOM WAVE : HEIGHT sig = 20.00 FEET PERIOD sig = 10.00 SEC

32 FREQUENCY COMPONENTS WITH MINIMUM = 0.05 HZ MAXIMUM = 0.25 HZ

DT = 0.0625 SEC DEPTH = 250.0 FEET DATA SIZE = 2048

GRID IN X DIRECTION HAS 7 POINTS SPACED AT 50.000 FEET

GRID IN Y DIRECTION HAS 3 POINTS SPACED AT 25.000 FEET

RESULTS COMPUTED AT (300.000,-25.00) FEET

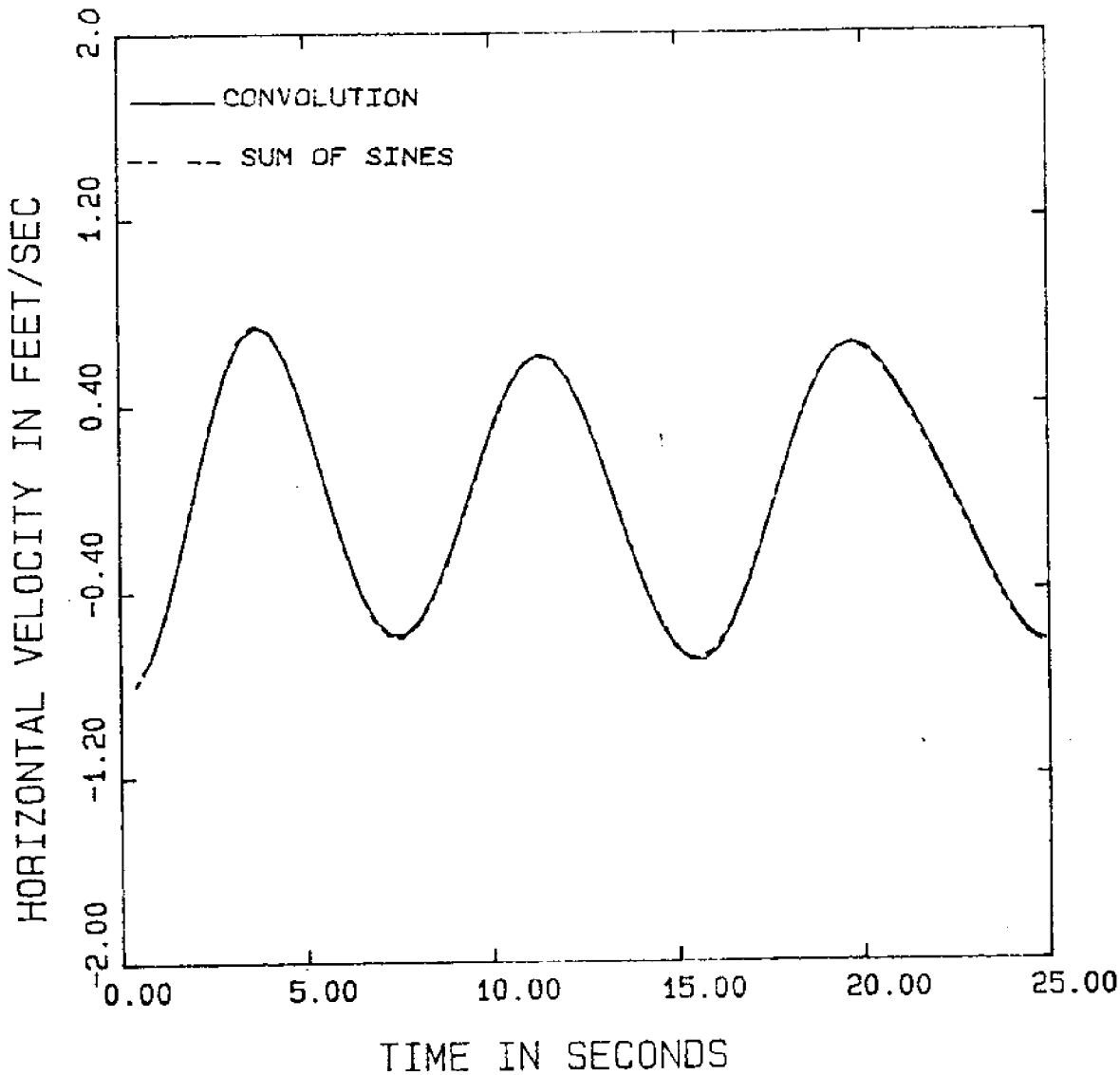

FIGURE 23: SIMULATED KINEMATICS (HORIZONTAL VELOCITY)

RANDOM WAVE : HEIGHT sig = 20.00 FEET PERIOD sig = 10.00 SEC

32 FREQUENCY COMPONENTS WITH MINIMUM = 0.05 HZ MAXIMUM = 0.25 HZ

DT = 0.0625 SEC DEPTH = 250.0 FEET DATA SIZE = 2048

GRID IN X DIRECTION HAS 7 POINTS SPACED AT 50.000 FEET

GRID IN Y DIRECTION HAS 3 POINTS SPACED AT 25.000 FEET

RESULTS COMPUTED AT (300.000,-25.00) FEET

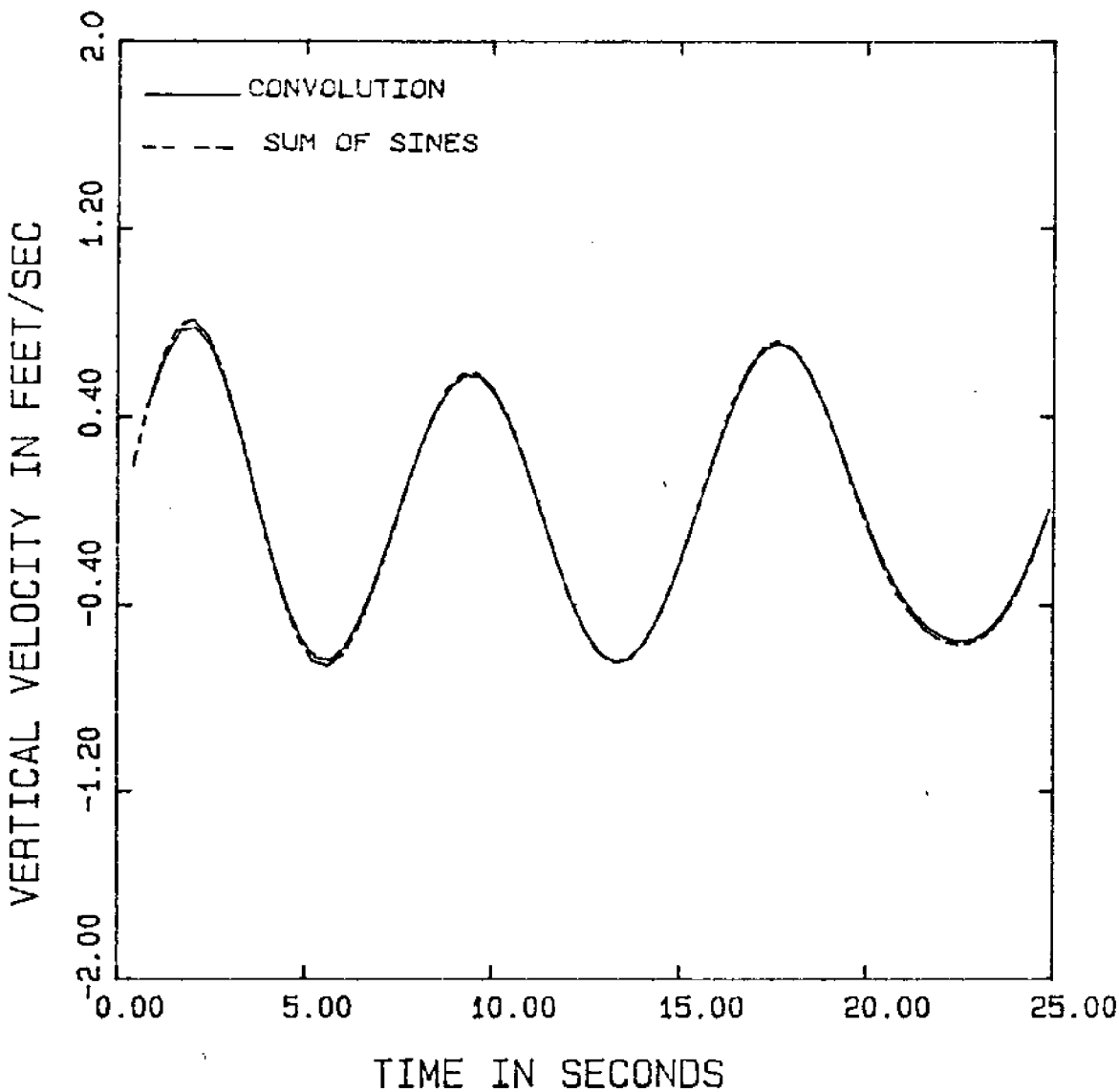

FIGURE 24: SIMULATED KINEMATICS (VERTICAL VELOCITY)

RANDOM WAVE : HEIGHT sig = 20.00 FEET PERIOD sig = 10.00 SEC

32 FREQUENCY COMPONENTS WITH MINIMUM = 0.05 HZ MAXIMUM = 0.25 HZ

DT = 0.0625 SEC DEPTH = 250.0 FEET DATA SIZE = 2048

GRID IN X DIRECTION HAS 7 POINTS SPACED AT 50.000 FEET

GRID IN Y DIRECTION HAS 3 POINTS SPACED AT 25.000 FEET

RESULTS COMPUTED AT (300.000,-25.00) FEET

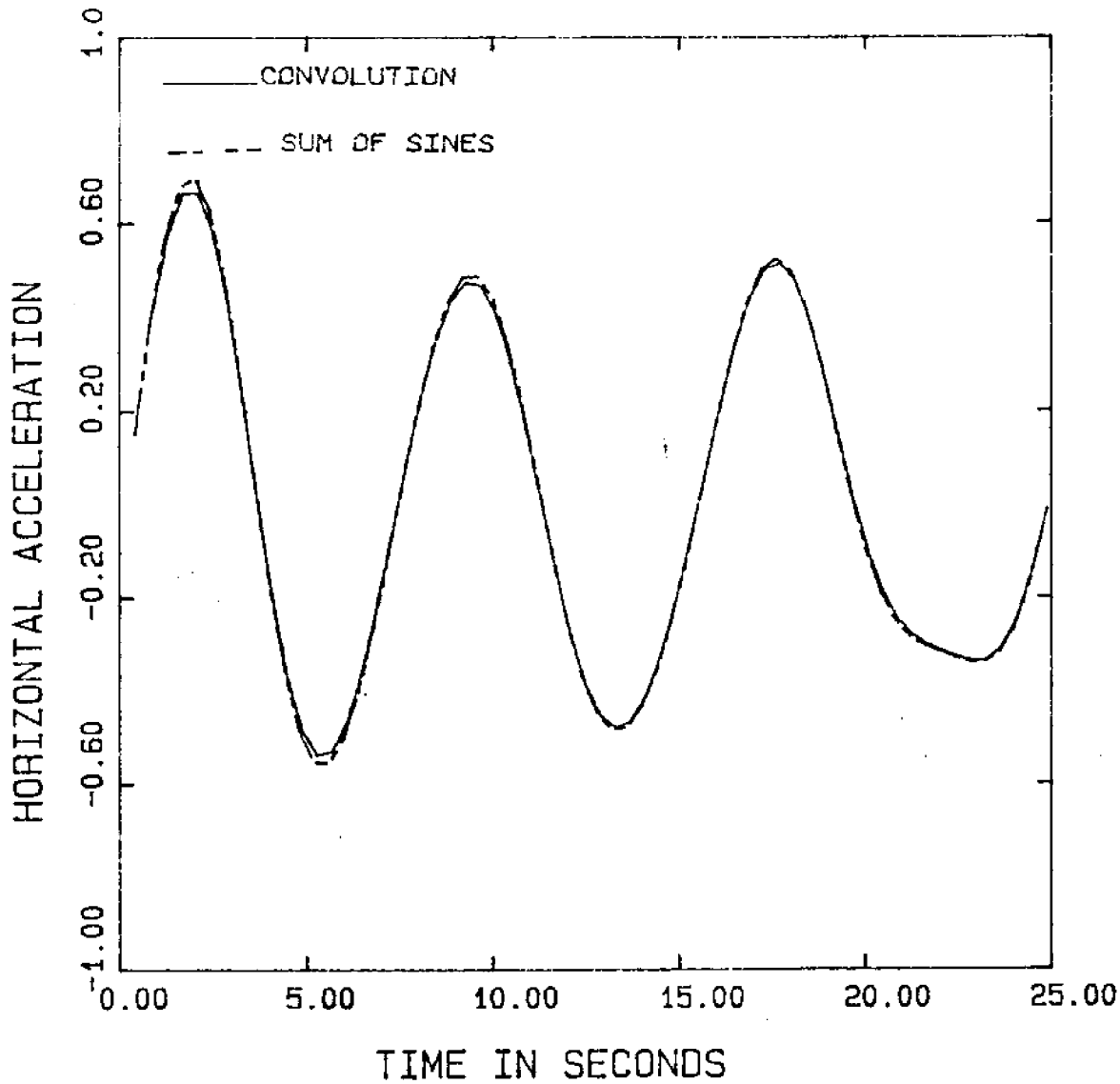

FIGURE 25: SIMULATED KINEMATICS (HORIZONTAL ACCELERATION)

RANDOM WAVE : HEIGHT sig = 20.00 FEET PERIOD sig = 10.00 SEC

32 FREQUENCY COMPONENTS WITH MINIMUM = 0.05 HZ MAXIMUM = 0.25 HZ

DT = 0.0625 SEC DEPTH = 250.0 FEET DATA SIZE = 2048

GRID IN X DIRECTION HAS 7 POINTS SPACED AT 50.000 FEET

GRID IN Y DIRECTION HAS 3 POINTS SPACED AT 25.000 FEET

RESULTS COMPUTED AT (300.000,-25.00) FEET

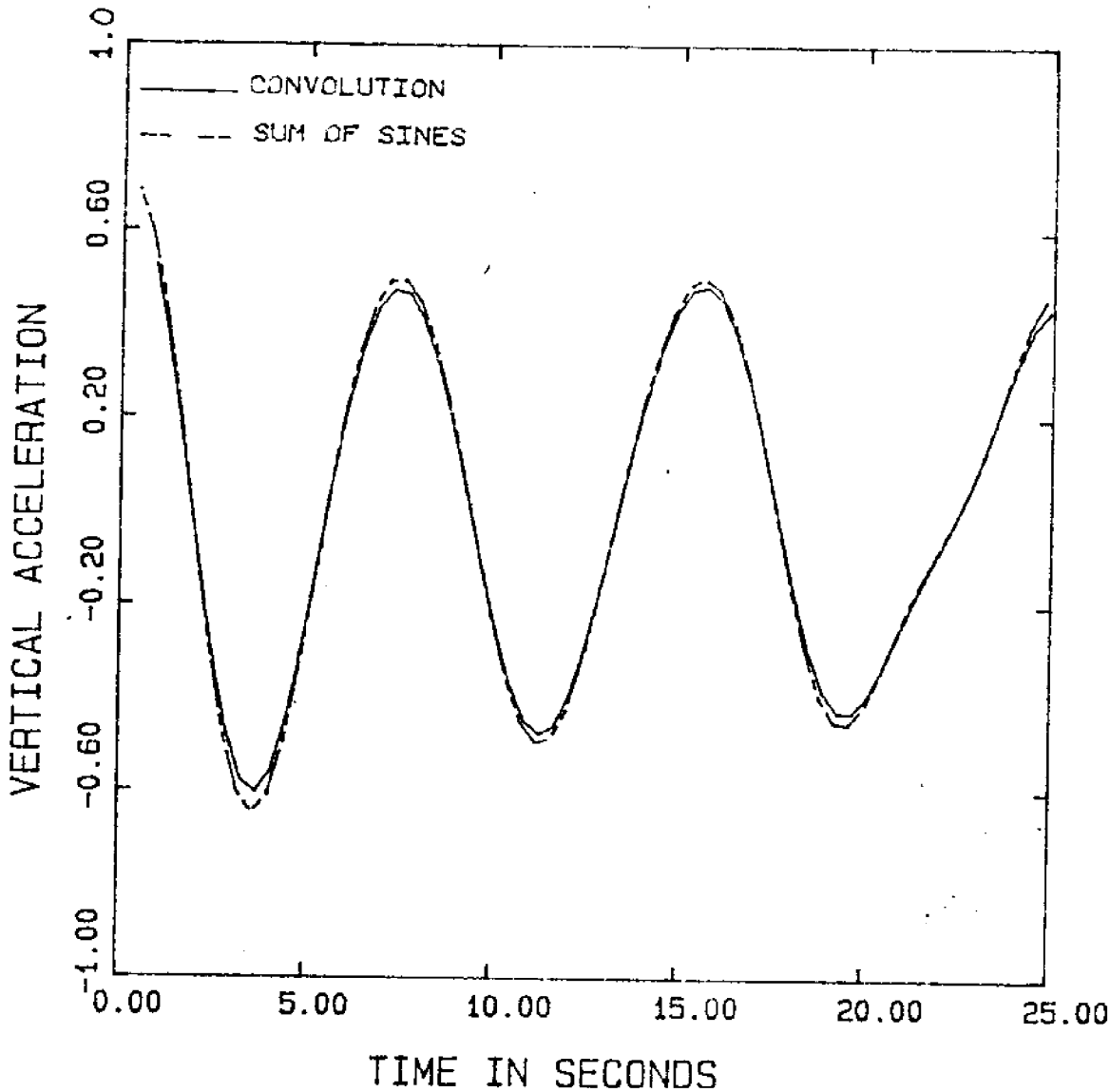

FIGURE 26: SIMULATED KINEMATICS (VERTICAL ACCELERATION)

REGULAR WAVE : AMPLITUDE = 00.100 FEET PERIOD = 00.50 SEC

DT = 0.0625 SEC DEPTH = 004.0 FEET DATA SIZE = 2048

X GRID DETAILS

9 POINTS SPACED AT 0.16 FEET, S=Lc /8, SHOWN BY -- --

5 POINTS SPACED AT 0.32 FEET, S=Lc /4, SHOWN BY —·—

3 POINTS SPACED AT 0.64 FEET, S=Lc /2, SHOWN BY —|—

Lc = SHORTEST WAVE LENGTH S = GRID SPACING

GRID IN Y DIRECTION HAS 3 POINTS SPACED AT 05.0000 FEET

RESULTS COMPUTED AT (00.480,-00.00) FEET

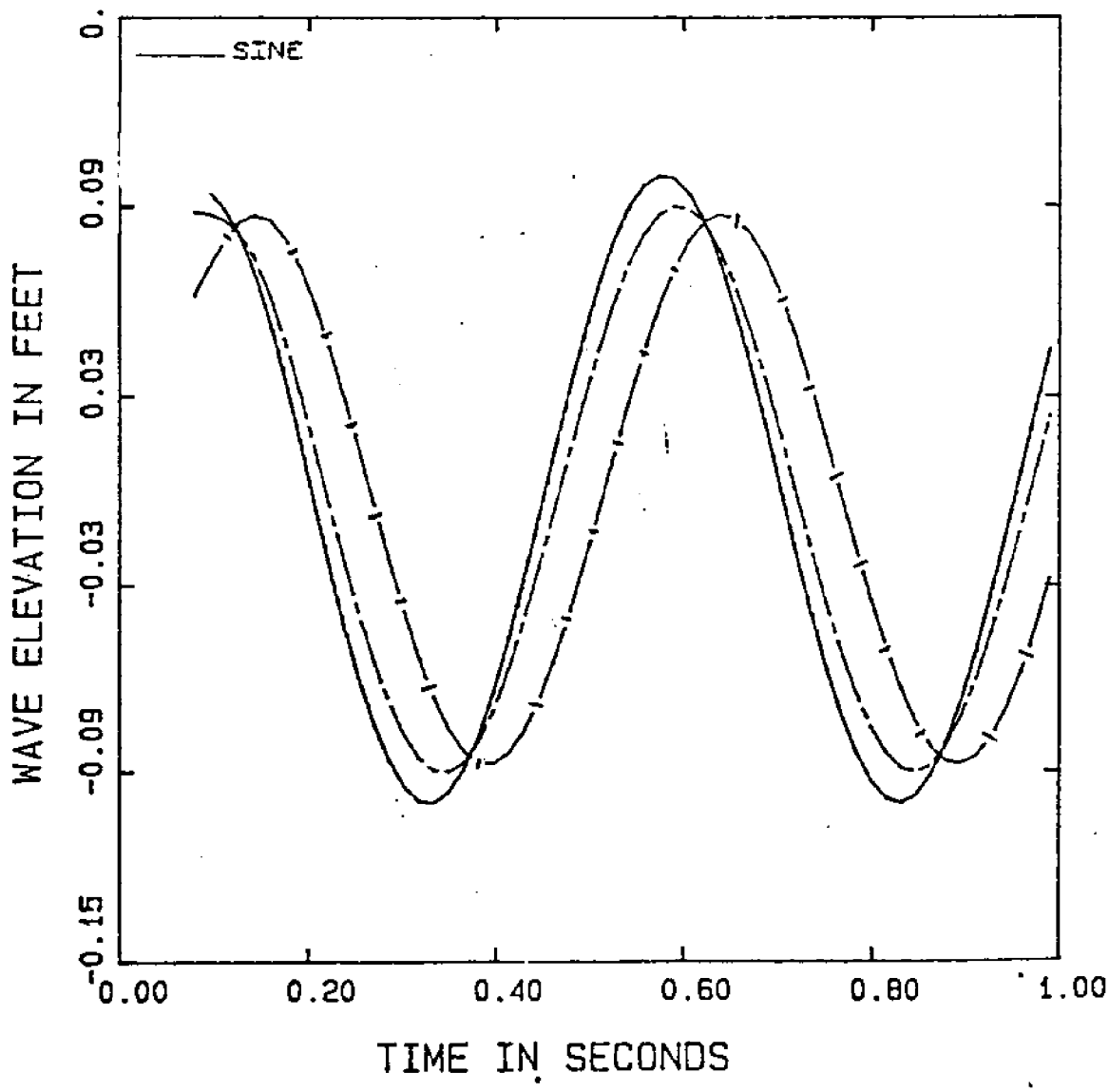

FIGURE 27 : EFFECT OF GRID SPACING ON SIMULATIONS

REGULAR WAVE : AMPLITUDE = 00.100 FEET PERIOD = 00.50 SEC

DT = 0.1500 SEC DEPTH = 004.0 FEET DATA SIZE = 1024

GRID IN X DIRECTION HAS 3 POINTS SPACED AT 01.2500 FEET

GRID IN Y DIRECTION HAS 3 POINTS SPACED AT 05.0000 FEET

RESULTS COMPUTED AT (002.500,-00.00) FEET

SINE ——— CONVOLUTION —▲—▲—

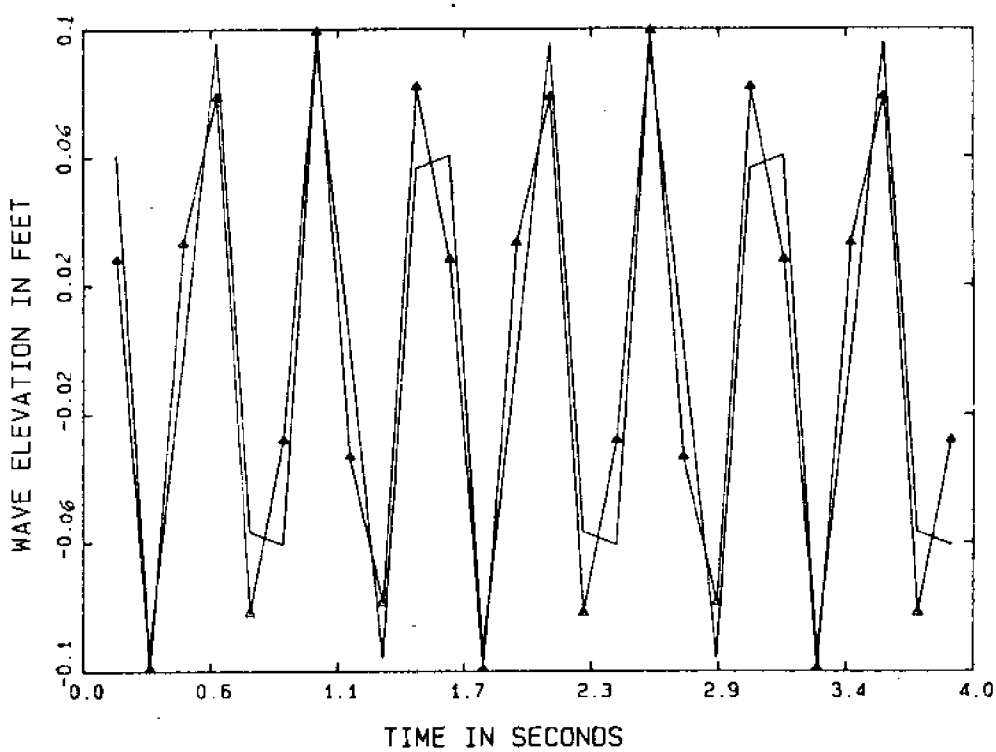

FIGURE 28 : UNDERSAMPLING

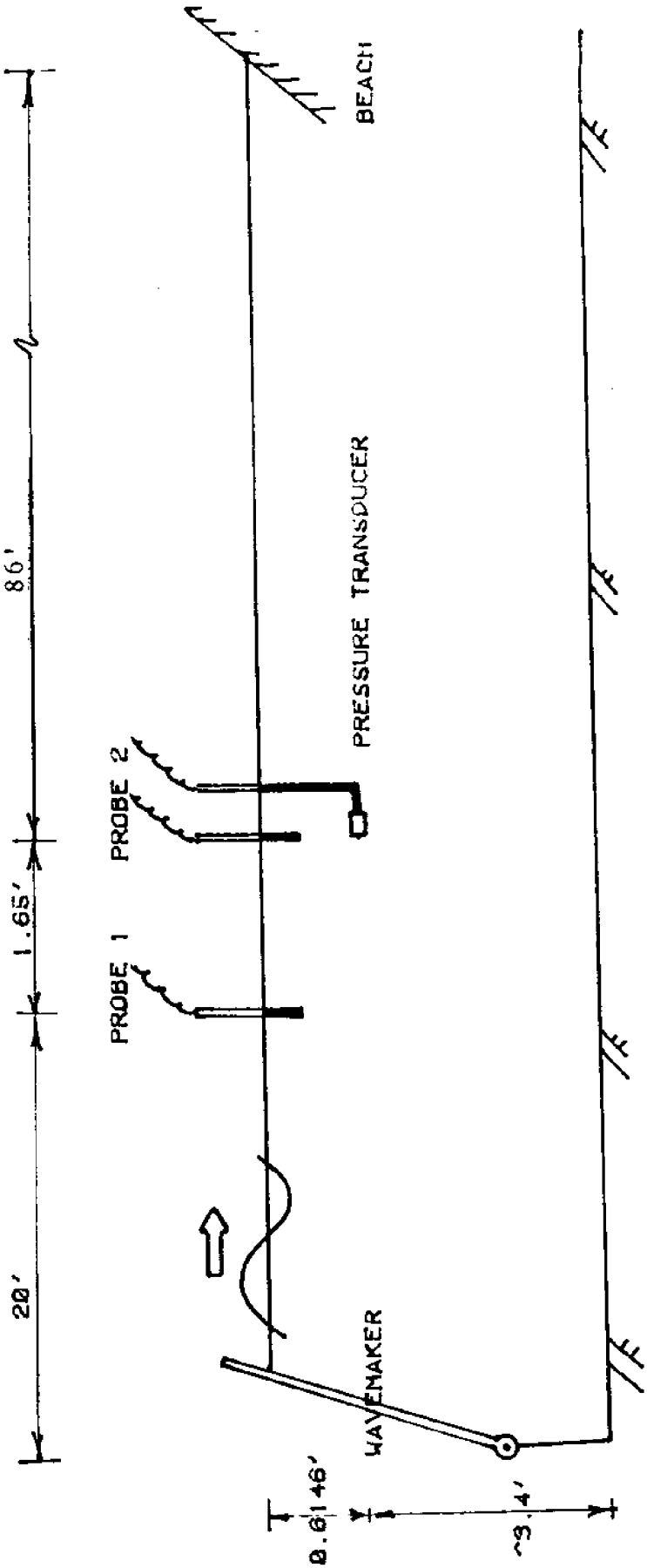

FIGURE 29. TEST SETUP IN THE WAVE TANK

DT = 0.0375 SEC DEPTH = 004.0 FEET DATA SIZE = 2048

GRID IN X DIRECTION HAS 3 POINTS SPACED AT 0.8125 FEET

GRID IN Y DIRECTION HAS 3 POINTS SPACED AT 0.6146 FEET

RESULTS COMPUTED AT (001.625,-00.00) FEET

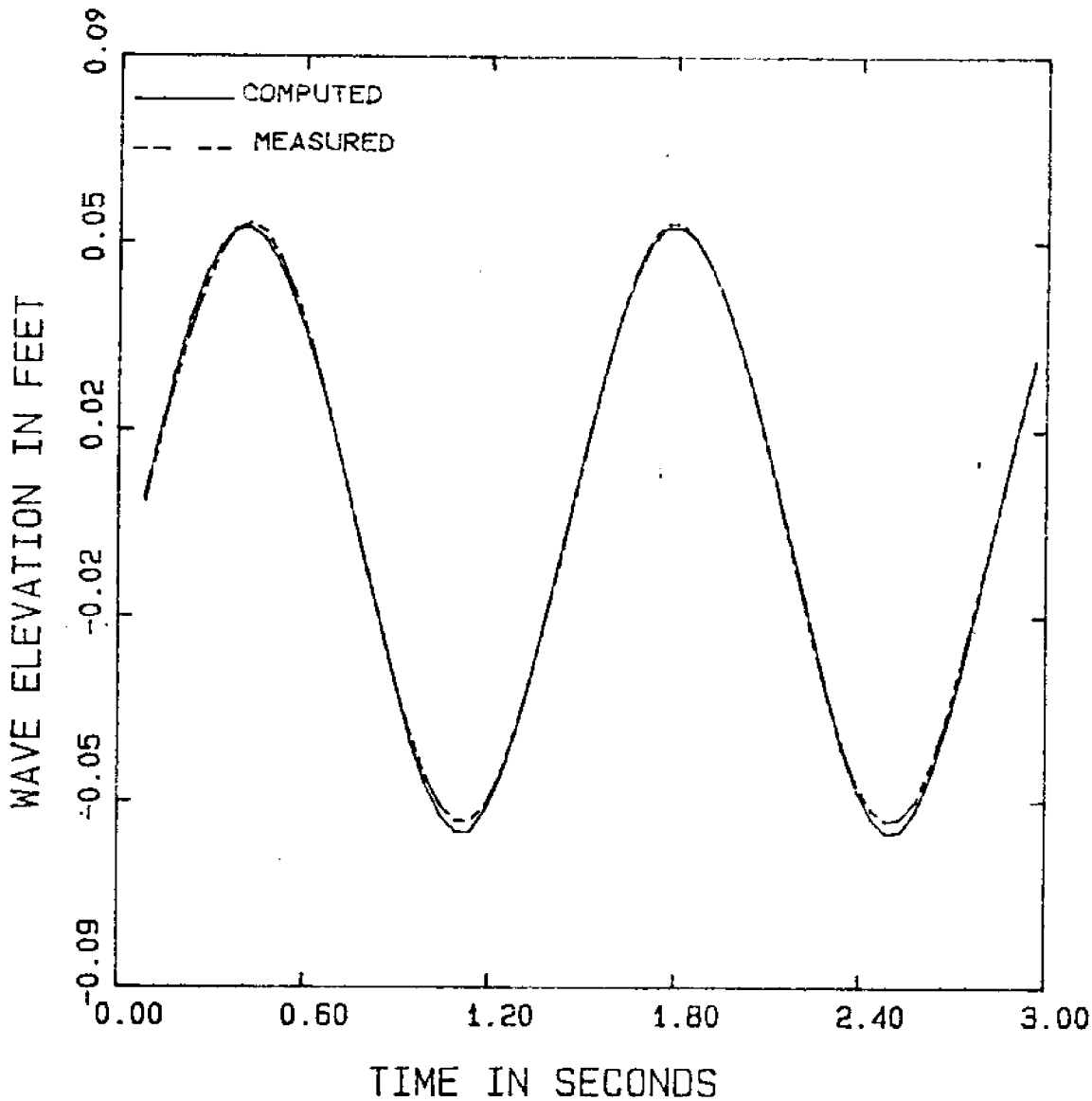

FIGURE 30 : PROPAGATED AND MEASURED WAVEFORMS

DT = 0.0375 SEC DEPTH = 004.0 FEET DATA SIZE = 2048

GRID IN X DIRECTION HAS 3 POINTS SPACED AT 0.8125 FEET

GRID IN Y DIRECTION HAS 3 POINTS SPACED AT 0.6146 FEET

RESULTS COMPUTED AT (001.625,-00.6146) FEET

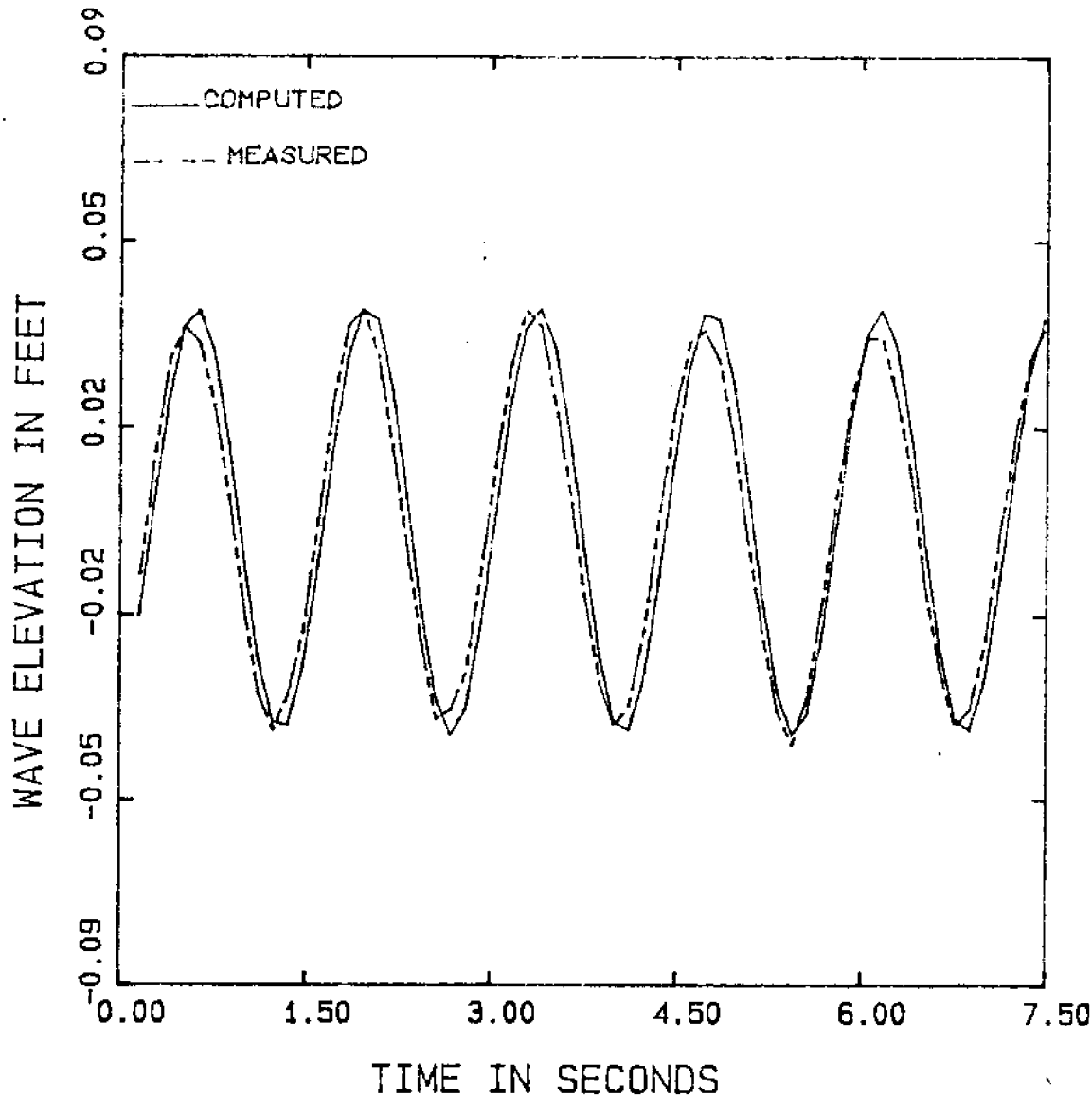

FIGURE 31 : PROPAGATED AND MEASURED WAVEFORMS

FIGURE 32: INPUT SPECTRUM AT PROBE 1

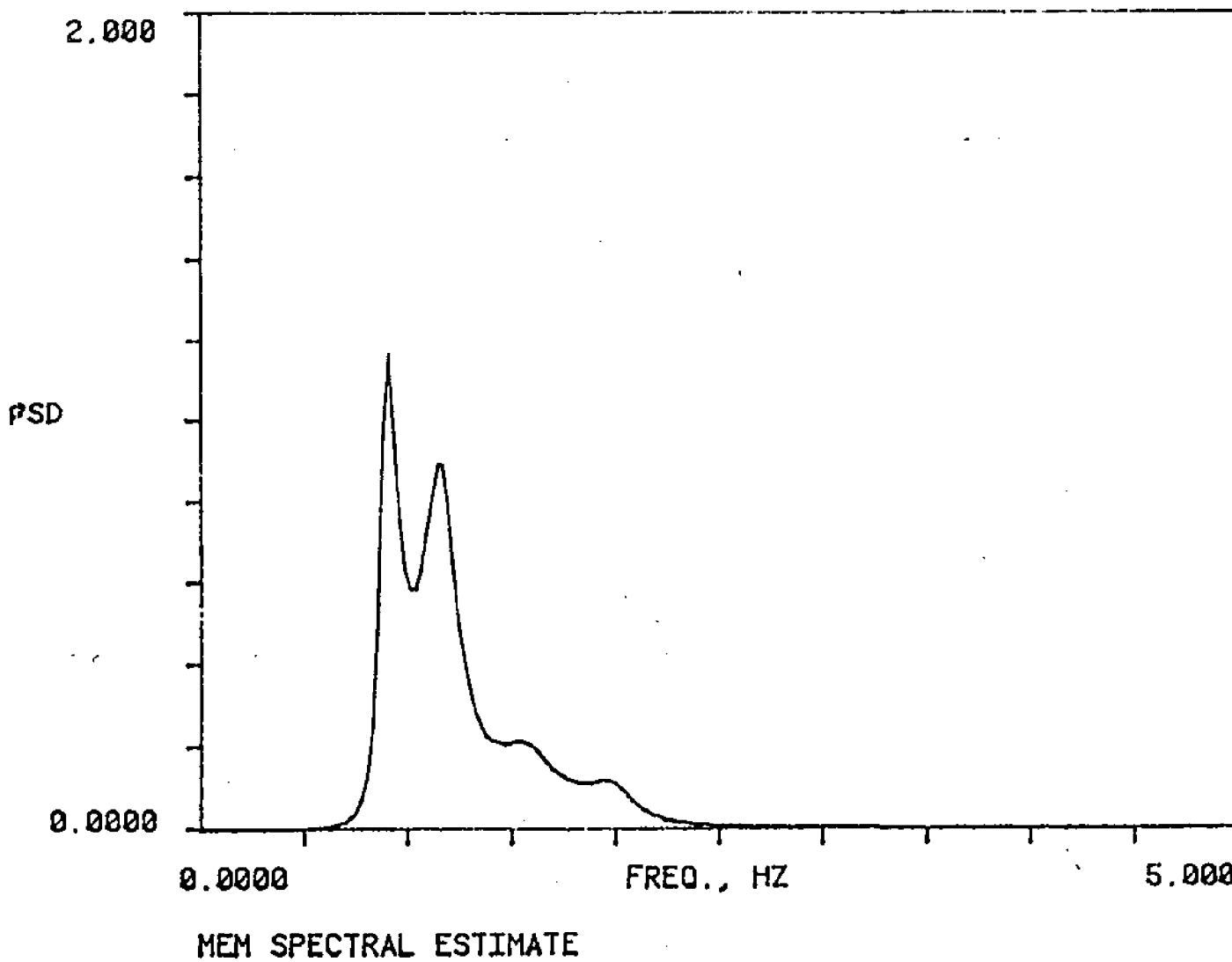

FIGURE 33 : INPUT SPECTRUM AT PROBE 2

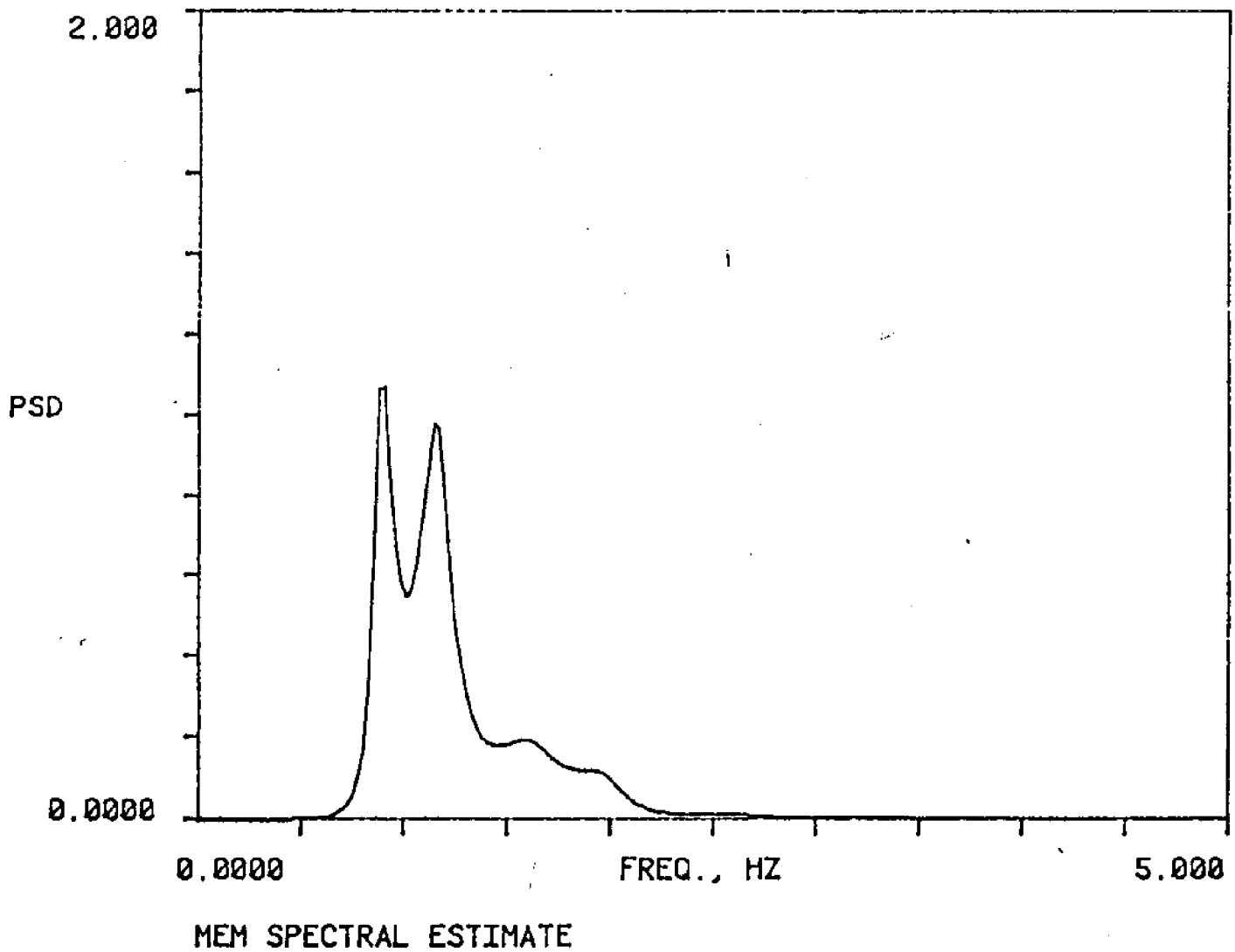

DT = 0.0375 SEC DEPTH = 004.0 FEET DATA SIZE = 2048

GRID IN X DIRECTION HAS 3 POINTS SPACED AT 0.8125 FEET

GRID IN Y DIRECTION HAS 3 POINTS SPACED AT 0.6146 FEET

RESULTS COMPUTED AT (001.625,-00.00) FEET

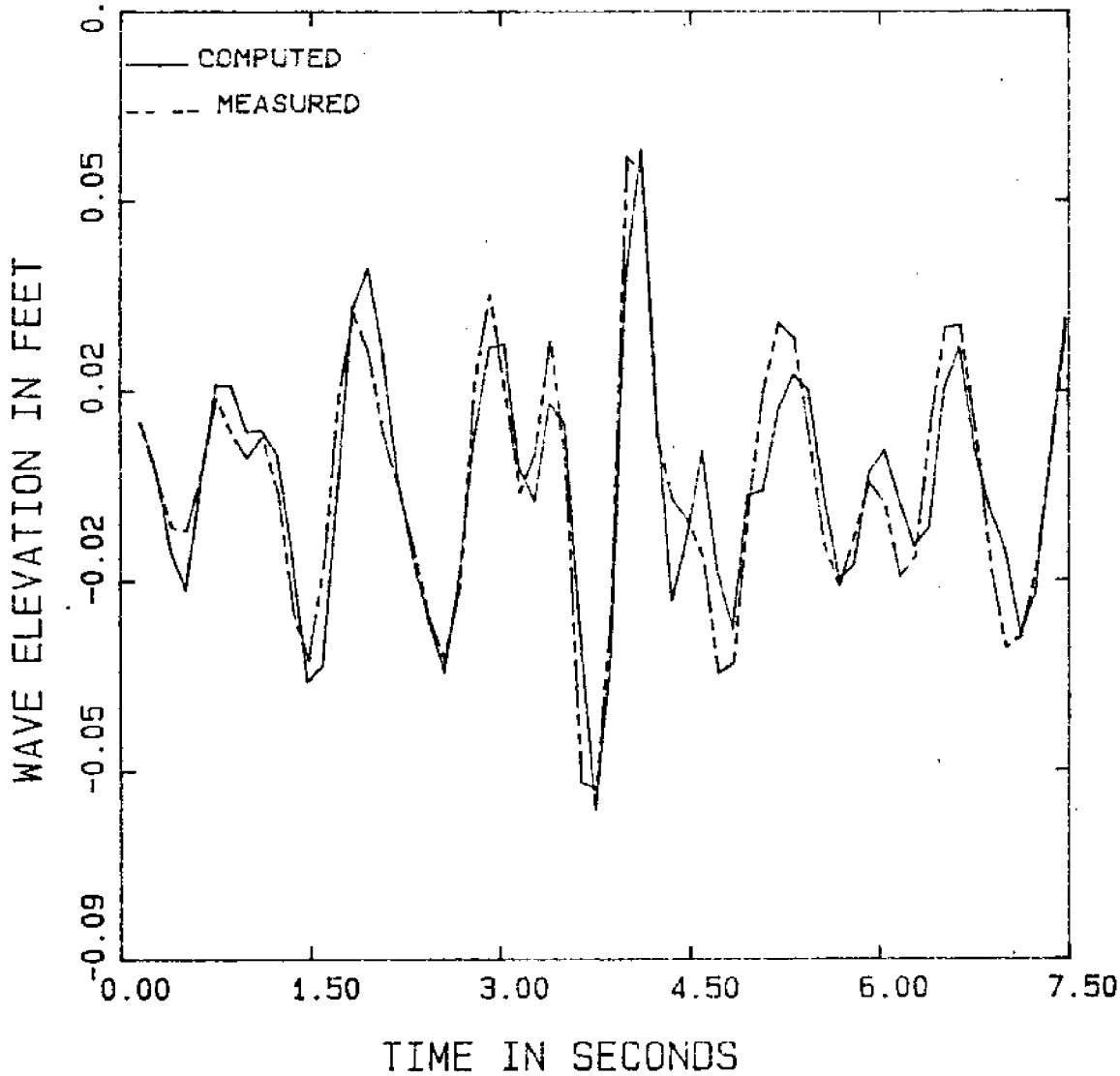

FIGURE 34 : PROPAGATED AND MEASURED WAVEFORMS

DT = 0.0375 SEC DEPTH = 004.0 FEET DATA SIZE = 2048

GRID IN X DIRECTION HAS 3 POINTS SPACED AT 0.8125 FEET

GRID IN Y DIRECTION HAS 3 POINTS SPACED AT 0.6146 FEET

RESULTS COMPUTED AT (001.625,-00.6146) FEET

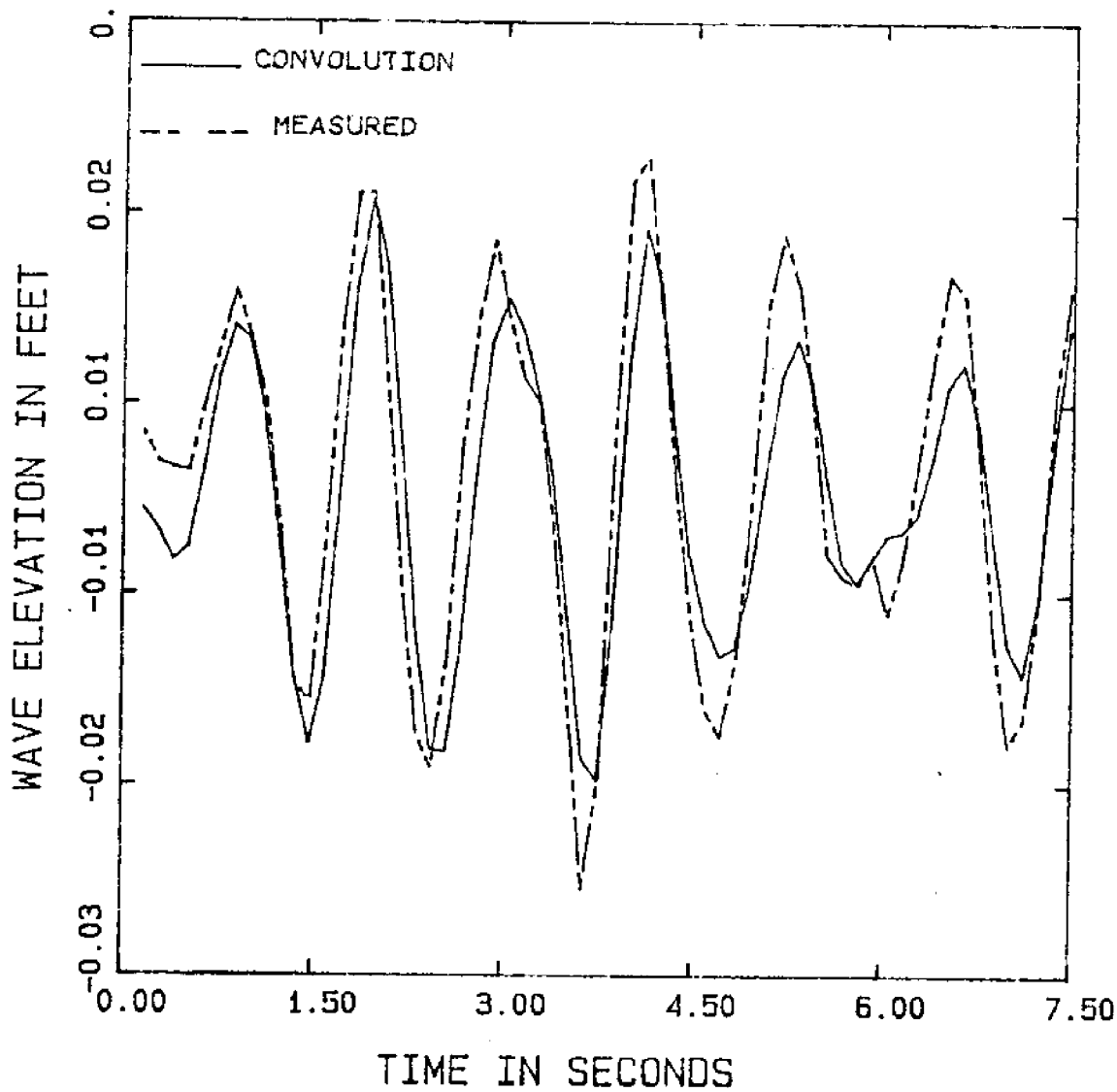

FIGURE 35 : PROPAGATED AND MEASURED WAVEFORMS

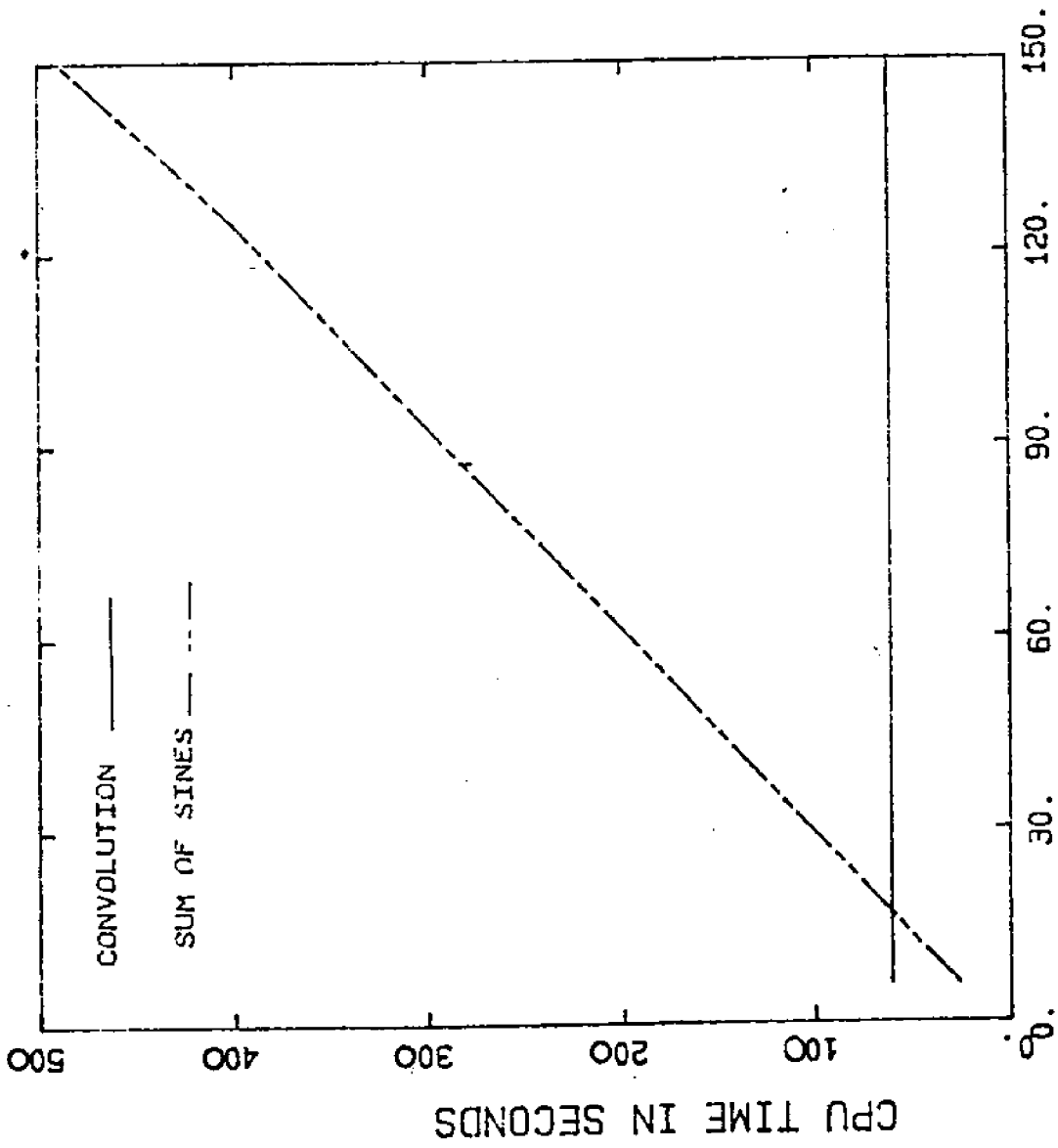

FIGURE 36: EFFECT OF NUMBER OF FREQUENCIES ON CPU TIME

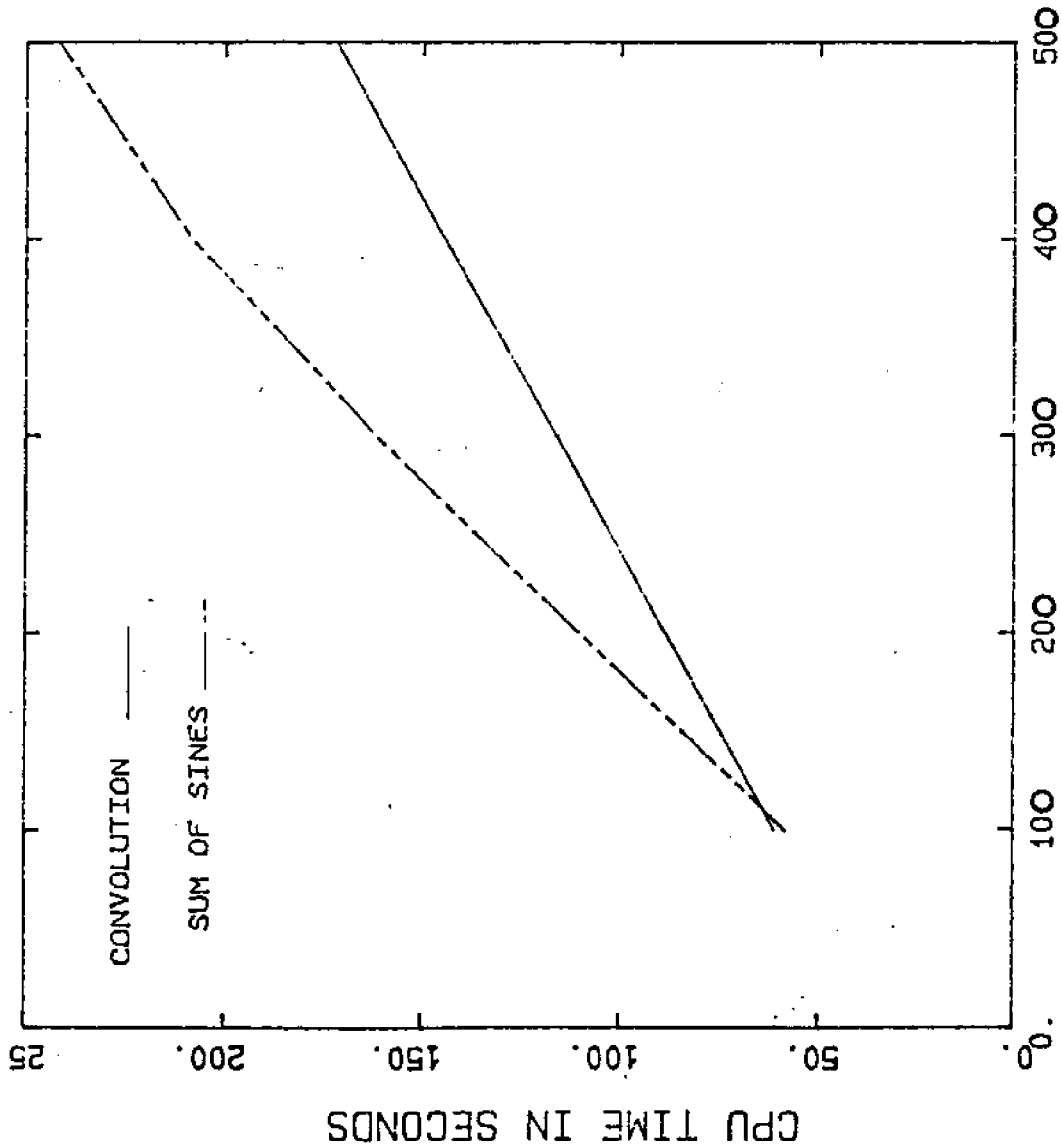

FIGURE 37: EFFECT OF NO OF STEPS ON CPU TIME

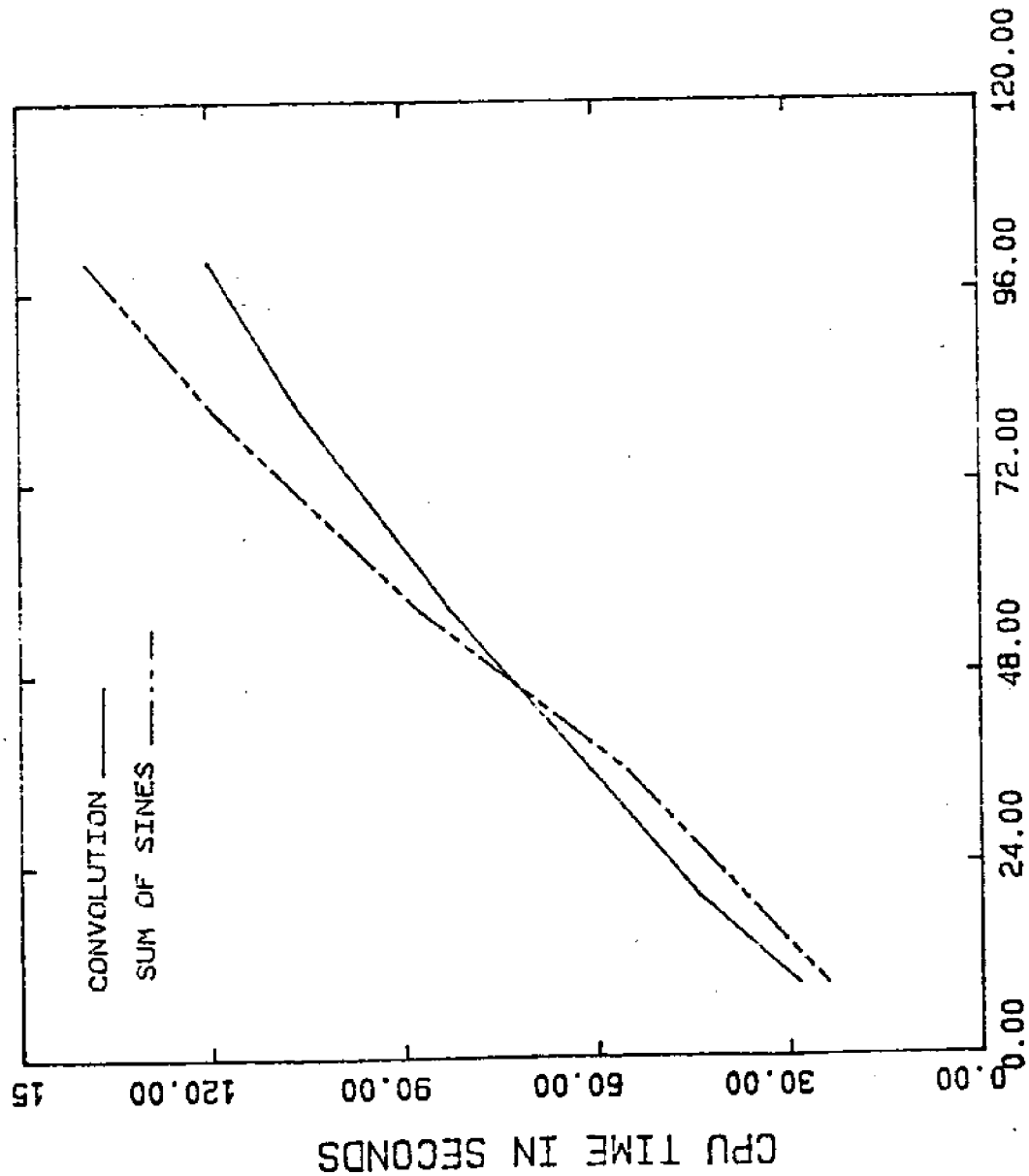

FIGURE 38: EFFECT OF GRID SIZE ON CPU TIME

REGULAR WAVE : AMPLITUDE = 10.00 FEET PERIOD = 14.59 SEC

DT = 0.5 SEC DEPTH = 250.0 FEET DATA SIZE = 2048

GRID IN X DIRECTION HAS 3 POINTS SPACED AT 125.000 FEET

GRID IN Y DIRECTION HAS 3 POINTS SPACED AT 025.000 FEET

RESULTS COMPUTED AT (250.400,-25.00) FEET

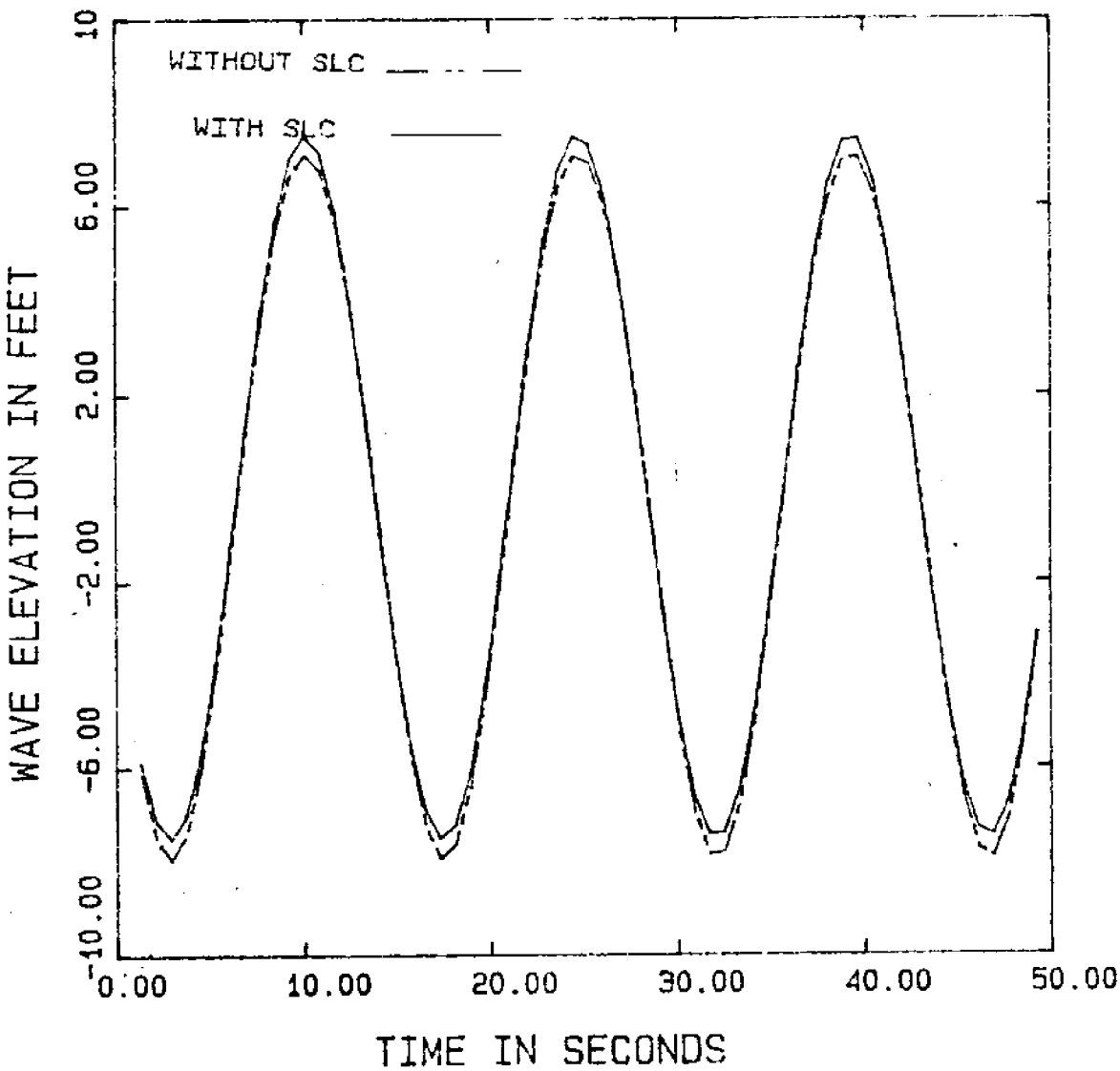

FIGURE 39 : SIMULATED WAVE WITH STRETCHED LINEAR CORRECTION

FIGURE 40 ERROR ANALYSIS OF CENTRAL DIFFERENCE METHOD

The relative error of the central difference method increases as the number of samples per wave decreases. As the sampling rate approaches infinity, the relative error error approaches one. As the sampling rate approaches two samples per wave, the relative error goes to zero.

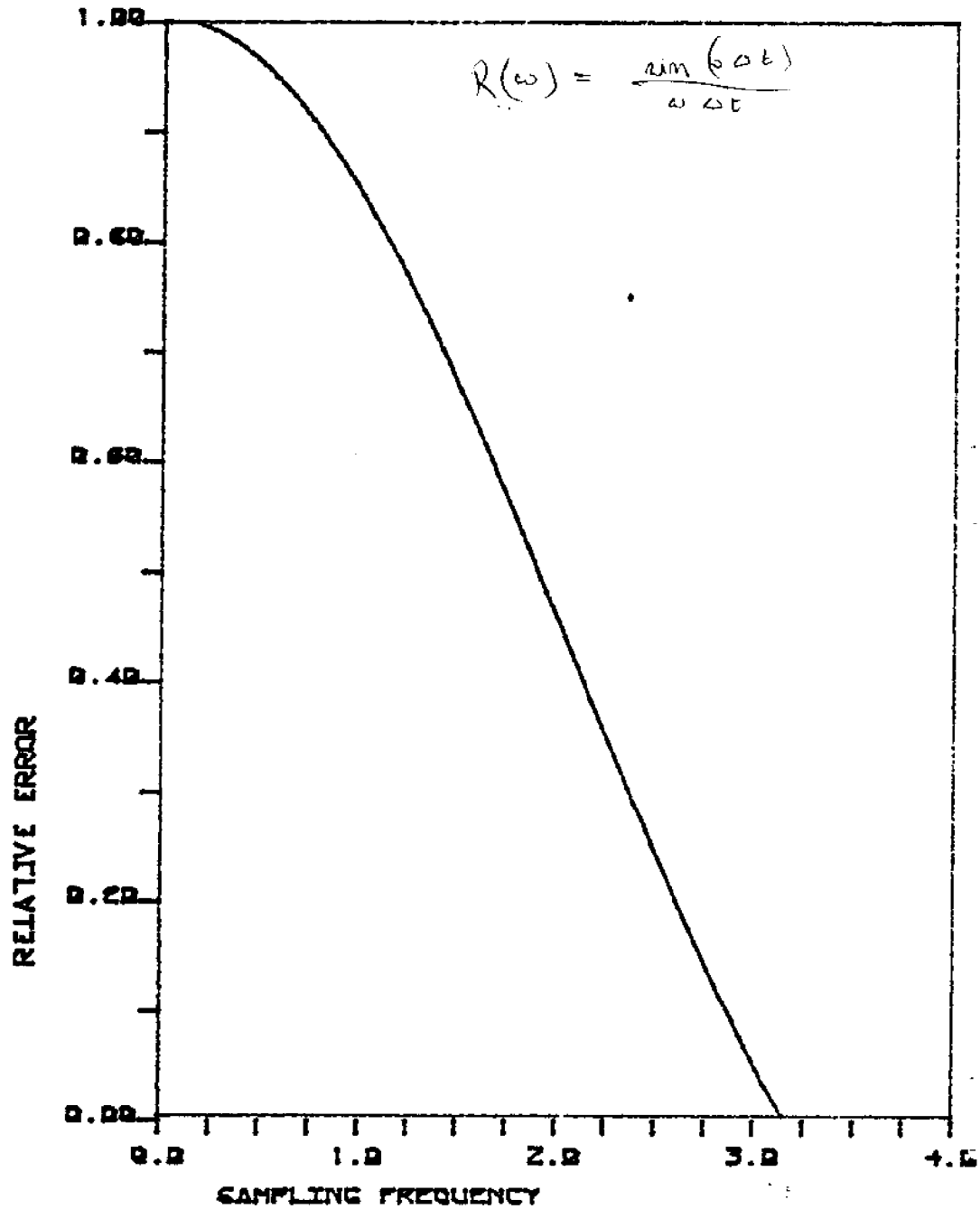

FIGURE 41 SINUSOIDAL WAVE CONTAMINATED WITH NOISE

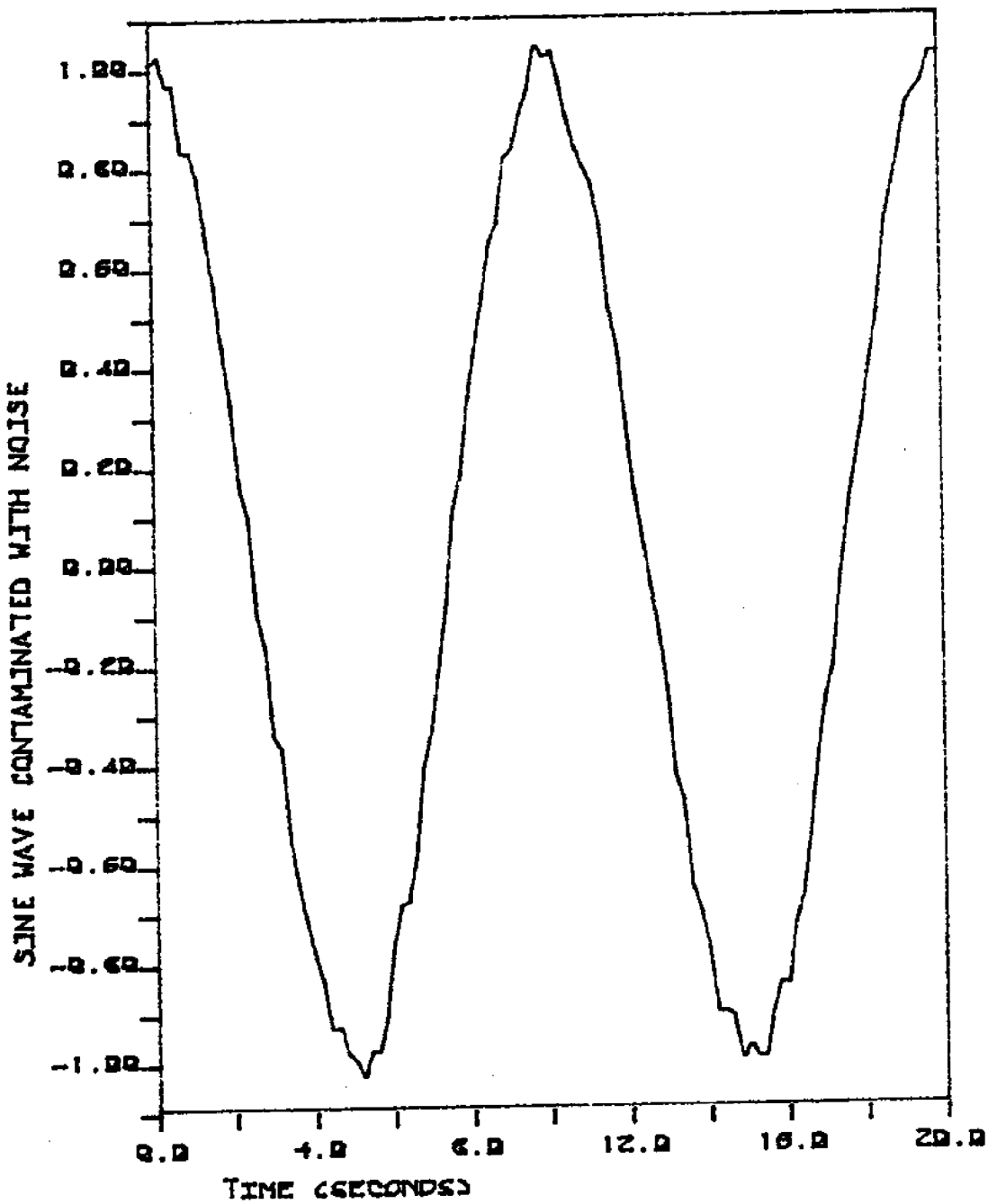

FIGURE 42 DERIVATIVE OF A WAVE CONTAMINATED WITH NOISE I

Numerical differentiation amplifies noise. In fact, the amplification increases as the number of sample points per wave increases. In this case, the central difference method has been used to evaluate the derivative of the function plotted in figure J.19. The sampling rate is 25 samples per wave. The solid line is the derivative of the function when it is not contaminated with noise. The symbols represent the derivative of the function as calculated by the central difference method.

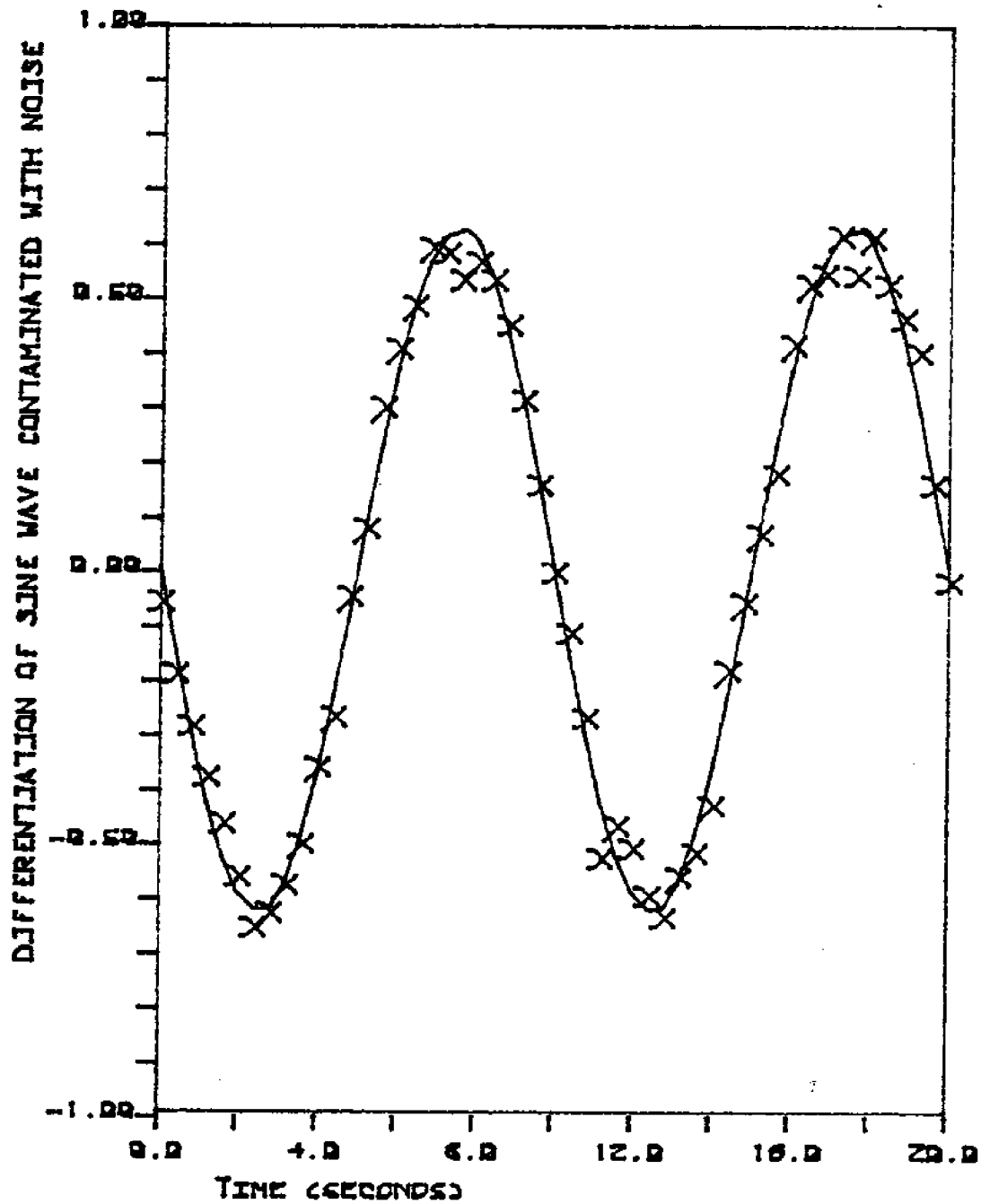

FIGURE 43 DERIVATIVE OF A WAVE CONTAMINATED WITH NOISE II

Numerical differentiation amplifies noise. In fact, the amplification increases as the number of sample points per wave increases. In this case, the central difference method has been used to evaluate the derivative of the function plotted in figure J.19. The sampling rate is 50 samples per wave. The solid line is the derivative of the function when it is not contaminated with noise. The symbols represent the derivative of the function as calculated by the central difference method. Clearly, the error at this sampling rate is greater than the error at the lower sampling rate shown on the preceding page.

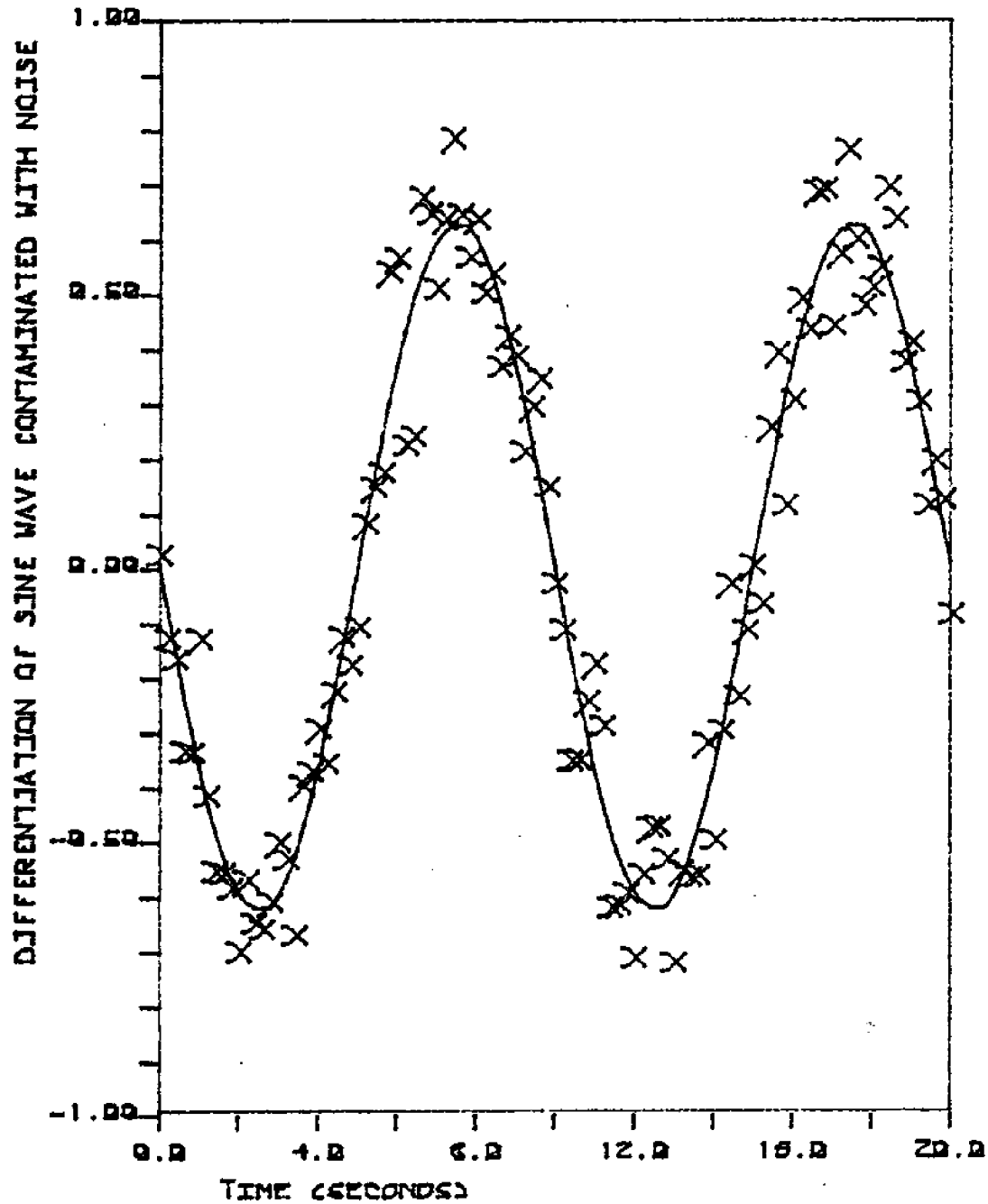

APPENDIX G

TABLES

TABLE G-1 AIRY WAVE THEORY IN FINITE WATER DEPTHS

Free surface elevation	$\eta = Re\, e^{i(kx-\omega t)}$
Horizontal particle velocity	$u = Re\, \omega A \frac{\cosh(k(z+h))}{\sinh(kh)} e^{i(kx-\omega t)}$
Vertical particle velocity	$w = Re\, -i\omega A \frac{\sinh(k(z+h))}{\sinh(kh)} e^{i(kx-\omega t)}$
Horizontal particle acceleration	$\dot{u} = Re\, -i\omega^2 A \frac{\cosh(k(z+h))}{\sinh(kh)} e^{i(kx-\omega t)}$
Vertical particle acceleration	$\dot{w} = Re\, -\omega^2 A \frac{\sinh(k(z+h))}{\sinh(kh)} e^{i(kx-\omega t)}$
Dynamic component of water pressure	$P_D = Re\, \rho g A \frac{\cosh(k(z+h))}{\cosh(kh)} e^{i(kx-\omega t)}$
Dispersion relation	$\omega^2 = kg \tanh(kh)$

TABLE G-2 AIRY WAVE THEORY IN DEEP WATER

Free surface elevation	$\eta = Re\, A e^{i(kx-\omega t)}$
Horizontal particle velocity	$u = Re\, \omega A e^{kz} e^{i(kx-\omega t)}$
Vertical particle velocity	$w = Re\, -i\omega A e^{kz} e^{i(kx-\omega t)}$
Horizontal particle acceleration	$\dot{u} = Re\, -i\omega^2 A e^{kz} e^{i(kx-\omega t)}$
Vertical particle acceleration	$\dot{w} = Re\, -\omega^2 A e^{kz} e^{i(kx-\omega t)}$
Dynamic component of water pressure	$p_D = Re\, \rho g A e^{kz} e^{i(kx-\omega t)}$
Dispersion relation	$\omega^2 = kg$